ABSTRACT

SHIN, PETER HANCHUL. Non-destructive Inspection in Adhesively Bonded Joints using Pulsed Phase Thermography. (Under the direction of Dr. Kara J. Peters.)

This study investigates the use of pulsed phase thermography for the inspection of an adhesively bonded, carbon fiber-epoxy laminate, single lap joint. Damaged area assessments from the majority of previous PPT research studies were mainly dependent on user decisions, based on the difference in phase contrast across the sample. These decisions can lead to false detections or misinterpretation of defected areas. This project derived a PPT imaging technique with a threshold filtering method, where the threshold value is determined mathematically.

In this research, two types of specimens were fabricated for quantification of the pulsed phase thermography (PPT) performance. The first specimen was a single lap-joint specimen with artificial defects at adherend-adhesive interface. The second type was a single lap-joint specimen, following ASTM standards, for damage detection after manufacturing and after fatigue cycles. Using a fully developed open source MATLAB program for PPT, the optimal parameters for specific bonded joint sample were first determined to maximize the visibility of the artificial defects. Next, the sizing threshold for phase contrast was calculated from the artificial defect specimen, by comparing the phase contrast distribution to the known sizes of the defects with different thicknesses. A single threshold value worked well for the different defect materials and thicknesses. This threshold was then applied to fatigue cycled specimens for the sizing of defects both present after manufacturing and progressing in the adherend-adhesive interface after fatigue loading cycles. The results of the threshold sizing method compared well with visual observations of the fracture surfaces after

final failure of the lap joint specimens. The growth of fatigue damage was more difficult to identify for brittle fractures, but was well captured by the PPT for the failure dominated by plastic deformation in the adhesive.

Non-destructive Inspection in Adhesively Bonded Joints using Pulsed Phase Thermography

by
Peter Hanchul Shin

A thesis submitted to the Graduate Faculty of
North Carolina State University
in partial fulfillment of the
requirements for the degree of
Master of Science

Aerospace Engineering

Raleigh, North Carolina

2013

APPROVED BY:

Dr. Kara Peters Committee Chair	Dr. Rudolf Seracino

Dr. Fuh-Gwo Yuan

DEDICATION

This work is dedicated to God (Matthew 19:26), my parents, sister, and brother-in-law. Also dedicated to the memory of my best friend, my grandfather; a role model of my life and a dearly missed family member.

BIOGRAPHY

Peter Shin was born in Baton Rouge, Louisiana on January 13th, 1985 to Hyun and Wha Shin. His family moved back to South Korea little after he turned seven, and Peter spent 15 years in his mother land. Peter attended Kum-Ho Elememtry School, Kwang-Hee Middle School, and Seoul High School while he was there.

Regardless of his interest in aircrafts, Peter attended Hong-Ik University as a Mechanical Engineering major for a year before he decided to study in the States. Upon his completion of his mandatory service in the Republic of Korea Army 39th Homeland Defense Infantry Division, Peter transferred to North Carolina State University to pursue a degree in Aerospace Engineering. He was actively involved in American Institute of Aeronautics and Astronautics and American Helicopter Society International as several officer positions during his undergraduate career at NC State. In senior year, he took part in design and construction of a long endurance UAS, Kestrel, as a structures specialist. He was responsible for stress analysis for the airframe, and fabrication of the components. Outside of school Peter has been active in Grace Community Church. He also enjoys cooking, photography, running, hiking, playing sports, and listening to music.

Peter decided to pursue his Master degree in Aerospace Engineering with passion in aircraft structures, composite materials, and experiments. He joined the Smart Composites Laboratory under supervision of Dr. Kara Peters to explore the field of non-destructive inspection in composite materials.

ACKNOWLEDGMENTS

I would like to take this opportunity to thank my advisor Dr. Kara Peters for her guidance, patience and support during this research. Her knowledge and enthusiasm for non-destructive inspection in composite material helped my understanding. I could not appreciate more about her great advises throughout the course of this research.

I would also like to thank my committee members including Dr. Kara Peters, Dr. Rudolph Seracino, and Dr. Fuh-Gwo Yuan for their willingness to review my work and provide helpful feedback. Furthermore, I would like to thank my fellow students in the Smart Composites Lab, Chun Park, Young Song, Kevin McCants-Brown, Sean Webb, Drew Hackney, Kyle Oman, and William Stewart for their help and support in many different ways. Particularly, I would like to thank Sachin Pawer for teaching me about the infrared thermography equipment and software. I also thank Wenbin Huang for assistance in servohydraulic fatigue testing system.

Finally, I would like to acknowledge my family and friends for their prayers and support in many different ways. This research would not have been possible without all these supports.

TABLE OF CONTENTS

LIST OF FIGURES

CHAPTER 1 INTRODUCTION

1.1. OVERVIEW

The goal of this study is to investigate the ability of pulsed phase IR thermography to detect and size defects in carbon fiber reinforced polymer (CFRP) adhesive bonded single lap-joints. Specifically, manufacturing and fatigue-induced defects are studied. The main goal is to develop a reliable and rapid inspection method without any required contact to the tested object surface. The experiments in this research focus on a small scale representation of aerospace structural lap joint during low frequency cyclic loading, similar to inflight structural fatigue loading. Due to manufacturing variabilities and their effect on the strength of the bonded lap joint region, the initial quality of the sample will also be tested. The high speed inspection technique developed in this study can save cost and time for inspections on larger vehicles.

Chapter 1 presents the overall goal of this study, and provides a literature review of related pulsed phase thermography imaging and non-destructive inspection studies on adhesive bonded joints. Chapter 2 describes the experimental instrumentation and procedures that were used for both artificial and fatigue-induced damage detection in adhesively bonded joints. The results and analysis of these experiments follows in Chapter 3 and Chapter 4. Finally, Chapter 5 presents conclusions of this research and proposes future work.

1.2. MOTIVATION AND BACKGROUND

Aerospace vehicle components can be expected to encounter aging problems such as fatigue cracking, stress corrosion cracking, corrosion, and wear. The importance of inspection and maintenance of aging aircraft was recognized around the late 1980s, after an Aloha Airlines 737 fuselage failed, due to a combination of disbonding and extensive fatigue cracking in a lap joint (Aviation week & Space Technology, 1989; Achenbach, 2000). Unlike traditional metallic air/spacecafts, where most of the structural aging is visible externally, the use of modern composite airframe materials presents both new challenges and new opportunities for inspection of aircraft structures. Fiber reinforced polymer (FRP) type composites comprise a major portion of these composite aircraft materials, due to their high strength to weight ratio.

Common FRP joining methods use adhesives to constraint multiple laminates at an overlapping area. Adhesive bonds offer substantial advantages over the traditional rivet in terms of the stress distribution across bonded area, the low part counts, and the high strength to weight ratio of loading joint region. Environmental conditions during fabrication, including surface preparation, have a great effect on the strength and quality of these bonded joint (Ashcroft *et al.*, 2000). Bonded joints can have two prime areas of defects during manufacturing, one is the adhesive layer and the other is the adherend-adhesive interface. In the adhesive layer, porosity or voids are often caused by air entrapment during the adhesive layup process, and cracks can be introduced due to incorrect mixing or thermal shrinkage

during curing process. At the adherend-adhesive interface, adherend surface contamination by grease or a loose oxide layer often leads to weak bonding. Disbonding can occur at the adherend-adhesive interface due to poor adherend surface preparation. The adhesive edge shape during sample production can affect the overall fatigue strength of an adhesively bonded joint by more than 25%. Following the nucleation phase in the center of the bondline, cracks propagate towards the outer edges, regardless of the bond geometry. Scanning electron microscope images, as shown in Figure 1.1, show that the majority of these cracks propagated at the adhesive-adherend interface (Figure 1.1 (a)). Exceptional cases of resin rich areas or fiber bundle result in vertically crack propagation through the laminae layers (Figure 1.1 (b)) (Quaresimin & Ricotta, 2006).

In order to prevent potentially catastrophic, premature failures due to poor manufacturing quality and/or service damage to the FRP structure, various non-destructive inspection (NDI) technologies are used after manufacturing and after regular amounts of flight cycles. Currently aerospace industries rely on ultrasonic, radiography, tap test, and infrared thermography to conduct NDI of composite materials. Ultrasonic imaging is one of the most popular NDI techniques because of its high resolution scanning. However, ultrasound imagines requires a liquid couplant, between the probe and the structure, which can penetrate the test object and reduce the contrast between damaged and undamaged area by reducing the acoustic impedance. Also, ultrasonic transducers are limited to scan 10-20 mm in a single scan. Radiography, which uses X-ray techniques, can also be used in the adhesive bonded joint FRP because of similarity in density between the adherends and

adhesive (Adams & Drinkwater, 1997; Adams and Cawley, 1988). On the other hand, radiography requires high operational costs and excessive time for set up.

Infrared thermography uses the temperature contrast in non-defective and defective areas to determine the damaged region. This method provides accurate and reliable NDI as compared to other techniques for imaging damage in composite materials, as presented by Roach in Figure 1.2 (Roach, 2009). It is rapid and also applicable to a broader region of area at a time, compared to other NDI methods. When the specimen (test object) cannot produce heat by itself, a heat source is required to provide thermal energy to the specimen, and an infrared camera applied to detect the infrared radiation reflected from or transmitted through the object. This is called active thermography. Pulsed thermography (PT) uses a thermal pulse to heat the specimen and measures the heating or cooling of the surface temperature. Differences in temperature profiles indicate damaged areas. Figure 1.3 shows theoretical measurements from PT during sample cooling. However, PT data contains noise due to environmental reflections, emissivity variations, non-uniform heating and surface geometry, and also requires prior knowledge of non-defective area location for comparison (Ibarra-Castanedo *et al.*, 2007; Madague and Marinetti, 1996). In lock-in thermography (LT), the structure is heated with a periodic thermal wave at a fixed frequency to investigate damage at a corresponding depth. The phase delay value is calculated the signal response in this technique. The phase information is much less sensitive to surface variations and uneven heating than the amplitude information collected from pulse thermography. Nevertheless, this technique requires multiple tests for each corresponding depth which is time consuming because the structure must cool before each test.

1.3. PULSED PHASE THERMOGRAPHY

Pulsed phase thermography (PPT), a recently developed technique in active thermography, combines the advantages of the two previous techniques: pulsed thermography and lock-in thermography. PPT uses a square pulse to heat the sample, which can then be decomposed into a multitude of individual sinusoidal waves using Fourier series with frequency ranging from 0 to ∞. The technique applies Fourier transforms to acquire the phase data of each pixel in the image in order to minimize the environmental reflections and non-uniform heating effect. In PPT, thermal data are acquired in the cooling transient regime, which can be post-processed as different frequencies from a single test. These thermal image sequence can be converted to frequency components $F(n)$ using the discrete Fourier transform for each pixel which can be written as (Brigham, 1988; Madague & Marinetti, 1996),

$$F(n) = \frac{1}{N}\sum_{t=0}^{N-1} f(t)\exp(-\frac{2i\pi nt}{N}) = R(n) + I(n)i \qquad (1.1)$$

where t is the image sequence index, n designates the frequency increment amongst N total frames, and $R(n)$ and $I(n)$ are the real and imaginary component of corresponding frequency. The phase value, ϕ, is computed for each transform component terms by,

$$\emptyset(n) = \tan^{-1}\left(\frac{I(n)}{R(n)}\right) \qquad (1.2)$$

The data acquisition time increment Δt limits the minimum frequency increment (Δf) that can be calculated from N total frames by $\Delta f = 1/N\Delta t$. The phase image presents less

sensitivity to surface coating, surface disturbances, and quick data acquisition for high thermal conductivity materials (Madague & Marinetti, 1996). In summary, pulsed phase thermography adopts the quick thermal data acquisition of pulsed thermography and obtains the low-noise phase images as in lock-in thermography using the discrete Fourier transform.

1.4. IMPROVEMENTS TO PULSED PHASE THERMOGRAPHY

Maldague et al. (2002) demonstrated extending the thermal pulse in time domain to narrow the spectrum in the resolution of frequency domain, improving the defect visibility. The same amount of total energy was provided to a steel sample separately; one with a double amplitude and normal pulse duration, and the other with normal amplitude and double pulse duration. The second experiment provided better damage visualization as shown in Figure 1.4. However, practically the long duration pulse cannot be extended too long as the resulting calculations are limited by the computational resources.

In other studies, additional post processing methods were emphasized in order to reduce the noise of PPT images for enhanced visibility. The baseline subtraction method, a commonly used technique in signal processing, was applied to PPT results on a disbonded composite patch joint, provided data easier to interpret. The size determination of this study relied on the operator's interpretation skills which can be confused with other thermal variations in occasion. The inspection results through PPT correlated well with traditional ultrasonic method, but with faster data image acquisition (Genest *et al*., 2009).

In order to calibrate thermography or other inspection methods, it is necessary to introduce simulated defects with controlled sizes. Polytetrafluoroethylene (PTFE) is commonly used to replicate debonding defects either in laminate or adherend-adhesive interfaces. For example, phase contrast data profiles from CFRP laminates, with identical size PTFE insertions in different layers, can be used for depth calibration of the PPT. Phase difference values varies dependent on the defect location, however, deeper defects also experience a reduction in contrast which makes their edges less sharp. Waught et al. (2011) conducted an experiment by fabricating a secondary bonding CFRP adhesively bonded joint with a PTFE film inserted in the adherend-adhesive interface. However, this study concluded that this defect was not visible due to submersion of the insert into the adhesive. Also during this process, uncertain phase variation was discovered in the adhesive layer along with the artificially added defect as shown in Figure 1.5. Automation effort for defect visualization was conducted by Lahiri et al. (2012). Flat bottomed holes were found using phase calculation image, and then a threshold value was applied to the entire image in order to visualize the defected area and non-defected area as binary images. These binary images showed relative size contrast corresponding to different size of the defects as expected. However, the study relied on trial and error method rather than a mathematical systematic way of finding the threshold for binary image.

IR-View, an open source MATLAB software (Figure 1.6), was developed at Laval University to reduce repetitive and time consuming tasks in previous command based IR NDI software (Klein et al., 2008). The graphical user interface also assists researchers with post processing of the images. Each frame of a two dimensional multi-frame data set can be

displayed in this program using the display control. The processing menu enables user to select FFT modes for phase and amplitude calculations. Also, this menu enables users to choose the region of interest (ROI), which focuses on a smaller area of the image. For mathematical calculations, the program requires certain user input values such as the 3-D thermal data matrix in the time domain and the data acquisition rate. The time window and total number of images, which are critical to the FFT calculation and results, are determined automatically based on these inputs.

1.5. OBJECTIVES

The primary goal of this research is to develop a rapid and reliable inspection method for adhesively bonded CFRP single lap joints under fatigue damage using pulsed phase thermography. This goal was divided into several smaller objectives as follows:

- To verify that pulsed thermography can detect artificial inserts at the adherend-adhesive interface in adhesively bonded lap joints.
- To derive a sizing algorithm for defects based on the artificial inserts. The algorithm, based on the known size of the artificial defect, should provide a method to distinguish the boundary between defective and non-defective areas.
- To qualitatively evaluate manufacturing defects and failures using pulsed phase thermography. The manufacturing defects should represent typical fabrication variations.

- To quantify the extent of fatigue damage using the algorithm in fatigued lap joint specimens and compare with experimentally measured failure surfaces to vary the algorithm’s capability to size damage.

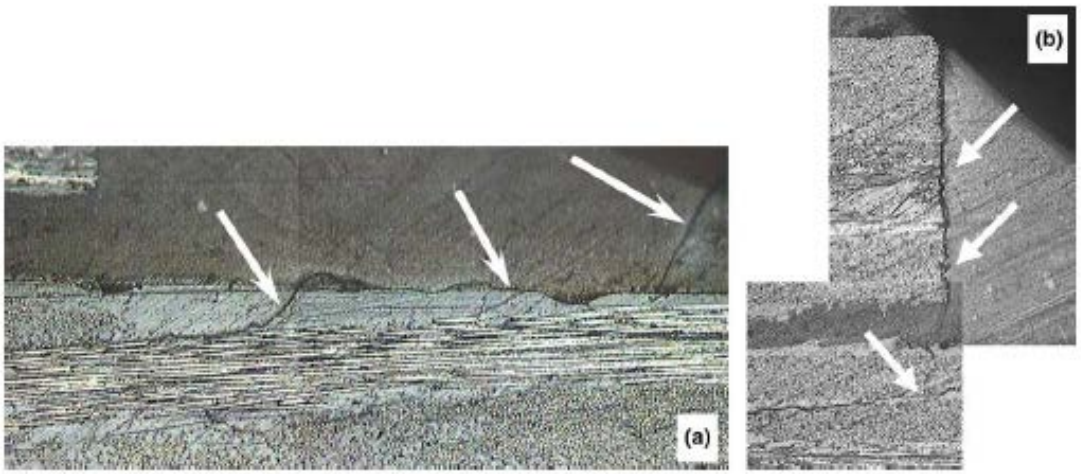

Figure 1.1 Crack nucleation site and path in spew fillet joints (a) propagation through adhesive-adherend interface; (b) propagation perpendicular to the crack front (Quaresimin & Ricotta, 2005).

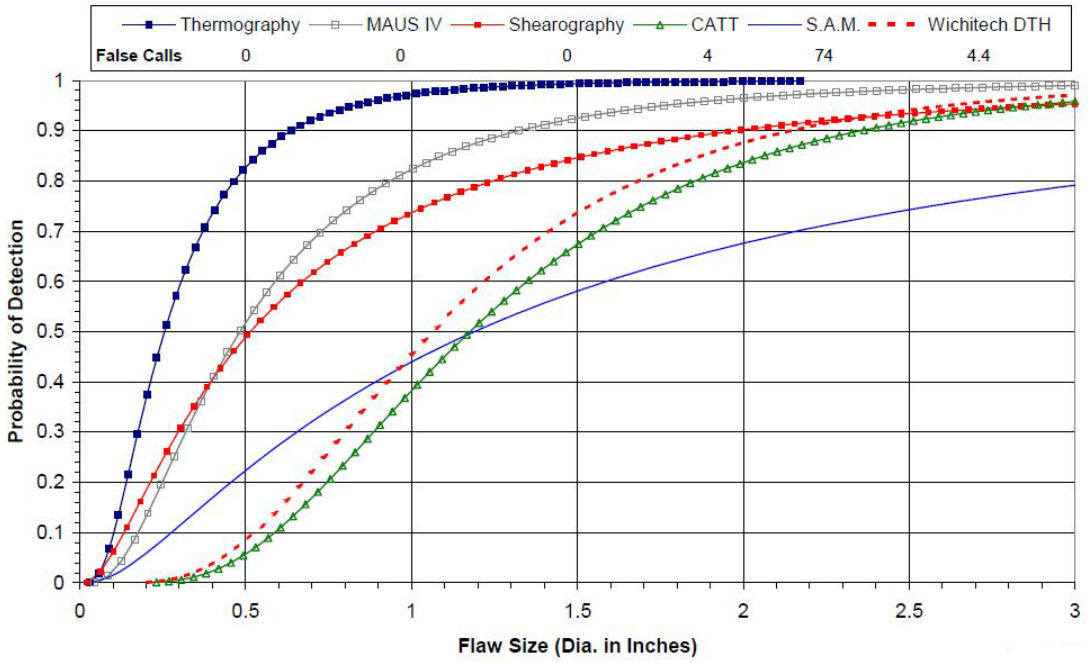

Figure 1.2 Comparison of advanced inspection techniques with best conventional NDI results on 9 ply carbon (Roach, 2009).

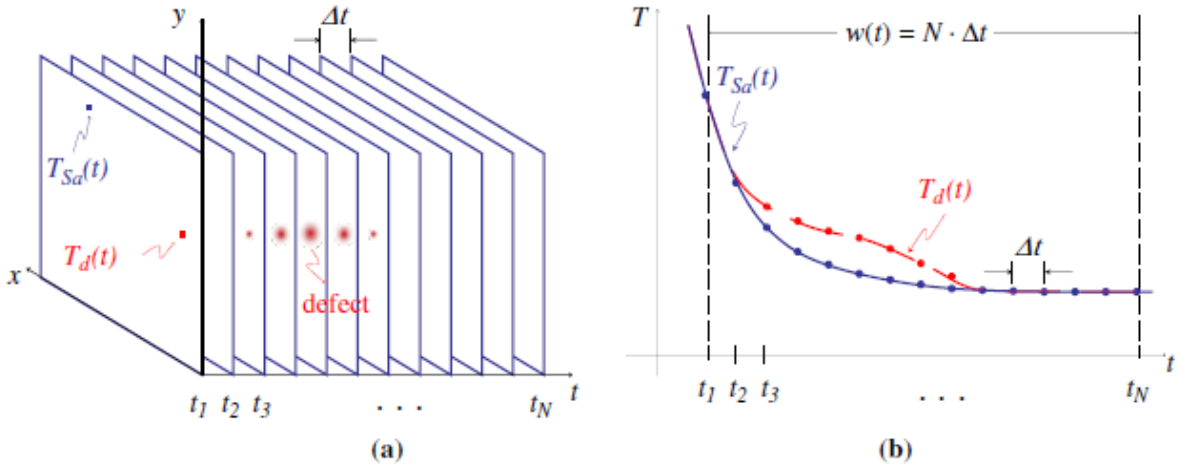

Figure 1.3 Thermal data: (a) 3D matrix; (b) thermal profile for two pixels in defective area (red) and non-defective area (blue) (Ibarra-Castanedo, 2007).

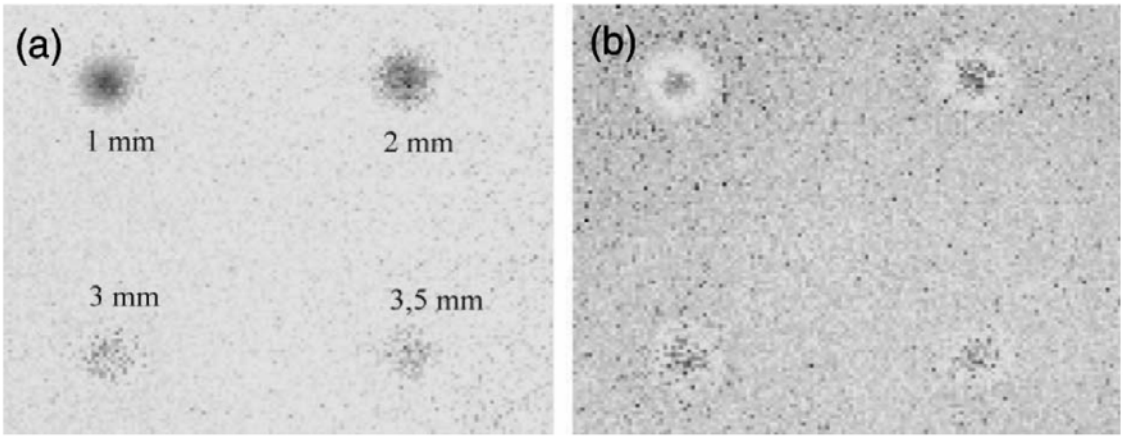

Figure 1.4 Phase images at 1.25 Hz in a steel specimen with four flat-bottom hole defects for two cases (a) one Δ duration pulse of amplitude 2A; (b) two Δ duration pulses each of amplitude A and separated by 3ms (Maldague *et al.*, 2002).

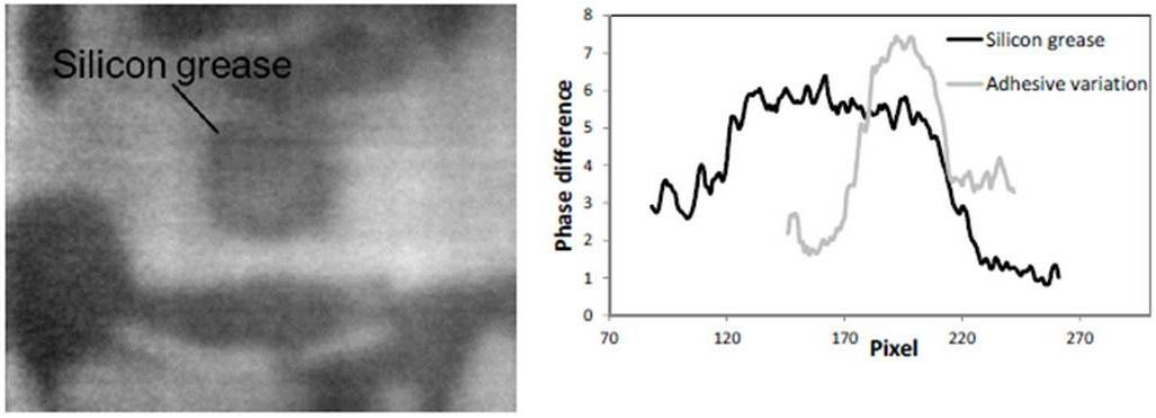

(a) (b)

Figure 1.5 (a) Phase difference image for secondary bonding adhesive joint with 20 mm circular silicon grease contamination; (b) comparison of phase difference caused by silicon contamination and an accidental adhesive variation (Waugh et al., 2011).

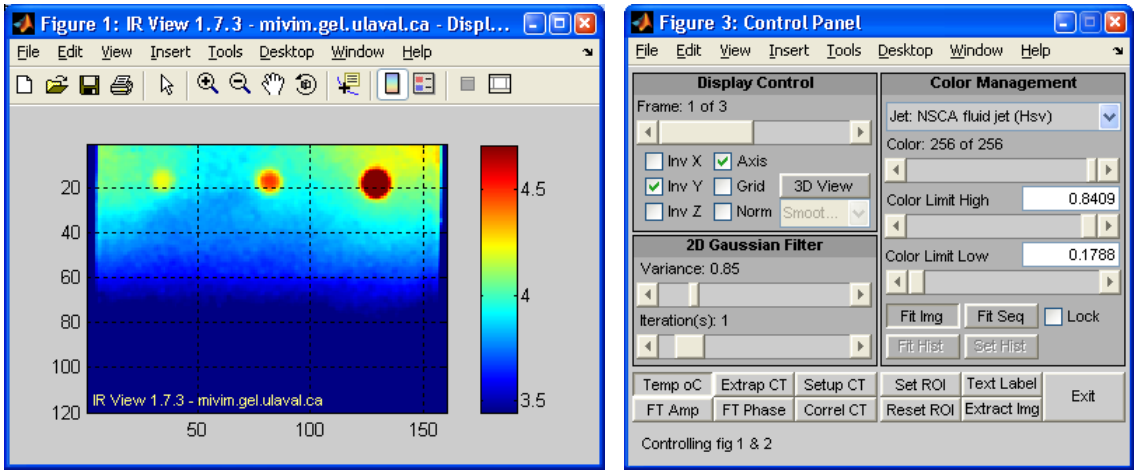

(a) **(b)**

Figure 1.6 IR-View: (a) display window; (b) control panel (Klein et al., 2008).

CHAPTER 2 EXPERIMENTAL METHODS

This chapter describes the sample fabrication methods for two different bonded CFRP composite specimens: calibration samples and validation (fatigue) samples. In addition, the experimental setup for pulsed phase thermography measurements will be described in detail. Finally, the fatigue loading sequences to be applied to the validation specimens are specified. The results from these experiments are presented in Chapters 3 and 4.

2.1. SAMPLE FABRICATION

All carbon fiber reinforced polymer laminated adherends used for this research were fabricated from 8 layers of pre-impregnated 2x2 twill woven carbon fiber (Advanced Composites LTM22/CF0300). Each lamina was sized 254 mm x 279.4 mm with the plies aligned in the 0°-90° directions. Prior to the laminate layup, a layer of Mylar vacuum bag, two layer of breather, and a single layer of peel ply were placed on an aluminum plate to prevent excessive resin on laminate surface. Each pre-preg layer was stacked on top of each other in the 0°-90° orientation, and the final assembly was covered by peel ply, breather, and finally Mylar as the bottom layer. The edge of the vacuum bag was sealed using sealing compound, and the air between the two Mylar layers was drawn out using a vacuum line. An additional aluminum plate was placed on the top and bottom of the Mylar sheet to evenly distribute the heat and pressure throughout the curing process. The sample was placed in a

hotpress, preheated to 50 °C, and pressurized to a constant pressure of 8.27 MPa. Following the curing cycle specified by the manufacturer, the hot-press temperature was increased every 15 minutes at 15 °C increments until it reached 80 °C. The laminate was then cured for an additional 3 hours at 80 °C and then allowed to cool for 12 hours at room temperature.

These carbon fiber reinforced polymer laminates were then used to fabricate two types of specimens for the following experiments: a calibration specimen and lap joint specimens. The goal of the calibration specimen was to determine the optimum pulse phase imaging properties and calibrate the defect size as a function of the calculated phase image using artificially introduced defects. For the calibration specimen, the cured laminate was cut into two 252 mm x 101.6 mm panels using a Felker TM-75 wet tile saw. The joining surfaces were prepared by sanding and cleaning each adherend with Al_2O_3 60 grit sanding paper and isopropyl alcohol. The artificial defects were created from various layers of 25.4 mm x 25.4 mm Polytetrafluoroethylene (PTFE or Teflon) tape and a single layer of polypropylene (PP) tape of the same dimensions. Four different simulated damages were applied between the two laminates as shown in Figure 2.1. Note that this image was captured prior to the application of the adhesive layer. Each layer of the PTFE tape had a thickness of 0.089 mm. All defects were placed 38.1 mm apart from each other.

Hysol EA 9394 adhesive was applied and distributed manually on the surface of the second laminate, using a steel blade parallel to the surface and perpendicular to the length of the plate. Hysol EA 9394 is a paste type adhesive commonly used in aerospace industries for composite bonding. Its main advantages are its low curing temperature, long pot life, room temperature storability, and high strength performance at both low and high temperatures.

Next, the second laminate was placed on top of the laminate shown in Figure 2.1 and the entire assembly placed between two sheets of Mylar to prevent the excess adhesive from curing on surrounding surfaces. The specimen was cured in the hotpress for an hour at 66℃. The total thickness of the adhesively bonded laminates was measured after curing to determine the level of variation due to the manual process, as will be discussed in the following chapter.

For the lap joint specimens, a single laminate was cut into twenty two 101.6 mm x 25.4 mm panels using the wet tile saw as shown in Figure 2.2. Each lap joint sample consisted of four laminate panels as adherends, based on the ASTM D3165 standard (ASTM, 2007). The full dimensions of the specimens are shown in Figure 2.3 Dimensions of composite lap joint specimens based on ASTM D3165. The joining surfaces were sanded and cleaned using Al_2O_3 60 grit sanding paper and isopropyl alcohol. Hysol EA 9394 was applied using a drywall scraper to evenly distribute the adhesive on the two treated surfaces per sample. A polyimide coated optical fiber containing a single FBG sensor was placed on top of adhesive layer of each lap joint during this process. These sensors were later used for independent measurements of the fatigue damage (Webb *et al.*, 2013), however were not visible in the PPT images due to their small size. These measurements will not be discussed in this thesis. After the placement of the optical fiber, the remaining laminate adherends were bonded to the exposed adhesive, as shown in Figure 2.3, to prevent bending of the specimen during tensile loading. The specimens were then placed between two Mylar sheets and placed in the hotpress, preheated to 66˚C, for an hour and allowed to cure at room temperature for 24 hours. Final lap joint samples are shown in Figure 2.4.

2.2. PULSED PHASE THERMOGRAPHY

The experimental setup used for pulsed phase thermography (PPT) is shown in Figure 2.5. Thermal images were acquired using a mid-wave infrared thermal camera, Cedip 560M, with a spectral response range of 3.6 to 4.9 μm, through an Indium Antimonide (InSb) detector. The size of recorded data points in a single frame was 640 x 512 pixels, at a maximum frame rate of 100 Hz. The thermal camera provides a noise equivalent temperature difference (NETD) less than 25 mK thermal sensitivity at 25℃. This IR camera was installed on an aluminum rail, perpendicular to the plane of the sample, so that the distance between the camera and object was adjustable. In the calibration experiment, the distance was chosen to capture all simulated defects in a single frame which was 1.16 m away from the sample surface. As shown in Figure 2.5, the sample was clamped parallel to the plane of the IR camera lens by two tension cables which were connected to vertical rails on each side of the sample. A function generator (Tektronics AFG3021B) provided a 5V square pulse signal for 7 seconds to the IR power module (IR Power control 330 US) The IR power module amplified the input signal to power the halogen lamps. Two Hedler halogen lamps were used as the heat source, each supplying 850W output power at the 5V input signal. These heat sources were positioned at a 30˚ angle and 0.5 m away from front surface of the specimen.

During the heating period, thermal images of the surface were captured from the thermal camera until 33.5 seconds after sample cooling using Altair software at a 60 Hz frame rate. The heating period data was removed in the software and then saved as proper file format for further processing in MATLAB. Software program Altair, provided by Cedip,

was designed optimal for thermal image data acquisition, which contains excessive information in post processing the surface temperature matrix (Cedip, n.d.). Past research using the same software required manual data extraction of each frames into separate files to eliminate unnecessary data in each file, which prolonged the data processing time. To reduce this conversion effort, a program was implemented in MATLAB, presented in Appendix C, to decrease the computational time by automatically eliminating unused portion of recorded data. The program also introduces flexibility in selecting sampling frequency at a lower range than the acquisition frequency. An open source MATLAB program, IR VIEW, was then used to calculate the phase images from the thermal data. Detailed post processing of the collected data will be described in the following chapters.

2.3. FATIGUE TESTING

For the lap joint specimens, fatigue loading blocks of 200 fatigue cycles were applied to create fatigue damage in the adhesively bonded joints. PPT images were obtained in between the 200 cycle loading blocks. For some specimens, the specimen was also loaded in tension and excited in vibration in between the fatigue loading blocks for the embedded sensor measurements (Webb *et al.*, 2013). In these cases, PPT images were obtained after the tension and vibration as well. The Instron Model 1331 servohydraulic fatigue testing system, with 50kN tensile strength capacity, shown in Figure 2.6, was used to apply the fully-reversed fatigue loading cycles. The amplitude of the fatigue load cycles was first determined by measuring the maximum force at quasi-static lap joint failure, in a displacement-

controlled tensile test at a rate of 0.5 mm/min. Using Wave Runner software, a peak-to-peak amplitude of low-frequency fatigue cycles at 3 Hz frequency in 200 cycles of increments was applied. If the sample did not fail after 1000 fatigue cycles, the cycle increments were increased over 1000 fatigue cycles at a time in between PPT imaging until failure. The experiments and data acquisition process described in this chapter are presented as a flow chart in Figure 2.7.

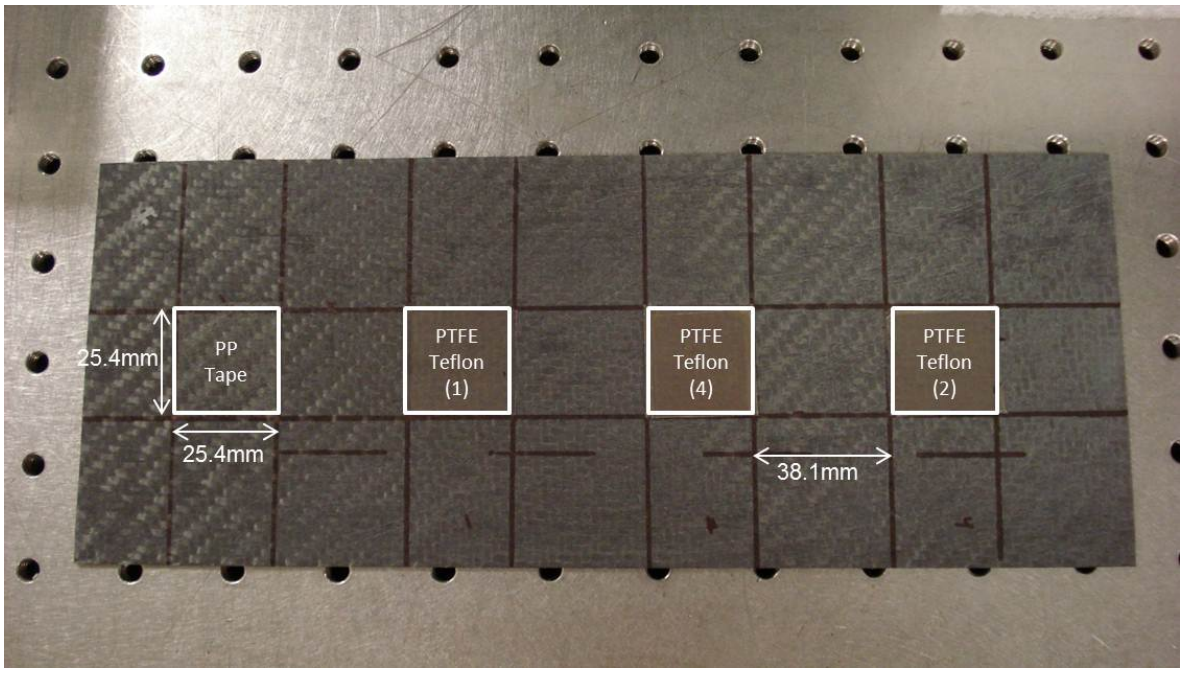

Figure 2.1 Location of simulated defects to be applied on joining surface of bonded joint. Number of PTFE tape layers is indicated in parentheses.

Figure 2.2 Resizing CFRP laminate for lap joint fabrication.

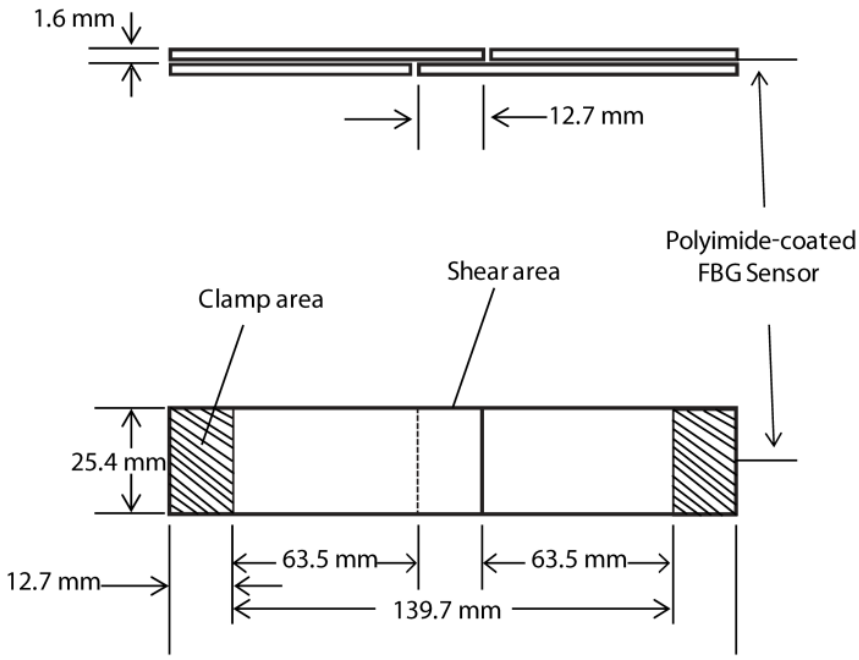

Figure 2.3 Dimensions of composite lap joint specimens based on ASTM D3165.

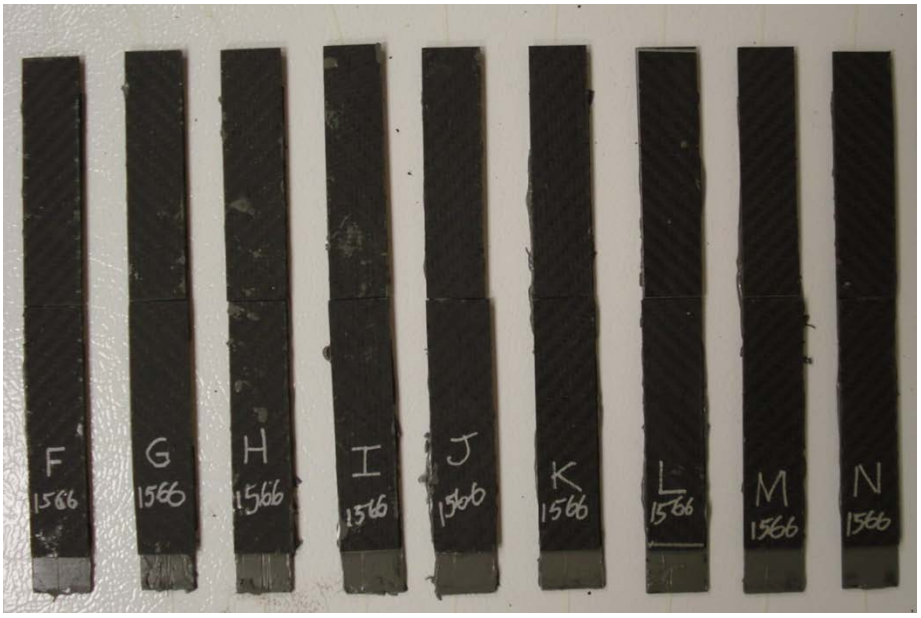

Figure 2.4 Lap joint specimens with FBG sensor after full curing.

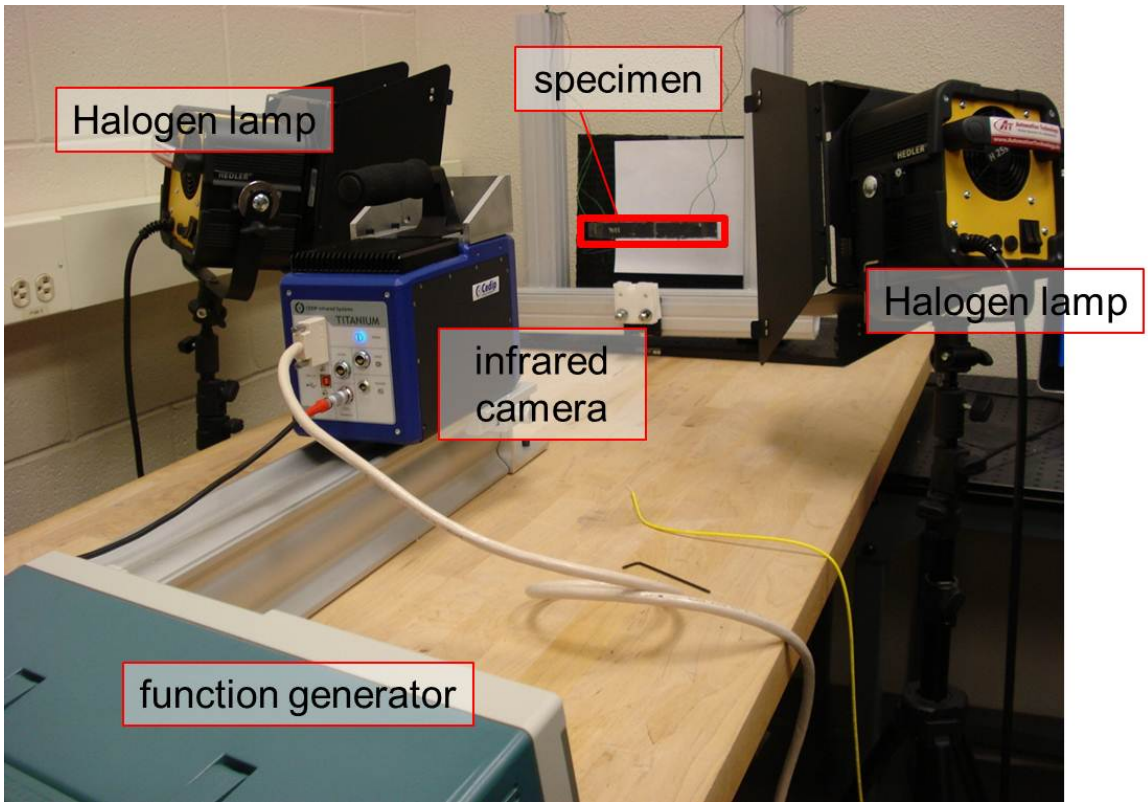

Figure 2.5 Pulsed phase thermography experimental setup.

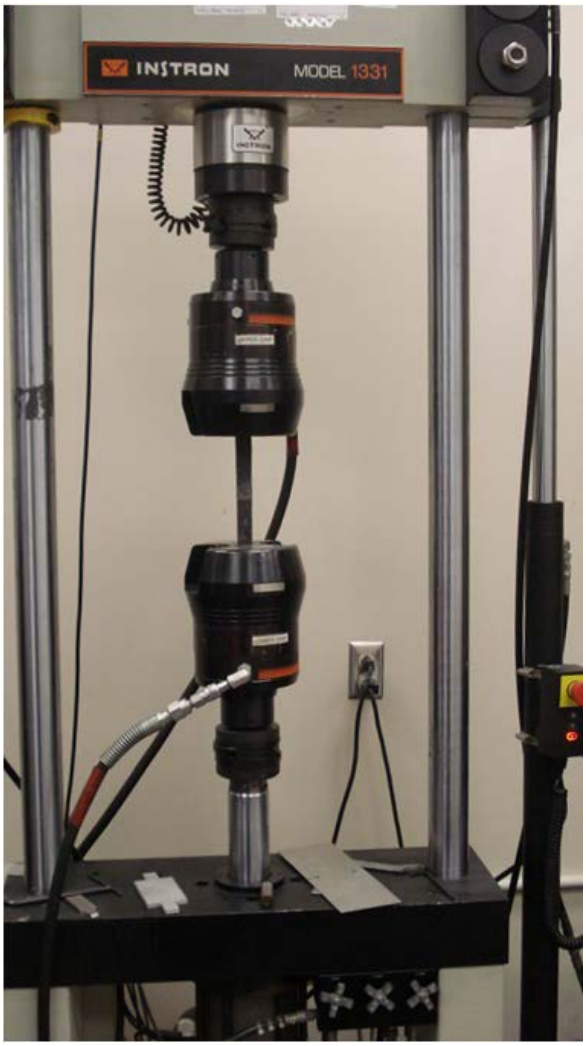

Figure 2.6 Lap joint sample mounted in Instron 1331 servohydraulic fatigue testing system.

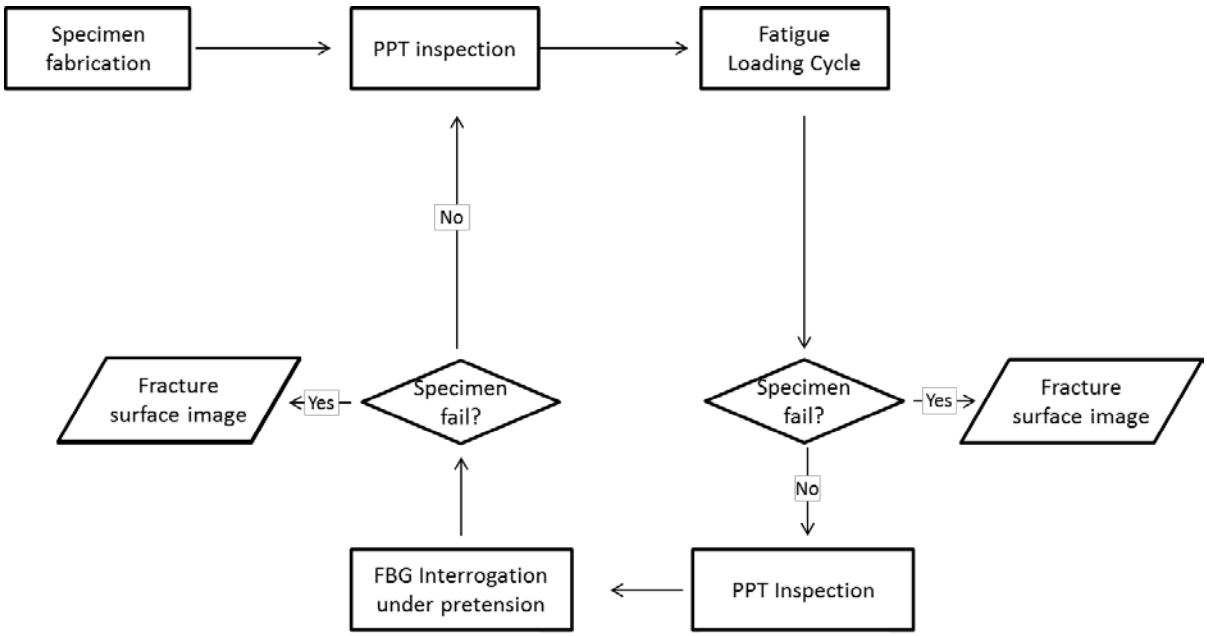

Figure 2.7 Flow chart of experimental procedures.

CHAPTER 3 CALIBRATION OF PULSED PHASE THERMOGRAPHY

A sample with artificial defects was fabricated to simulate manufacturing defects during the sample fabrication process, and artificial delaminations between the adherends and adhesive of the bonded lap joint. In addition to defect detection, this calibration sample was also manufactured to image damages at a known depth and geometry in order to set the PPT parameters for later imaging of the sample under fatigue damage. The artificial delaminations were created by inserting various layers of Polytetrafluoroethylene (PTFE) tapes and Polypropylene (PP) tape at different locations within the same joining surface. As compared to metallic materials, woven carbon fiber reinforced epoxy has a low thermal diffusivity value and also has a similar effusivity to PTFE tape which makes it difficult to detect these inserts in the unfiltered time domain temperature profile. However, pulsed phase thermography, which is based on the fast Fourier transform of the surface temperature measurement, is expected to improve the defect visualization for this sample. Finally, the known size of the simulated defects will be used to derive a criterion to determine the boundary of fatigue-induced damage which will be applied in later chapters.

3.1. THERMAL MEASUREMENTS

First, the 252mm x 101.6 mm bonded joint thickness was measured after full cure process using a micrometer, to inspect the manufacturing quality of the bonded sample. These measurements were taken 15 mm away from lengthwise edges, towards the defects. The result from this measurement is shown in Figure 3.1, where the origin of plot was at the edge near the polypropylene (PP) tape. From this graph, a thickness increase was observed along the length of the sample. As the adherend thickness did not vary significantly, this was primarily due to a thickness variation in the adhesive layer. However, the maximum percentage difference between the top and bottom thickness measurement was 3.71 %, indicating that the bond line thickness in the width wise direction is relatively uniform. A visible void on edge of the sample was also observed during this measurement around the 4 layer PTFE laminate edge location, as shown in Figure 3.2. This defect is likely to corrupt the phase angle data around this region due to the difference in thermal properties of the air and the composite.

After a square thermal pulse of 7 s was applied to the specimen, thermal images were recorded during the sample cooling period, acquired using the Altair software, some of which are shown in Figure 3.3. Significant non-uniform heating at the center of sample was observed from the surface temperature image immediately after the heat pulse as shown in Figure 3.3 (a). The diagonal rib of the twill weave appears at a negative 45˚ angle due to the twill formation between tows and picks in the material. The temperature difference between a single diagonal rib to a neighboring rib varied from 1.38 ˚C to 10.3 ˚C depending on the heated region. The image in Figure 3.3 (b) was acquired 33.5 s after the maximum

temperature of the specimen was achieved. The temperature difference between the minimum point and maximum point was less the 2 ˚C across the specimen surface. Notice the presence of the weave pattern in the cooling period image, which has a high probability of appearing in phase angle images.

The maximum temperature difference between the sound area and the known defective area after the 7 s heat pulse was approximately 2˚C above the 4 layer PTFE insert. The surface temperature change between pixels in the non-defective and defective regions is plotted in Figure 3.4. The rate of change in temperature for the defective area is lower than that of the non-defective area due to its lower thermal effusivity value. Effusivity represents the thermal energy exchange ability with its surroundings, in this case of the PTFE tape compared to the surrounding adhesive. However, due to this low contrast between the non-defective and defective regions, it is challenging to visually detect the defects in the surface thermal images (i.e. using pulsed thermography).

3.2. PHASE CALCULATIONS AND DEFECT SIZING

Phase contrast images of the calibration sample were calculated from the thermal data, an example of which is shown in Figure 3.5, using IRVIEW. Phase contrast value ($\Delta\phi$) is an expression commonly used in the pulsed phase thermography, which expresses the difference between phase value of each pixel and overall minimum phase value. The locations of defects marked in this figure were added later to indicate the inserts regions. This phase data was acquired using every one frame out of 10 frames of the 60 Hz surface thermal

image during a duration of 10 seconds, which corresponds to a 6 Hz sampling rate with a total of 60 frames. The truncation window for the following phase analyses was determined based on the time from the maximum overall temperature until the defective and non-defective regions were at the same temperature, seen in Figure 3.4, which in this calibration sample was approximately10 seconds. The initial temperature measurement up to 1 s, was neglected in the truncation process to eliminate the effect of heat saturation. A significant decrease in non-uniform heating effects was observed in the pulsed phased thermography, consistent with previous research (Ibarra-Castanedo, 2005). The values of the calculated phase contrast values varied from 0 rads to 0.234 rads at a minimum 0.1Hz frequency. Notice the high phase delay region in the upper right corner resembles the visible edge void from Figure 3.2, which was formed during manufacturing due to poor adhesive distribution between the two CFRP laminates.

The maximum phase angle value in the single layer PP tape region was 0.926 rads while that of the single layer PTFE tape was 0.910 rads, due to the difference in thermal conductivity between the two materials. For further analysis, the phase contrast data ($\Delta\phi$) across all four defects was obtained as shown in Figure 3.6. This figure highlights several challenges in defining a damage region from thermography images. The weave pattern clearly superimposes a noise on the data. In addition, the different defects each have different maximum phase contrast values. Finally, there are not sharp boundaries between the defective and non-defective regions.

The phase angle values from the maximum point of the PP tape region decrease gradually whereas phase angle values in the other defects rapidly decreases from the

boundary of the defect to its surrounding area. The difference in the PP measurements indicates possible contamination in the PP tape area. Also, observing the double layer PTFE Teflon tape region we see high phase angle values caused by the edge effect of the void region mentioned earlier. These contamination effects and void regions make it challenging to accurately predict the boundary of artificial damages for these two artificial defects. Therefore, the phase contrast distribution in the uncontaminated defect regions, the single and quadruple layer PTFE, were consider the most reliable data and will be used for the calculation of a damage boundary criterion.

The final goal of the calibration specimen was to derive a criterion to define the boundaries of damage regions, based on the known boundaries of the artificial inserts. In the following chapter, this criterion will be tested on the fatigue-induced damage in the lap joint specimens. The phase contrast distribution across all defects shows a change in the values inside and outside of each defect boundaries. However, these changes are relative to the maximum phase contrast for that particular defect. Therefore we will apply a percentage of the maximum phase contrast for a particular defect as a boundary estimate.

We first needed an image scale to convert the number of pixels into a physical length. The width of the adherend was measured using a ruler and was found to be 106.2 mm long. The same distance, marked in Figure 3.7 by the red line was measured in MATLAB to convert this length into equivalent pixels. The point-to-point measurement of Figure 3.7 resulted in 310 pixels which provided the image scale of 2.92 pixels per mm. Therefore, the artificial defect size of 25.4 mm x 25.4 mm was mapped to a 74 pixel x 74 pixel square as shown in Figure 3.8.

Next the ratio between the average boundary value and the maximum phase contrast value in each of the two artificial defects and was calculated to be 74.6 % and 70.5 % for the single and 4 layers PTFE respectively. The average boundary value was calculated by averaging the phase values in the pixels defined by the red lines in Figure 3.8 (a) and (b). Since these two values were reasonably close, it was assumed that a universal threshold value for percent change could be applied to any defect. Using the average value of those two (72.6 %) as the threshold limit between non-defective and defective regions, the two center defects are again plotted in Figure 3.9 where a binary system is used to mark pixels where black pixels indicate the values above this critical threshold as compared to the maximum value for each of the defects. Each point was compared to the maximum value of the spatially closest maximum pixel. This criterion requires the user to first define a neighborhood for each defect and then compare the points in that neighborhood.

As presented in Figure 3.9, the modified threshold filtering technique boundary well represented the actual defect boundary (plotted in red). It is notable that this method is a conservative calculation for the thicker defect on the right hand side as compared to the left hand side. Also, diagonal stripe patterns inside of the mapped boundary once again indicate the twill weave diagonal ribs which illustrate the significant difference in phase contrast especially on the top right corner of the defect of the thicker insert.

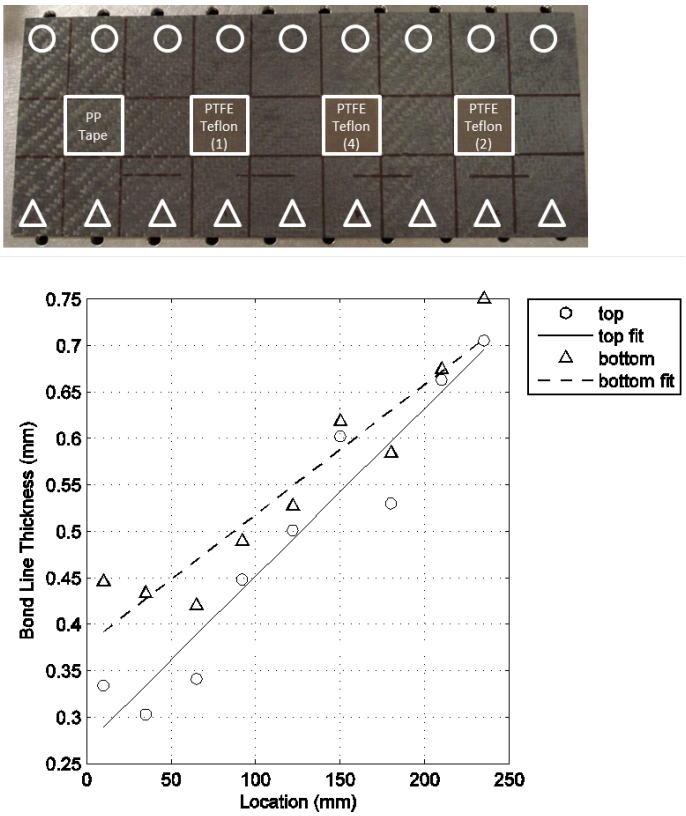

Figure 3.1 Sample thickness measurement location and variation along length.

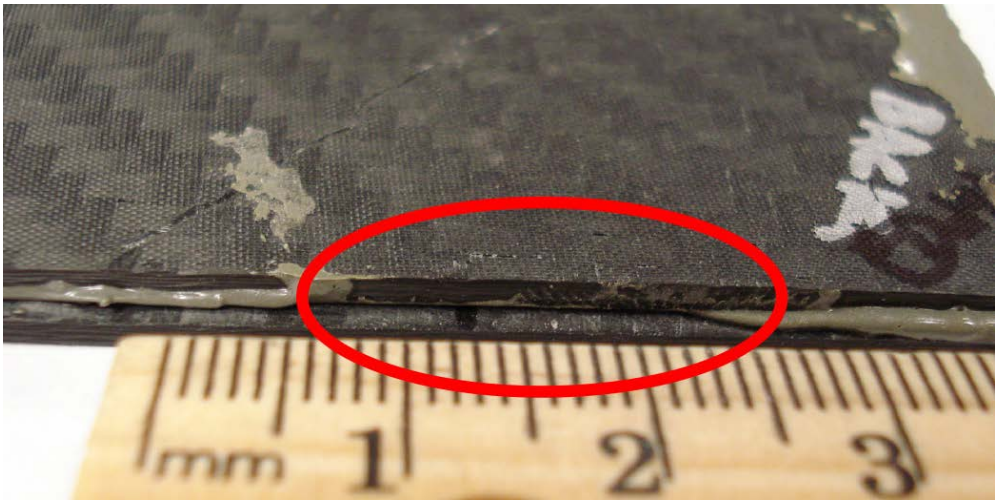

Figure 3.2 Visible edge voids between adherends.

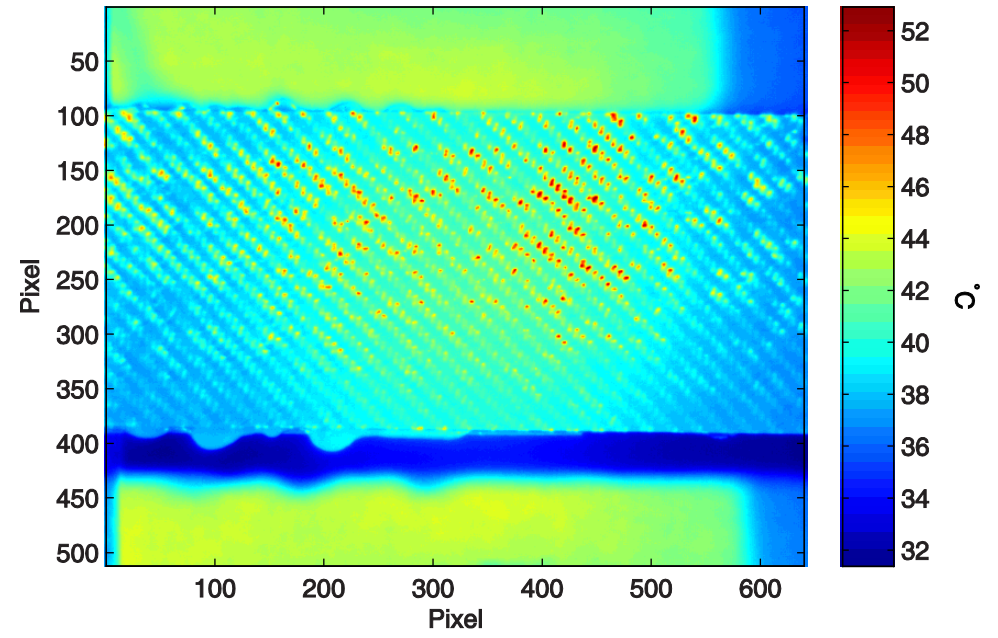

(a)

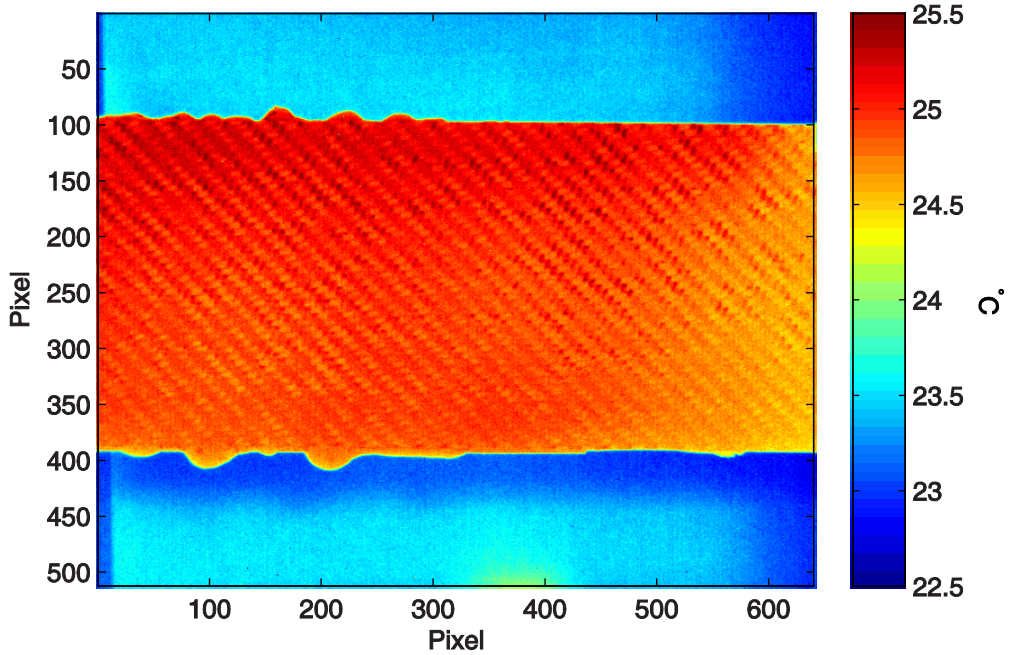

(b)

Figure 3.3 Thermal images: (a) maximum temperature immediately after heating, (b) after 26 seconds of cooling.

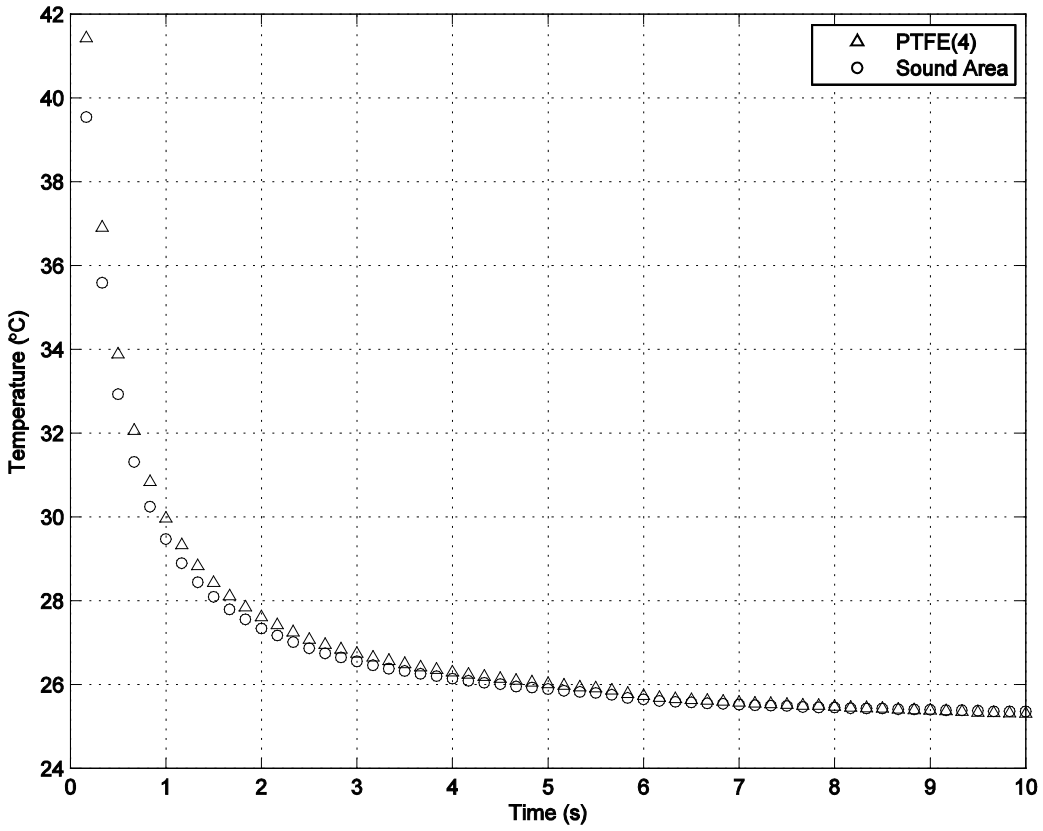

Figure 3.4 Surface temperature change between single pixels in non-defective and defective areas.

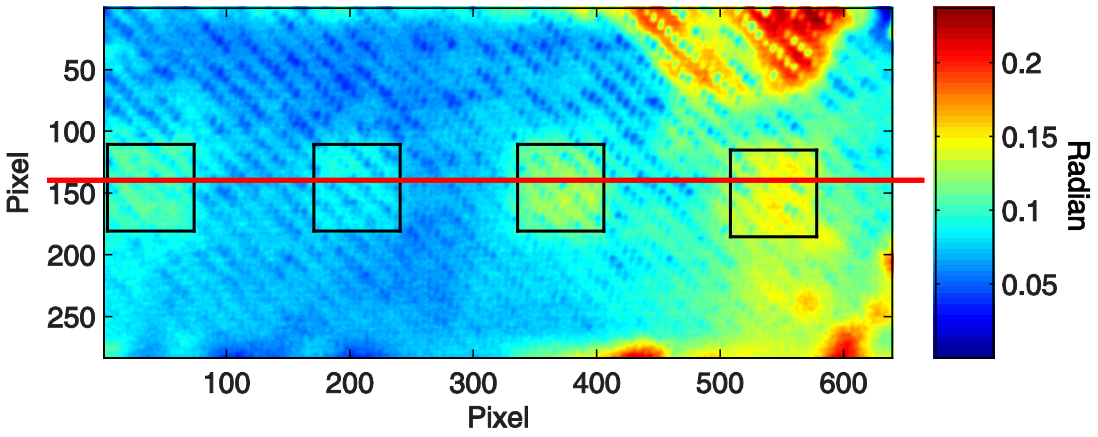

Figure 3.5 Phase image of specimen with artificial defects (f_s =0.16 s, N = 600, $w(t)$ = 10 s, f = 0.1 Hz). Defects from left to right are: PP tape, 1 layer PTFE tape, 4 layer PTFE tape, 2 layer PTFE tape.

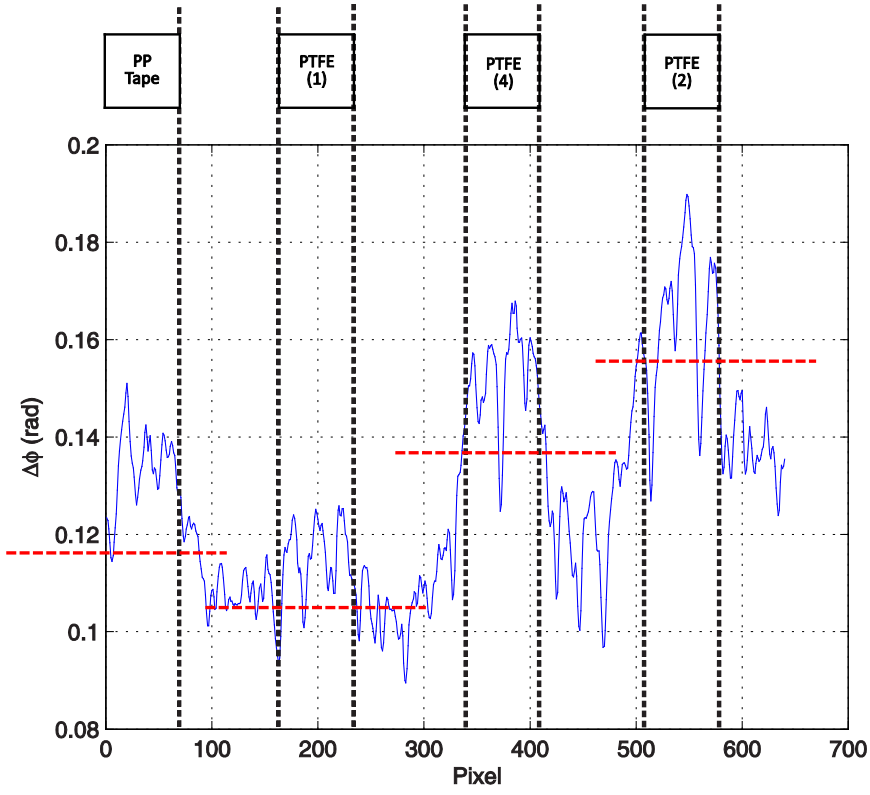

Figure 3.6 Phase contrast distribution across all defects. Location of phase contrast data is shown by red line in Figure 3.5

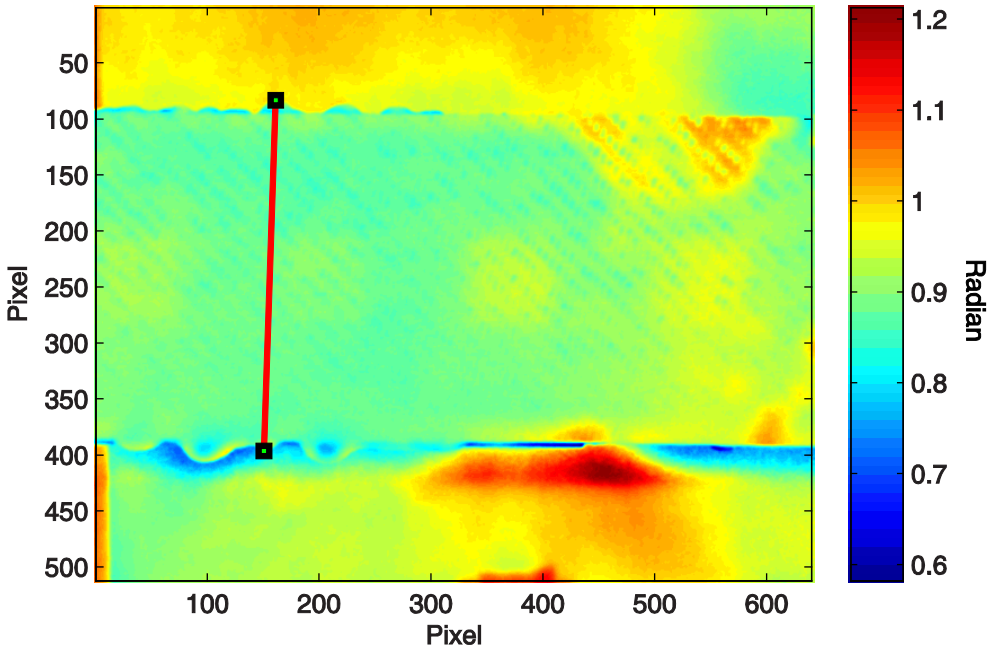

Figure 3.7 Location of size reference measurement.

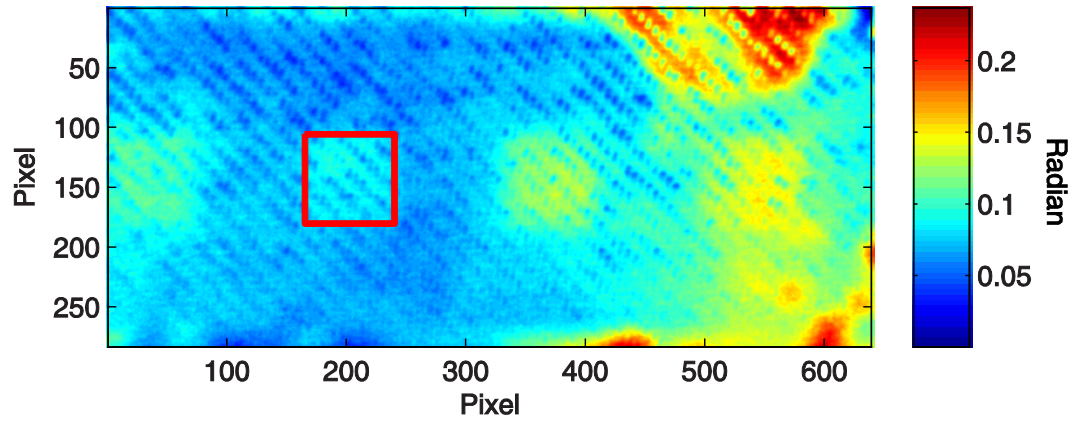

(a)

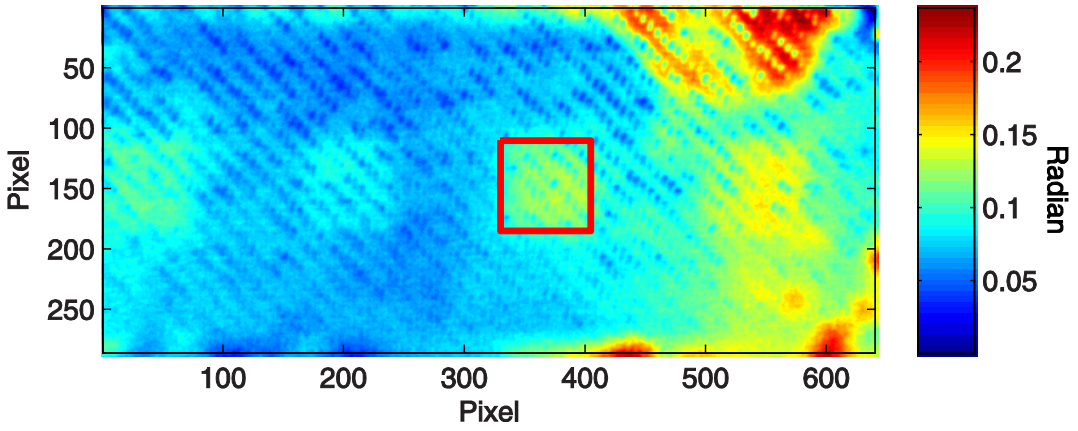

(b)

Figure 3.8 Actual defect size mapped on MATLAB phase contrast image (a) single layer PTFE location, (b) 4 layers PTFE location.

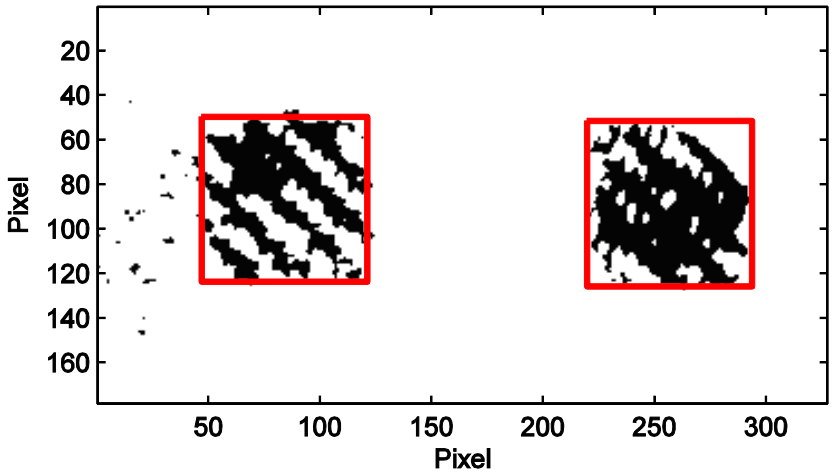

Figure 3.9 Damage locations calculations for two center defects of the calibration sample applying 72.6% of maximum defect phase contrast criterion. Actual regions of the artificial defects are plotted in red.

CHAPTER 4 DEFECT DETECTION OF PULSED PHASE THERMOGRAPHY

Low frequency fatigue loading cycles, which represents in-flight conditions that bonded joint members can possibly experience during flights, were applied to 12 samples, fabricated after ASTM standard D3165 with fiber Bragg grating (FBG) sensors. The fatigued samples were inspected in-between loading cycles using PPT to define the damage growth in the bonded joint region until failure. The goal of the tests was to maintain consistent measurement regardless of position and angle deviation from measurement to measurement, which represents a more realistic after-flight inspection condition, where the inspecting part location remains constant and position varies depending on the inspector. The damage size at the joining region will be determined after certain amount of cyclic loadings as well as the damage location, based on the methodologies from the defect calibration presented in the previous chapter.

4.1. THERMAL MEASUREMENTS

Temperature measurements of a single lap joint specimen at three different locations were acquired to determine the truncation window. The three areas were selected by visual inspection method around the edge and the surface temperature image. During this process, a visible void on the edge and an additional possible defect within the joining region were

detected. As shown in Figure 4.1, the defected area of interest at the bonded joint location has the lowest temperature decay rate in comparison to the other two areas. This region did not achieve equilibrium temperature of the non-defected area after full measurement time span of 33.5 seconds, unlike the air void region. However, the total measurement time remained consistent during the following data acquisition process due to limitation of data storage space in the equipment. After eliminating the early recorded thermogram, the first thermogram in use for PPT was acquired 1 second after the saturation. The truncation time (32.5 seconds) sets the frequency resolution (Δf) in PPT to 0.031 Hz. In addition, the increased truncation window corresponds to narrower frequency bandwidth with less rippling effects. Change in the parameters required recalibration for accurate measurement of fatigue damage. Repeating the calibration process from the previous chapter, the critical value was found to be relative to the 66.15 % of the nearest maximum phase contrast value, using the parameters described in this section.

4.2. LAP SHEAR TESTING

Initially, 12 samples were fabricated for static loading and cyclic loading tests to determine the appropriate load amplitude for later fatigue testing. Five samples among these 12 were utilized for static loading to measure the maximum shear load of the lap joint in order to prevent premature failure during the cyclic loading tests. Presented in Figure 4.2 is the displacement controlled test data at a displacement rate of 0.50 mm/minute until failure in the bonded region. The plots represent data points recorded every 5 seconds at a 10 Hz

sampling rate. The maximum load value of all samples broadly varied from 2.71 kN to 4.49 kN depending on the manufacturing quality, where the average maximum tensile force of the five samples was 3.74 kN. The peak-to-peak amplitude of cyclic loading was set to be approximately 10 % of this average maximum load, 0.445 kN.

4.3. FATIGUE LOADING

Twelve additional samples were fabricated under ASTM D3165 standard to investigate damages in the adherend-adhesive region under fatigue loading. Various qualities in the joining area due to non-uniform surface treatment and an adhesive layer with manufacturing flaws can be expected from the previous calibration sample quality. The life cycle of the corresponding specimen can be expected to withstand different amounts of fatigue cycles. In other words, the number of fatigue cycles at failure will be different from sample to sample.

The load input was originally planned to control 0.1* P_{max} peak-to-peak amplitude at a 3Hz cyclic loading with a data collection rate of 0.02 kHz for fatigue load cycle. Among the 12 samples, 3 samples failed due to mechanical load cell error prior to the fatigue cycle. Three samples were selected for further investigation of the bonded joint region from the 9 remaining samples. The Instron device was recalibrated after every set of cyclic loading since the sample position on the load cell and material stiffness of the bonded joint changed. In order to compile the full cyclic loading and displacement data, the maximum and minimum amplitude of each cycle was calculated. The graphs in Appendix A show the cyclic fatigue

loading and corresponding displacement plot of the bonded joint sample that were acquired from the 9 sample runs conducted. As predicted above, diverse behavior from one sample to another in fatigue life cycle and displacement was detected. A MATLAB code used to perform calculations of normalized peak-to-peak load and displacement is found in Appendix C.

The first sample was under pre-tension conditions after the 200 cycles and the 600 cycles. The left hand side of Figure 4.3 (a) shows discrepancy in the load-fatigue cycle recording between the maximum and minimum envelope of the load which shows change after pre-tension conditions. However, as it can be observed during 400-600 cycles and 800-1200 cycles, the load envelope curve recovers to its previous trend after no additional application of pre-tension. These variations were considered acceptable because we are studying the ability of PPT to image realistic, fatigue-induced damage and not the fatigue life of the specimens. Comparing the two plots in Figure 4.3 (a), one can see that as the number of fatigue cycles increases, the maximum and minimum load decreases. Unlike this trend, the envelope of the displacement at the bonded joint region indicates increase in displacement which shows a stiffness decrease in the material. Similar behavior was detected in Sample 2, where the pre-tension condition was introduced after 200 cycles and 400 cycles. This specimen failed during the pre-tension process after 600 cycles. A noticeable change occurred in both load envelope and displacement after the first pre-tension condition, as seen in Figure 4.3 (b). This also indicates change in the lap joint region's material properties. Sample 3, without any pre-tension condition in between cycles, indicated relatively small discrepancy compared to the other samples as shown in Figure 4.3 (c) . The two measured

components remained consistent throughout the entire life cycle of this sample. The extended life span of the specimen represents higher manufacturing quality.

4.4. PHASE CALCULATION AND FATIGUE DAMAGE DETECTION

The manufacturing quality in each adhesive bond joint sample was observed using PPT as shown in Figure 4.4. Phase angle images confirm quality variations shown in fatigue load and displacement data which explains the reasoning behind different fatigue life cycles from sample to sample. Notice form the phase calculation images (Figure 4.4 (a) - (c), (f) - (h)), the marker writing and laminate gap shows significant contrast compared to the other parts of the sample. The joint region, marked in red boundary, was located on the left or right side of the vertical low phase line value depending on the specimen orientation when attached to the tension cables. These boundaries were used as a rough estimation to plot the location. However, the orientation of the specimen remained consistent within the same specimen.

The following analysis is focused on the 3 samples that were analyzed in fatigue loading data (Sample 1 – Sample 3). The PPT images for the other 6 specimens are presented in Appendix B for reference. Figure 4.5 represents phase images of Sample 1 after manufacturing, 200 fatigue cycles, and pre-tension conditions in between 200 and 600 fatigue cycles. Notice that phase values after every set of cycles or pre-tension conditions did not contain a uniform scale that applies to every sample, due to specimen position variation on the IR camera platform. Phase angle values in the region of interest ranged approximately

0.2 rads for every sample even at Figure 4.5 (b) where phase value of the entire sample varied approximately at 0.8 rads. For these reasons, the phase contrast was applied to compare the damage in the bonded joint area. The phase contrast is defined as the phase difference between a pixel and the minimum pixel value on the specimen in a given phase image. The minimum phase value corresponding to a non-defected area cannot be selected automatically due to the disturbance of writing on the surface of the laminate and the laminate gap around the bonded joint region. These same issues would be seen in a real structural application due to paint or dirt on the surface. A multi-point user input method was selected to resolve this issue with a high fidelity. An average of 5 pixel by 5 pixel area around each point was calculated and compared to the other points to find the absolute minimum phase value. In general, 3 different points were typically used. This value was then used to subtract the amount from raw phase angle data, which results in the phase contrast value. Also, each image shows that the size of specimens within images was approximately 100 pixels to 120 pixels depending on the distance between the clamped location and the IR camera. Using length of the distinctive laminate gap (25.4 mm) as a reference width, a 12.7 mm x 25.4 mm overlap area to the left of the gap line was extracted for further investigation. Figure 4.6 presents 2 different cases of runs conducted separately by selecting 3 points from Sample 1each time as estimated minimum points. The two positions of the initial selection of the lap region gap were slightly misaligned with each another. However, the phase contrast range seen in both cases was near identical which proves the high accuracy in this method.

Based on the principle and theories stated above, the following steps were conducted as below to identify the prospected damage area after each fatigue cycle.

1. The direction of bonded area relative to the laminate gap was determined prior to the other user inputs.
2. Three points in the very last fatigue cycle phase image were selected, and then the length of the reference line was measured at the bonded joint gap.
3. The area of the bonded joint was calculated based on the length of the reference line selected in the previous step. Then, using the minimum value in the selected point areas, the phase contrast values were calculated in the bonded joint region.
4. Next, the maximum point was found within this area and multiplied by the threshold factor value found from the calibration sample (66.15%).
5. Steps 2 to 4 were repeated for all the collected phase images, throughout the cyclic loading and pre-tension conditions. Then, the threshold filter was applied to generate binary images of the adherend-adhesive joint location.

The full MATLAB code listing for these 5 steps can be found in Appendix C. The threshold filtering of Sample 1 at the bonded joint region indicates a defect on the bottom left had side of the sample from the initial stage shown in Figure 4.7 (a). Due to an error in original phase values at certain measurements, distortion of underestimate phase contrast data was found relative to the absolute maximum phase value. Hence, the filtered data was also corrupted as shown in Figure 4.7(b), (c), and (g). This potentially was caused during the thermal image data collection process because of the image processing speed and data storage speed. Other data in this series of binary figures shows a hint of damage after the

initial manufacturing flaw detection. The image of the actual fracture surface represents a combination of typical adhesive failure and light-fiber-tear failure as seen in Figure 4.8. Between the two exposed adherend-adhesive layers, the bonded region remained on the left hand side of the laminate gap. Hence, the right hand side part of the specimen was represented by the binary image of PPT. Comparing this image to the last threshold filter result in Figure 4.7 (i), the threshold filter result resembles the fracture line and debonded area accurately.

The second sample data neglects the writing on the surface to eliminate possible errors during post processing. Figure 4.9 shows PPT image resulting from the fatigue cycles and pre-tension condition mentioned in the previous section. A void region detected after the curing cycle is present on the left side of the laminate gap, and becomes more significant after the first 200 cycles (Figure 4.9 (b)). The bonded joint region, mapped in red on the right hand side of the vertical low phase line, shows significant increase in contrast within the joint location between the initial stage (Figure 4.9 (a)) and 600 cycles (Figure 4.9 (f)). This indicates change of properties in the area. Closer investigation of this area is shown by phase contrast values as in Figure 4.10 using the information of multi-point user input. From Figure 4.10 (a), possible defect region is visible across top 10 – 40 pixel location. This potential defect grows towards the edge and the sample center, as cyclic fatigue and pre-tension is introduced. Applying the critical value, acquired from phase contrast plot after final cycle, the damage progression is seen in Figure 4.11. As predicted from the phase contrast images, damage was detected at the top region of the bonded joint in Figure 4.11 (a). The damage growth can be traced by comparing this to the after 400 cycle image at Figure 4.11 (d) where

it becomes more distinctive. Figure 4.12 shows the actual fracture surface which failed during pre-tension condition after 600 cycles, Sample 2 failed by a combination of adhesive failure and light-fiber-tear failure, similar to Sample 1. Throughout the threshold filter data, the potential starting location of adhesive failure was predictable. The approximated size of the adhesive failure region was better predicted in Figure 4.11 (e) rather than the data after the last cyclic loading in this specimen.

Finally in Sample 3, the first PPT in Figure 4.13 (a) shows uniform distribution of low phase angle region which is an indication of wide non-defected area across the entire sample. There are certain locations in the supporting laminate near the laminate gap with potential defects; this is negligible for the purpose of this study however. The twill weave pattern in this particular sample appears more significantly compared to the previous samples phase angle images. The sample did not show any significant change in phase contrast images after the first set of fatigue cycles as shown in Figure 4.14. A distinctive diagonal pattern caused by the weave is observed at the 3000 cycle phase contrast image, as seen in Figure 4.14 (h), due to the placement of specimen at the IR thermography platform. The filtered data presented in Figure 4.15 proves all discussions previously mentioned about the quality of this particular sample quality. With exception of the 200 cycle and 3000 cycle threshold filter data due to the sample position, no significant defects or damages were detected. Comparing the final fracture surface in Figure 4.16 to the 50000 cycle binary image presented in Figure 4.15 (j), which was 2652 cycles prior to failure, indicates combination fiber-tear failure and light-fiber-tear failure due to brittle fracture.

From all cases, generally when the sound area (lower phase values) is located at the center of the joint regions, the specimen withstands longer fatigue cycles. Also, threshold filter using information of the after damage data is an accurate measurement of indicating manufacturing defects and predicting adhesive failure areas in early stages of fatigue cycles.

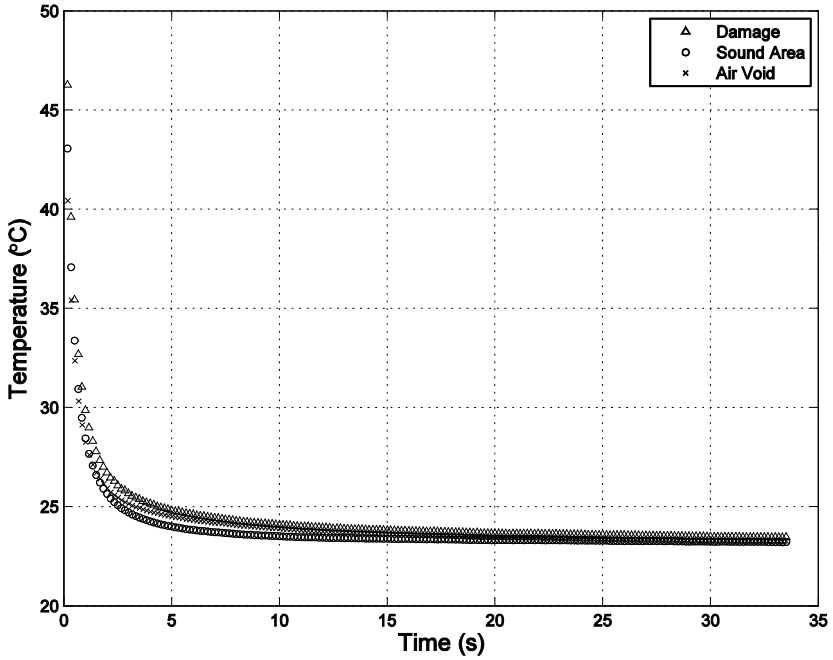

Figure 4.1 Surface temperature change between non-defective and defective area, as compared to air void.

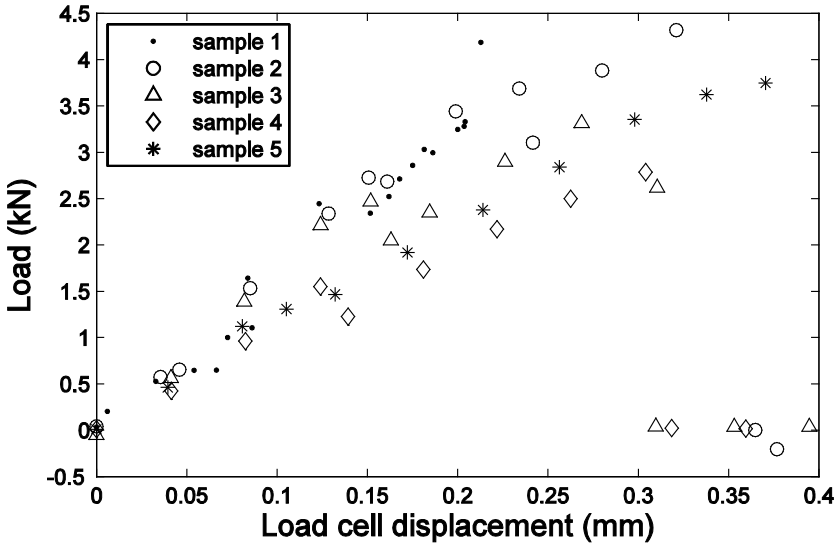

Figure 4.2 Load-displacement curve of lap shear test samples measured at 0.5 mm/min loading rate.

Figure 4.3 Fatigue cycle envelopes (thick line) and mean values (dotted line) controller load input and corresponding displacement of the bonded joint, where gaps between cycles indicate discrete loading due to IR thermography and pre-tension condition measurement; (a) Sample 1, (b) Sample 2, (c) Sample 3.

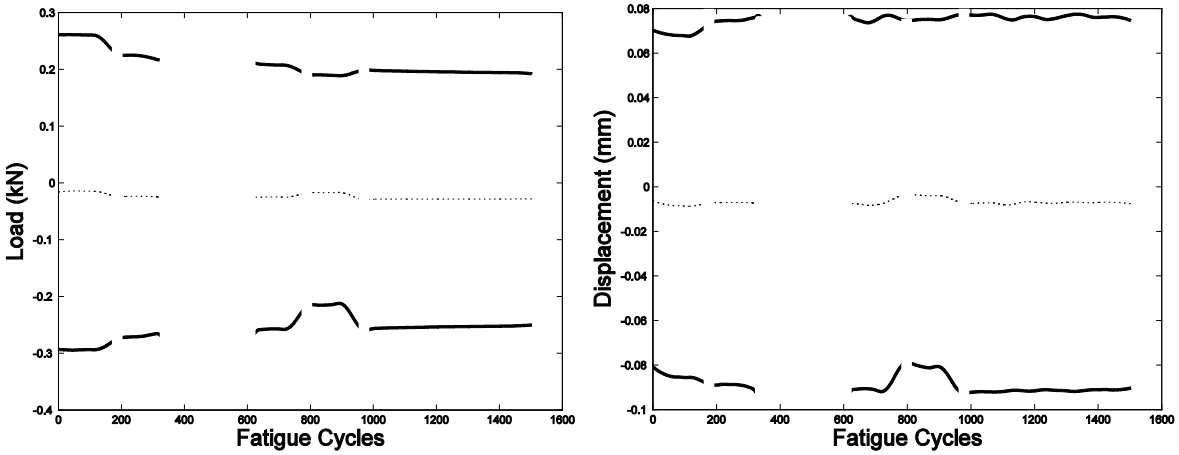
Load (kN)
Fatigue Cycles
Displacement (mm)
Fatigue Cycles

(a)

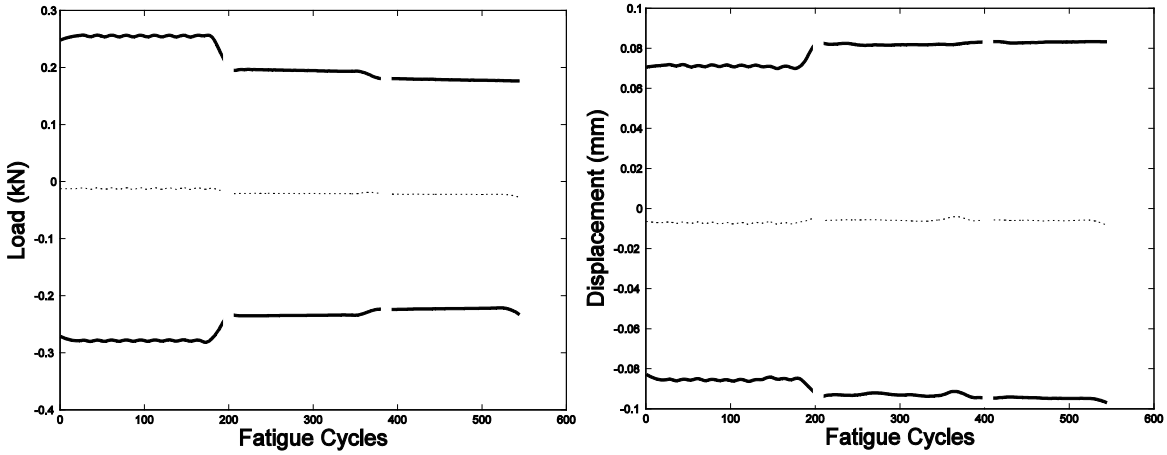
Load (kN)
Fatigue Cycles
Displacement (mm)
Fatigue Cycles

(b)

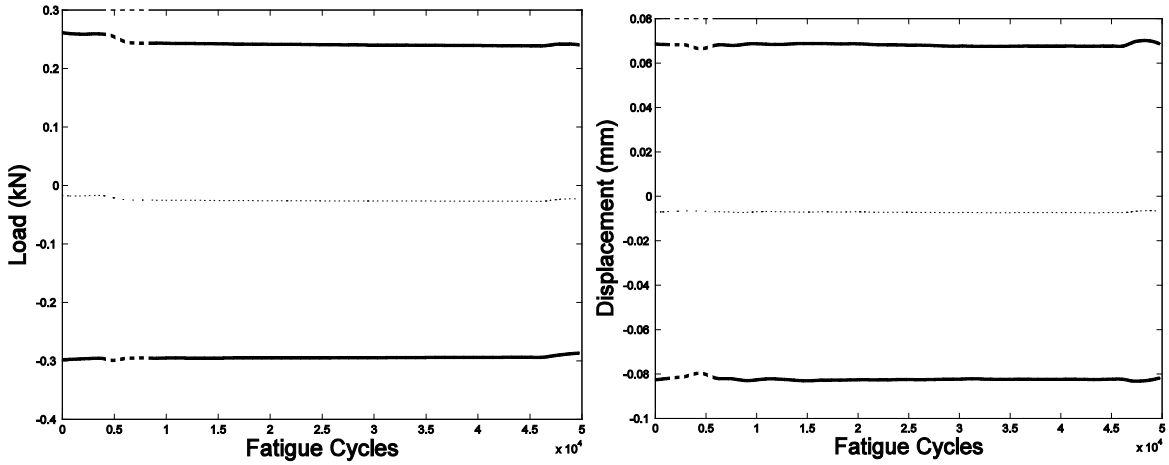
Load (kN)
Fatigue Cycles
x 10^4
Displacement (mm)
Fatigue Cycles
x 10^4

(c)

Figure 4.4 Initial PPT phase image of 12 samples after fabrication and adhesive bonded joint region (red) at f_s = 6 Hz, N = 196, f = 0.1 Hz; (a) – (l) Samples 1 – 12. Location of joint overlap region is shown by red box.

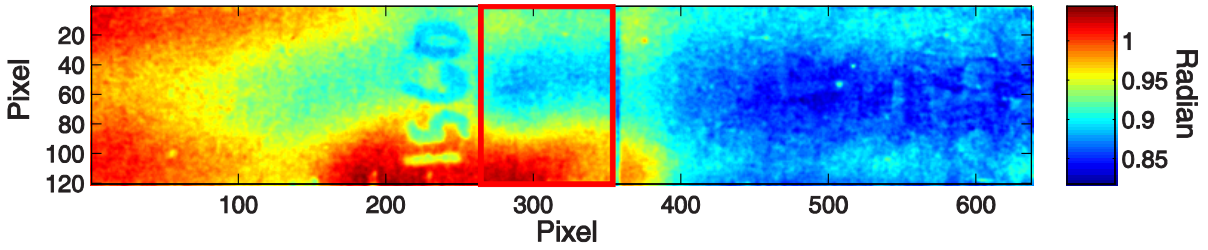
Pixel
20
40
60
80
100
120
100
200
300
400
500
600
Pixel
1
0.95
0.9
0.85
Radian

(a)

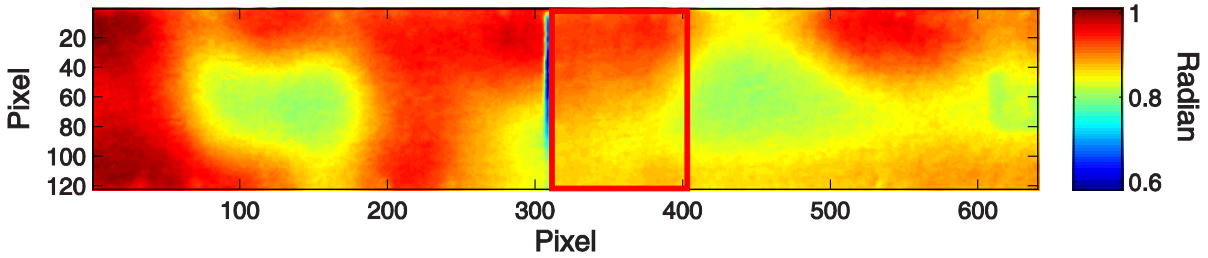
Pixel
20
40
60
80
100
120
100
200
300
400
500
600
Pixel
1
0.8
0.6
Radian

(b)

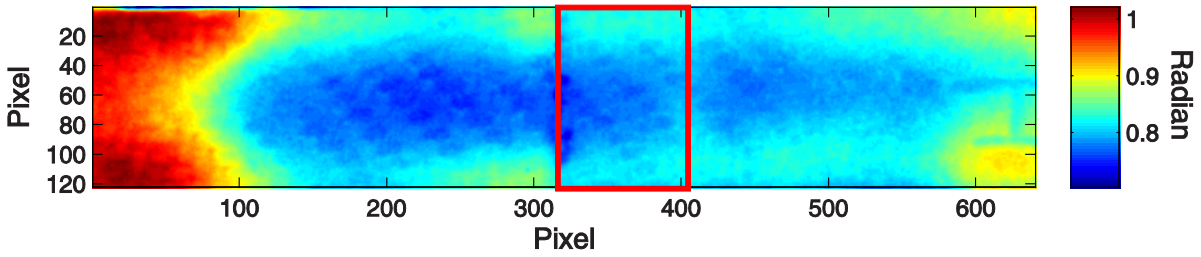
Pixel
20
40
60
80
100
120
100
200
300
400
500
600
Pixel
1
0.9
0.8
Radian

(c)

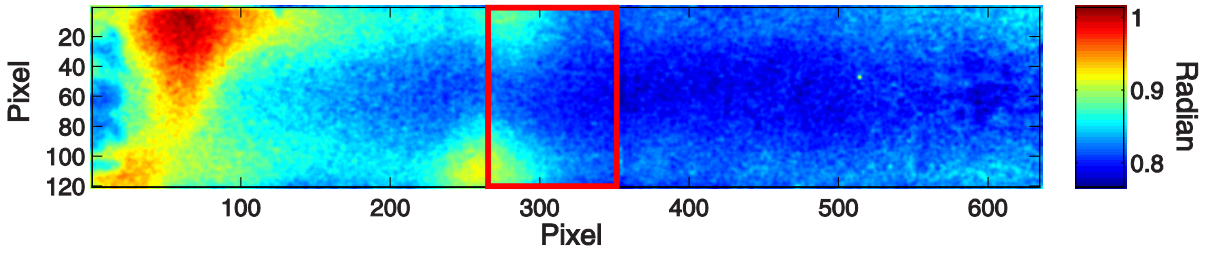
Pixel
20
40
60
80
100
120
100
200
300
400
500
600
Pixel
1
0.9
0.8
Radian

(d)

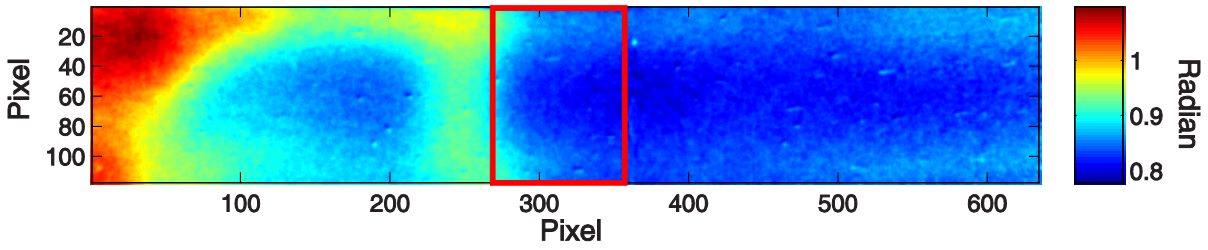
Pixel
20
40
60
80
100
100
200
300
400
500
600
Pixel
1
0.9
0.8
Radian

(e)

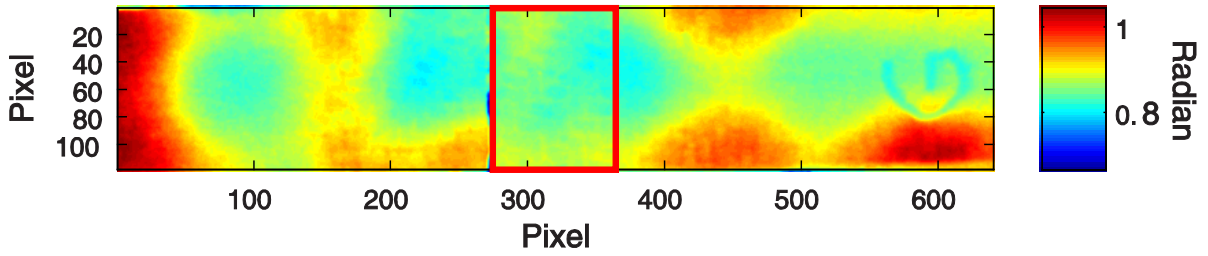
Pixel
20
40
60
80
100
100
200
300
400
500
600
Pixel
1
0.8
Radian

(f)

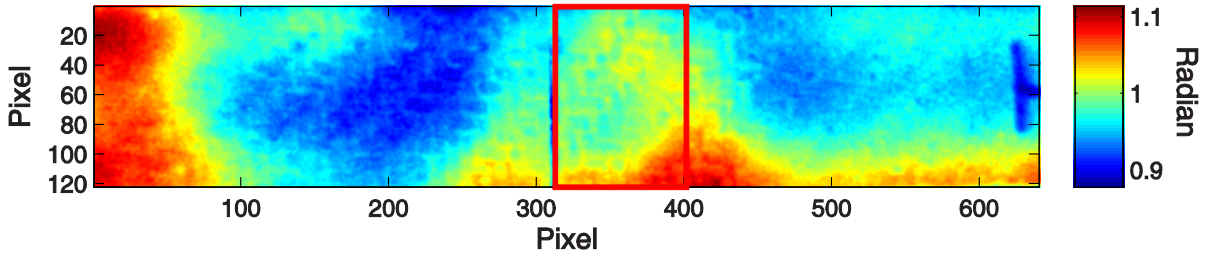
Pixel
20
40
60
80
100
120
100
200
300
400
500
600
Pixel
1.1
1
0.9
Radian

(g)

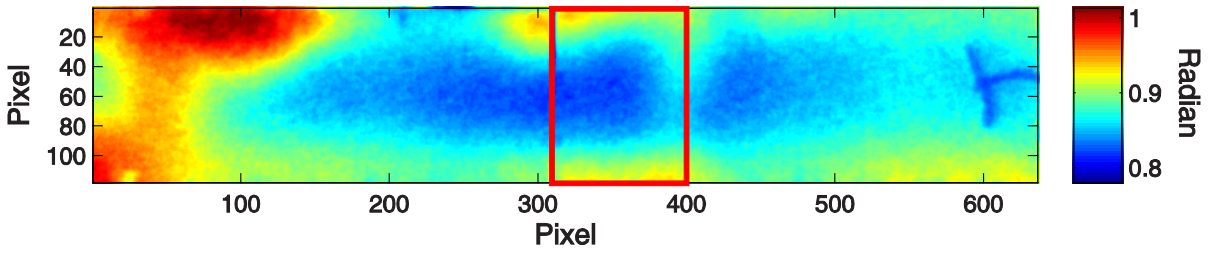
Pixel
20
40
60
80
100
100
200
300
400
500
600
Pixel
1
0.9
0.8
Radian

(h)

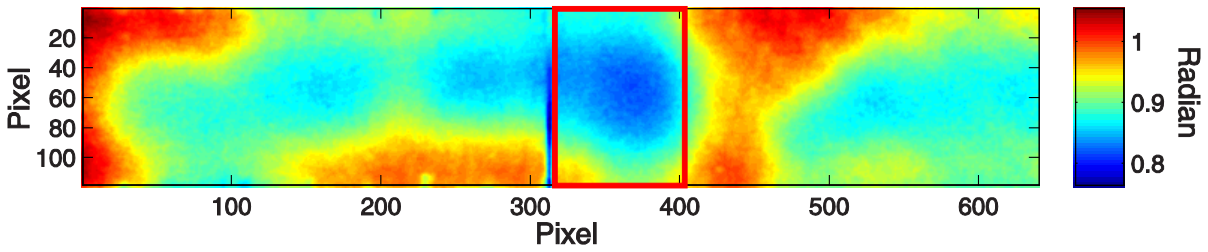
Pixel
20
40
60
80
100
100
200
300
400
500
600
Pixel
Radian
1
0.9
0.8

(i)

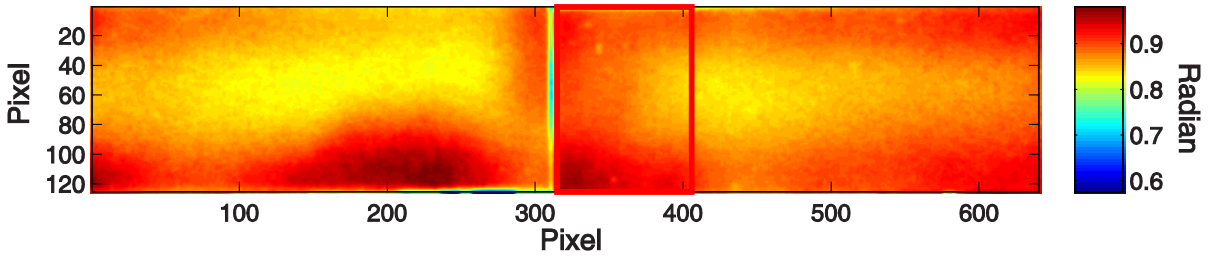
Pixel
20
40
60
80
100
120
100
200
300
400
500
600
Pixel
Radian
0.9
0.8
0.7
0.6

(j)

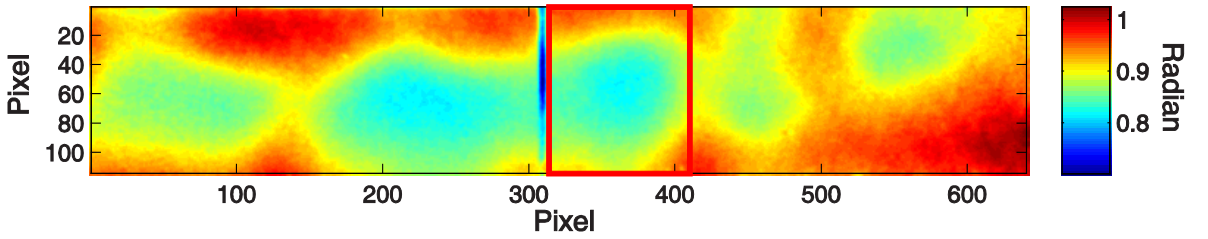
Pixel
20
40
60
80
100
100
200
300
400
500
600
Pixel
Radian
1
0.9
0.8

(k)

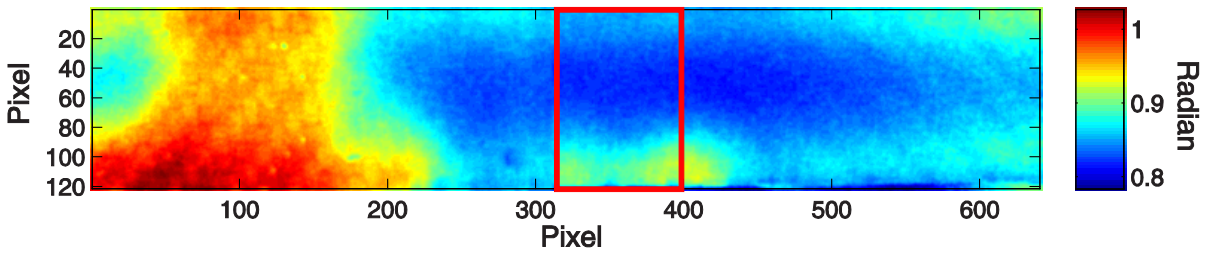
Pixel
20
40
60
80
100
120
100
200
300
400
500
600
Pixel
Radian
1
0.9
0.8

(l)

Figure 4.5 Phase image of Sample 1 (f_s = 6 Hz, N = 196, f = 0.1 Hz); (a) initial stage, (b) 200 cycles, (c) 200 cycles and pre-tension, (d) 400 cycles, (e) 600 cycles (f) 600 cycles and pre-tension, (g) 800 cycles, (h) 1000 cycles, (i) 1600 cycles. Location of joint overlap region is shown by red box in (a).

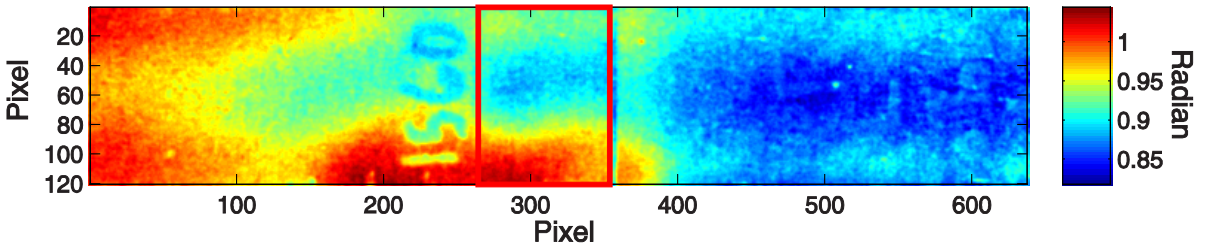
Pixel
20
40
60
80
100
120
100
200
300
400
500
600
Pixel
Radian
1
0.95
0.9
0.85

(a)

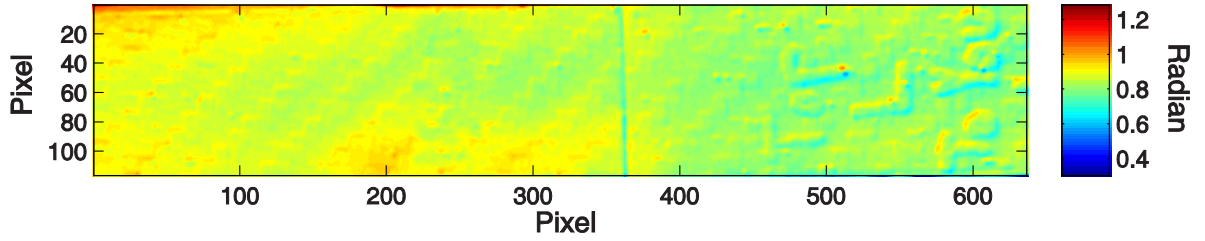
Pixel
20
40
60
80
100
100
200
300
400
500
600
Pixel
Radian
1.2
1
0.8
0.6
0.4

(b)

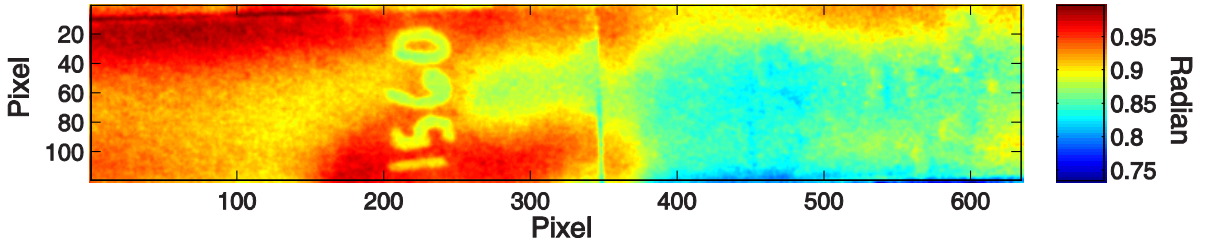
Pixel
20
40
60
80
100
100
200
300
400
500
600
Pixel
Radian
0.95
0.9
0.85
0.8
0.75

(c)

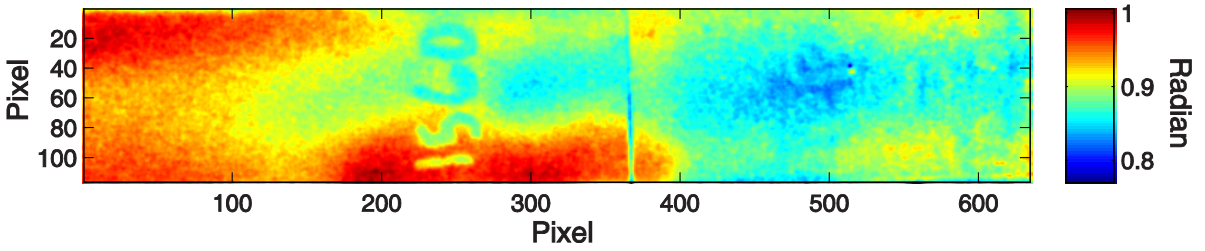
Pixel
20
40
60
80
100
100
200
300
400
500
600
Pixel
Radian
1
0.9
0.8

(d)

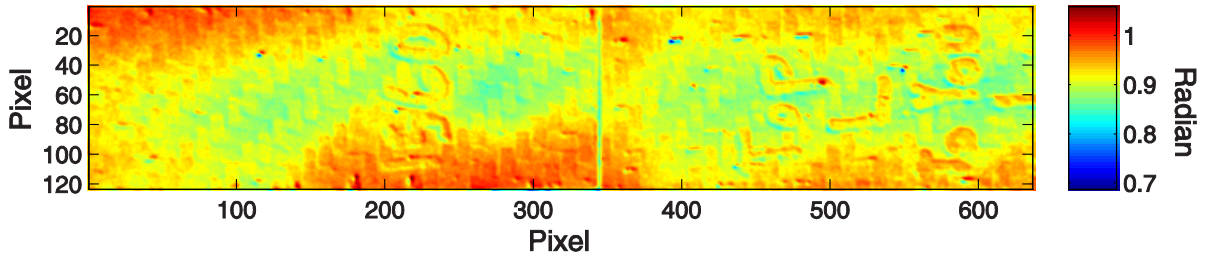
Pixel
20
40
60
80
100
120
100
200
300
400
500
600
Pixel
1
0.9
0.8
0.7
Radian

(e)

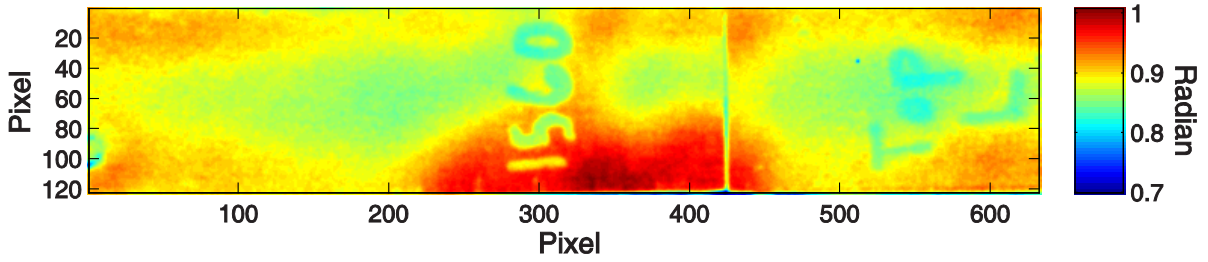
Pixel
20
40
60
80
100
120
100
200
300
400
500
600
Pixel
1
0.9
0.8
0.7
Radian

(f)

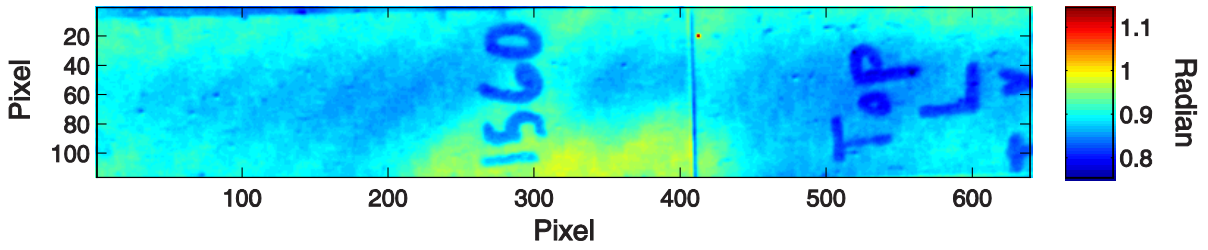
Pixel
20
40
60
80
100
100
200
300
400
500
600
Pixel
1.1
1
0.9
0.8
Radian

(g)

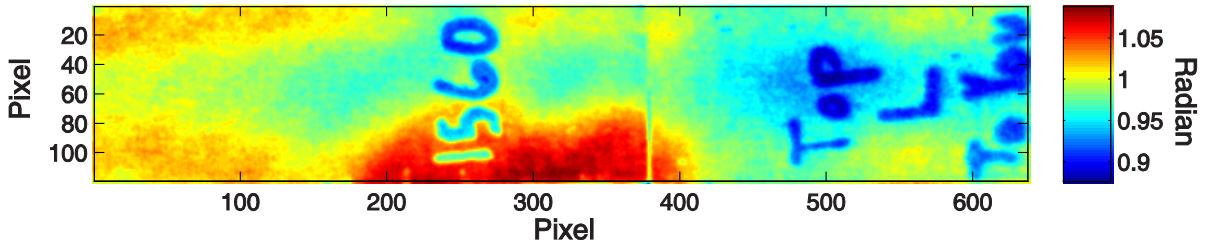
Pixel
20
40
60
80
100
100
200
300
400
500
600
Pixel
1.05
1
0.95
0.9
Radian

(h)

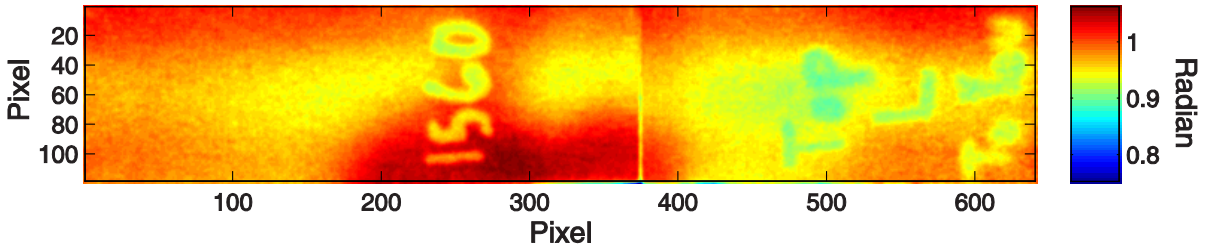
Pixel
20
40
60
80
100
100
200
300
400
500
600
Pixel
1
0.9
0.8
Radian

(i)

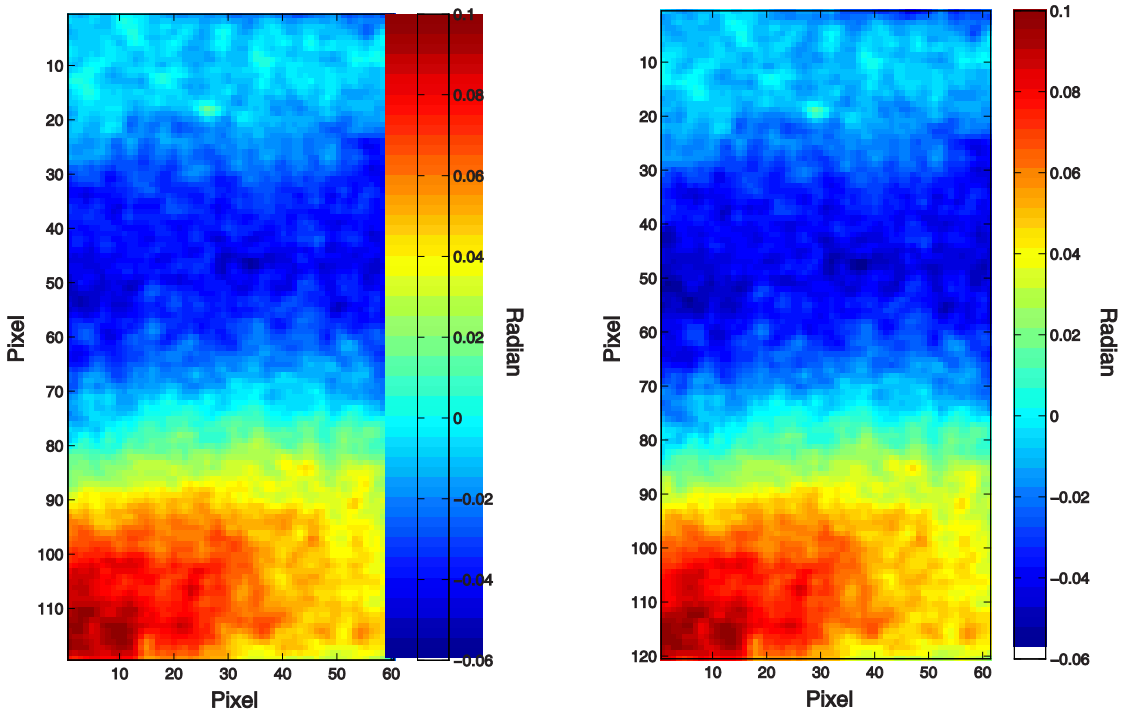

(a) **(b)**

Figure 4.6 Phase contrast image after fabrication using multi-point user input method for Sample 1 (f_s = 6 Hz, N = 196, f = 0.1 Hz); (a) run 1, (b) run 2.

Figure 4.7 Binary image expression of phase contrast value in Sample 1 after applying threshold value 0.66 of maximum phase value (f_s = 6 Hz, N = 196, f = 0.1 Hz); (a) initial stage, (b) 200 cycles, (c) 200 cycles and pre-tension, (d) 400 cycles, (e) 600 cycles (f) 600 cycles and pre-tension, (g) 800 cycles, (h) 1000 cycles, (i) 1600 cycles.

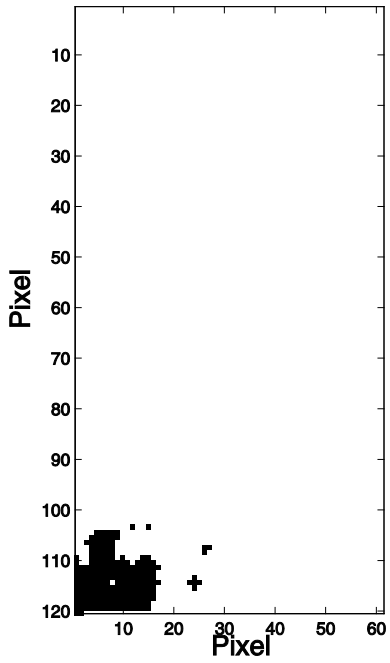
Pixel
Pixel
10
20
30
40
50
60
70
80
90
100
110
120

(a)

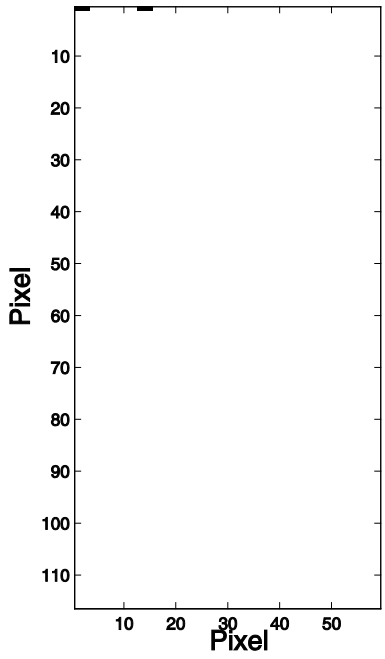
Pixel
Pixel
10
20
30
40
50
60
70
80
90
100
110

(b)

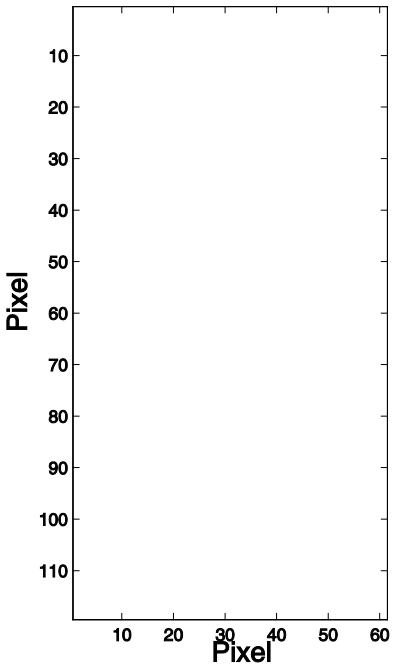
Pixel
Pixel
10
20
30
40
50
60
70
80
90
100
110

(c)

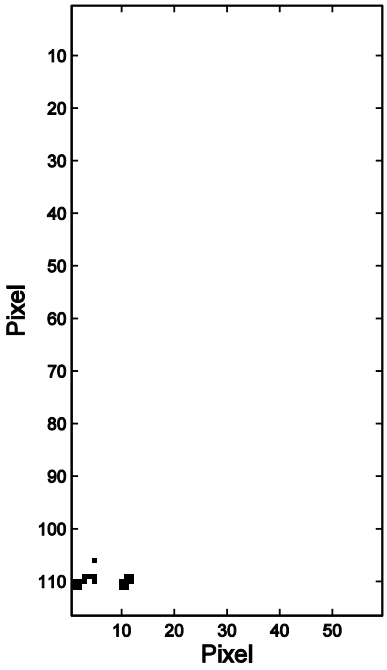
Pixel
Pixel
10
20
30
40
50
60
70
80
90
100
110

(d)

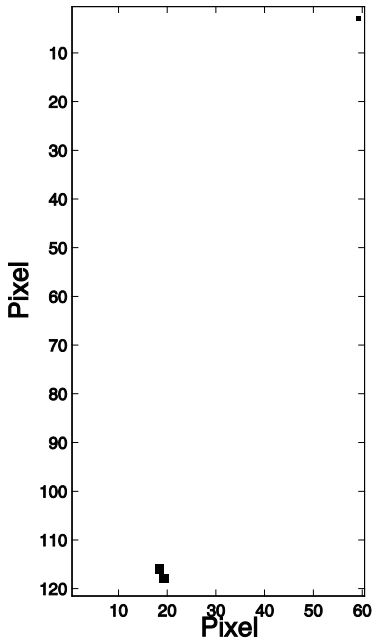
Pixel
Pixel
10
20
30
40
50
60
70
80
90
100
110
120

(e)

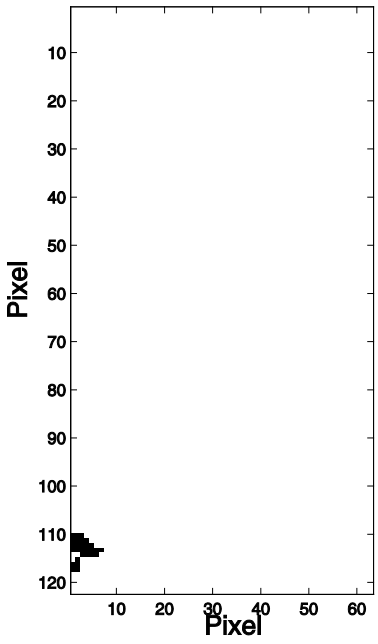
Pixel
Pixel
10
20
30
40
50
60
70
80
90
100
110
120

(f)

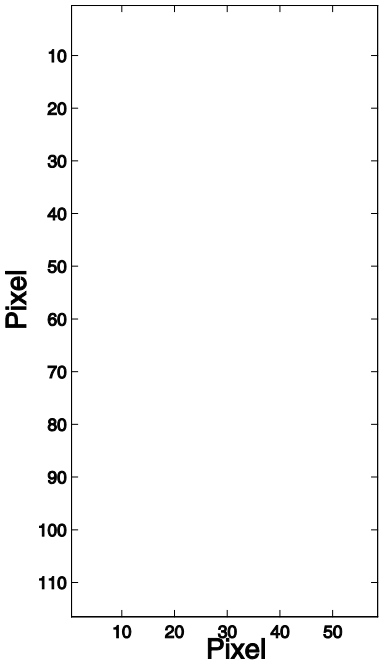
Pixel
Pixel
10
20
30
40
50
60
70
80
90
100
110

(g)

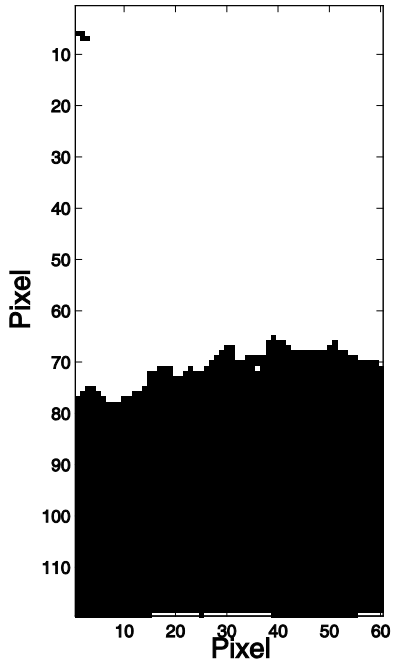
Pixel
Pixel
10
20
30
40
50
60
70
80
90
100
110

(h)

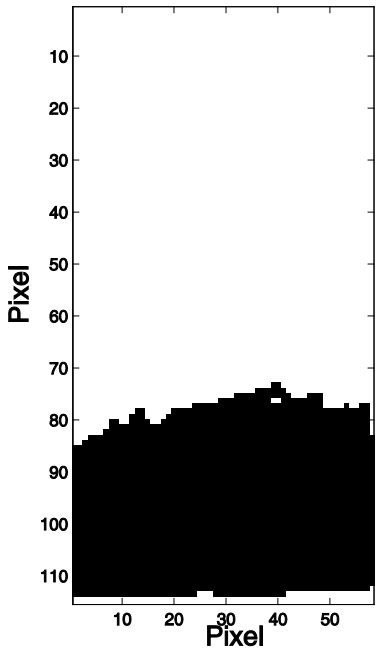

(i)

Figure 4.8 Facture surface after failure of Sample 1.

Figure 4.9 Phase image of Sample 2 (f_s = 6 Hz, N = 196, f = 0.1 Hz); (a) initial stage, (b) 200 cycles, (c) 200 cycles and pre-tension, (d) 400 cycles, (e) 400 cycles and pre-tension, (f) 600 cycles, (g) 600 cycles and pre-tension. Location of joint overlap region is shown by red box in (a).

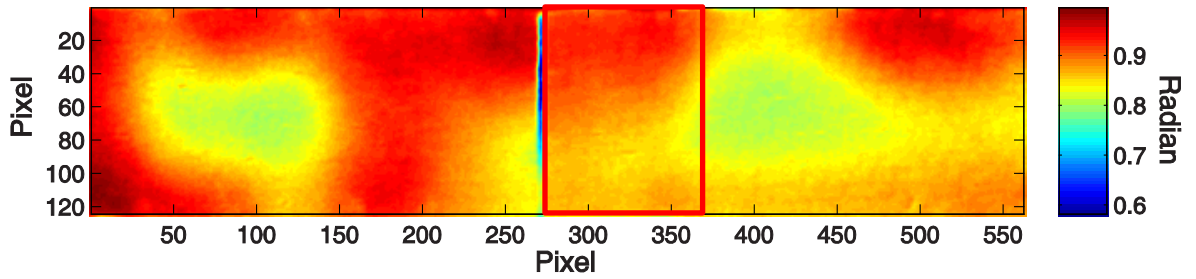
Pixel
20
40
60
80
100
120
50
100
150
200
250
300
350
400
450
500
550
Pixel
Radian
0.9
0.8
0.7
0.6

(a)

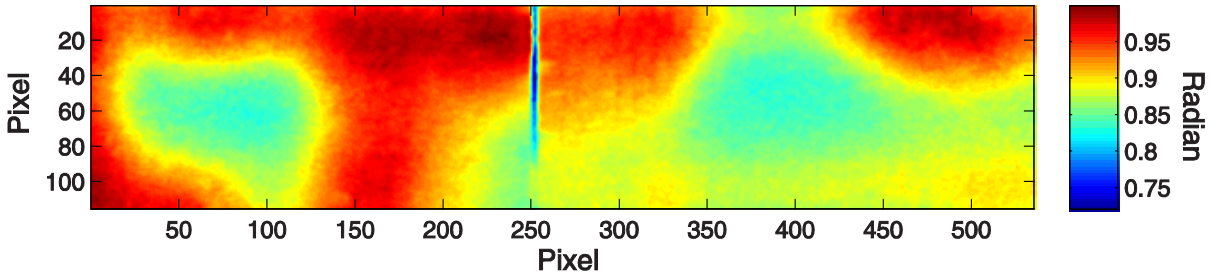
Pixel
20
40
60
80
100
50
100
150
200
250
300
350
400
450
500
Pixel
Radian
0.95
0.9
0.85
0.8
0.75

(b)

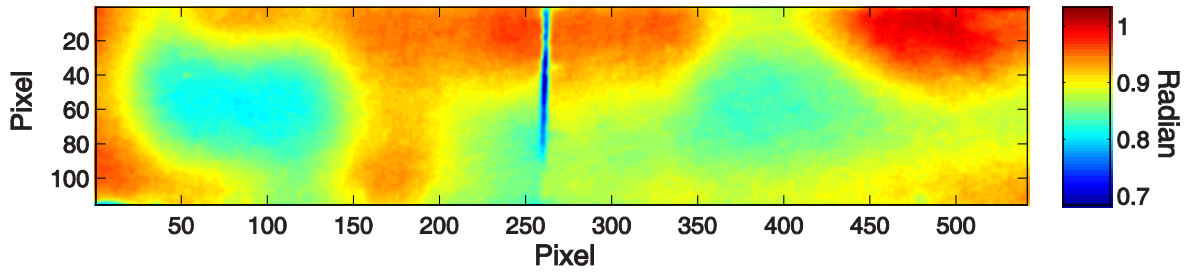
Pixel
20
40
60
80
100
50
100
150
200
250
300
350
400
450
500
Pixel
Radian
1
0.9
0.8
0.7

(c)

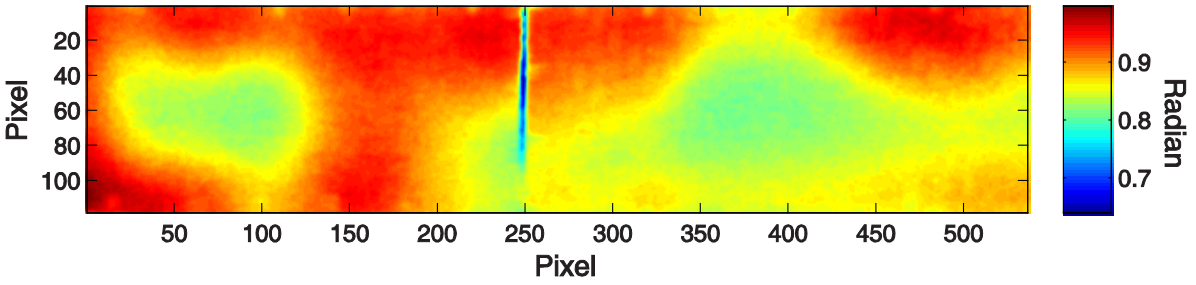
Pixel
20
40
60
80
100
50
100
150
200
250
300
350
400
450
500
Pixel
Radian
0.9
0.8
0.7

(d)

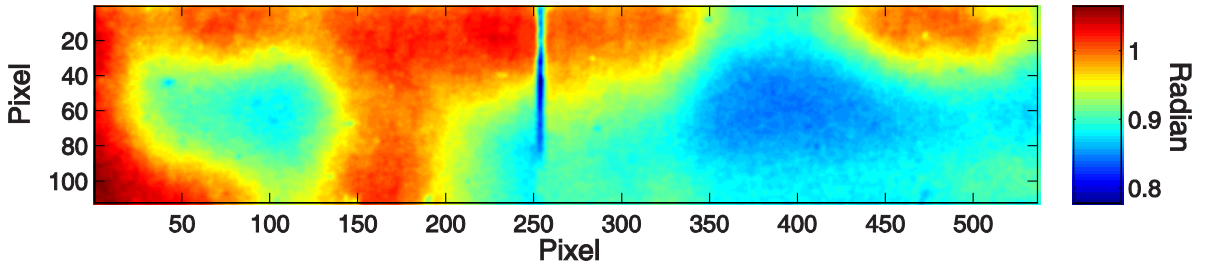
Pixel
20
40
60
80
100
50
100
150
200
250
300
350
400
450
500
Pixel
1
0.9
0.8
Radian

(e)

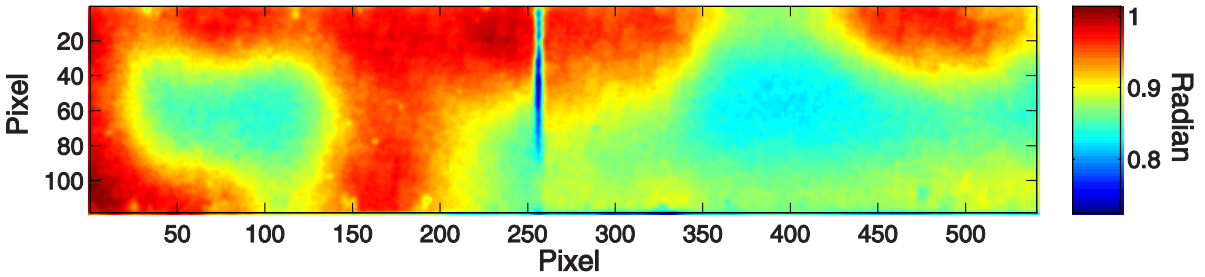
Pixel
20
40
60
80
100
50
100
150
200
250
300
350
400
450
500
Pixel
1
0.9
0.8
Radian

(f)

Figure 4.10 Phase contrast using multi-point user input method for Sample 2 (f_s = 6 Hz, N = 196, f = 0.1 Hz); (a) initial stage, (b) 200 cycles, (c) 200 cycles and pre-tension, (d) 400 cycles, (e) 400 cycles and pre-tension, (f) 600 cycles, (g) 600 cycles and pre-tension.

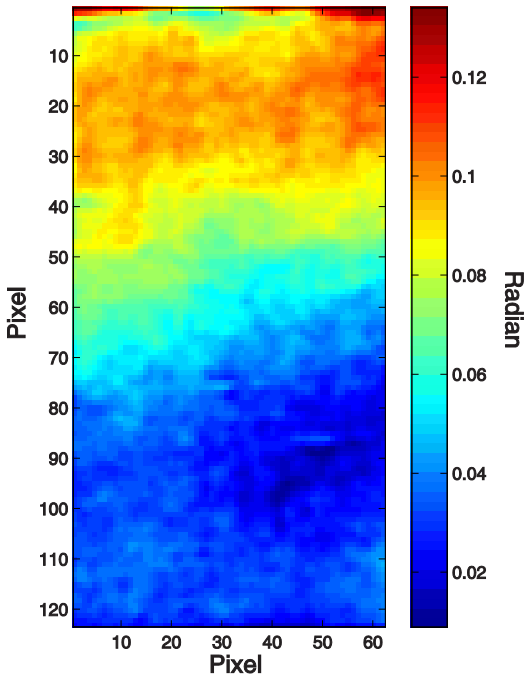
Pixel
Pixel
Radian
10
20
30
40
50
60
70
80
90
100
110
120
0.12
0.1
0.08
0.06
0.04
0.02

(a)

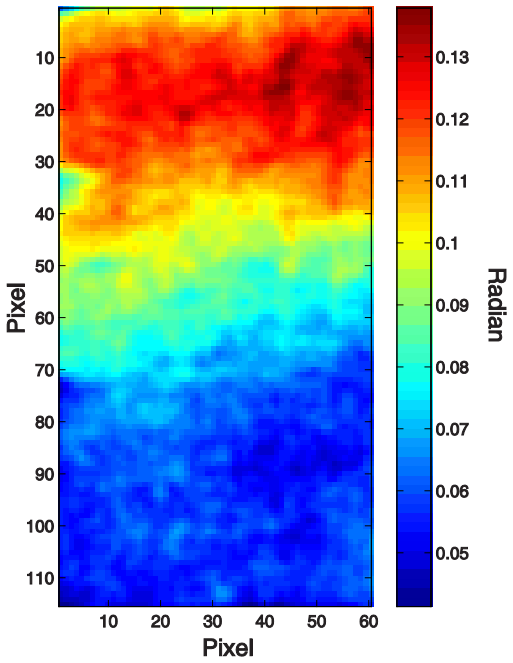
Pixel
Pixel
Radian
10
20
30
40
50
60
70
80
90
100
110
0.13
0.12
0.11
0.1
0.09
0.08
0.07
0.06
0.05

(b)

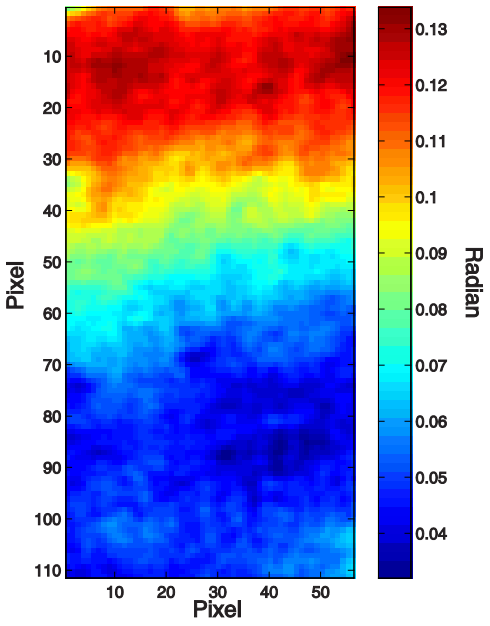
Pixel
Pixel
Radian
10
20
30
40
50
60
70
80
90
100
110
0.13
0.12
0.11
0.1
0.09
0.08
0.07
0.06
0.05
0.04

(c)

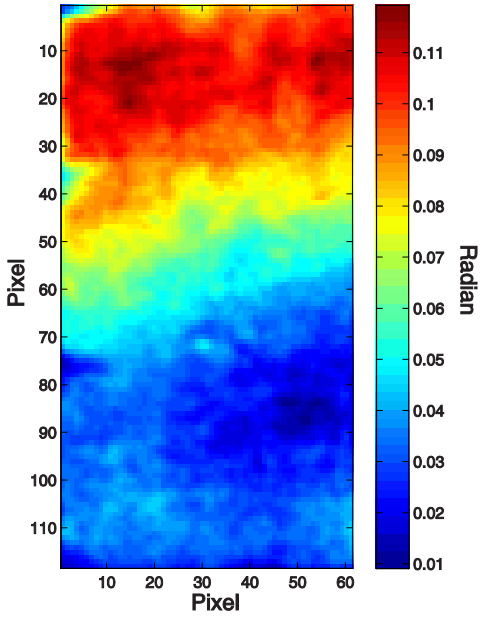
Pixel
Pixel
Radian
10
20
30
40
50
60
70
80
90
100
110
0.11
0.1
0.09
0.08
0.07
0.06
0.05
0.04
0.03
0.02
0.01

(d)

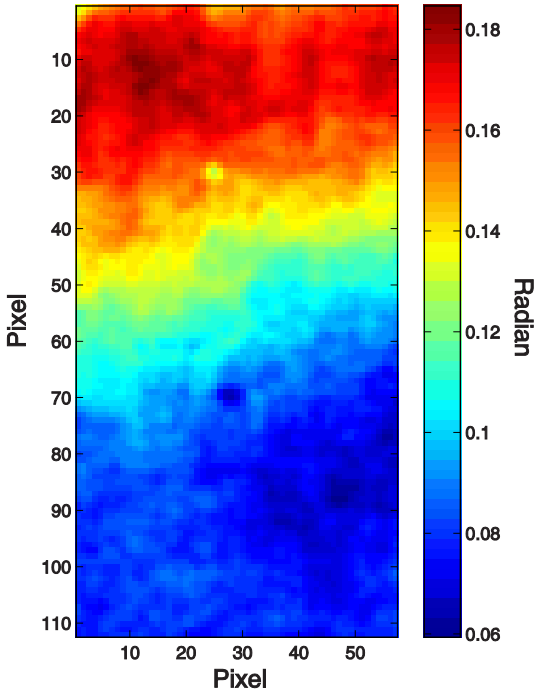
Pixel
Pixel
Radian
10
20
30
40
50
60
70
80
90
100
110
10
20
30
40
50
0.18
0.16
0.14
0.12
0.1
0.08
0.06

(e)

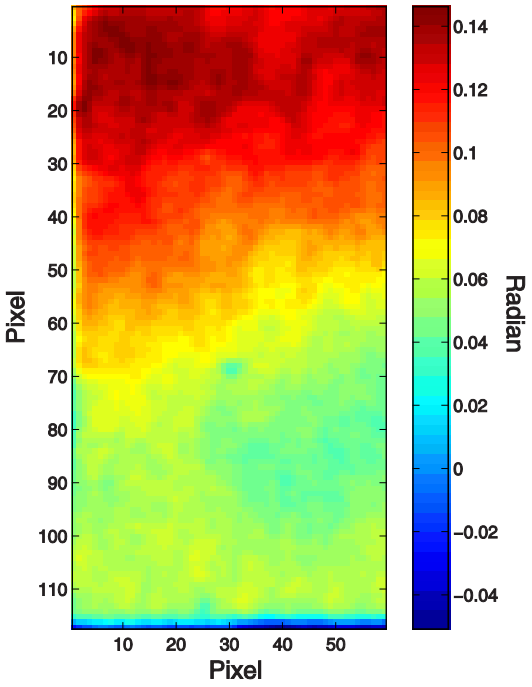
Pixel
Pixel
Radian
10
20
30
40
50
60
70
80
90
100
110
10
20
30
40
50
0.14
0.12
0.1
0.08
0.06
0.04
0.02
0
−0.02
−0.04

(f)

Figure 4.11 Binary image expression of phase contrast value in Sample 2 after applying threshold value 0.66 of maximum phase value (f_s = 6 Hz, N = 196, f = 0.1 Hz); (a) initial stage, (b) 200 cycles, (c) 200 cycles and pre-tension, (d) 400 cycles, (e) 400 cycles and pre-tension, (f) 600 cycles, (g) 600 cycles and pre-tension.

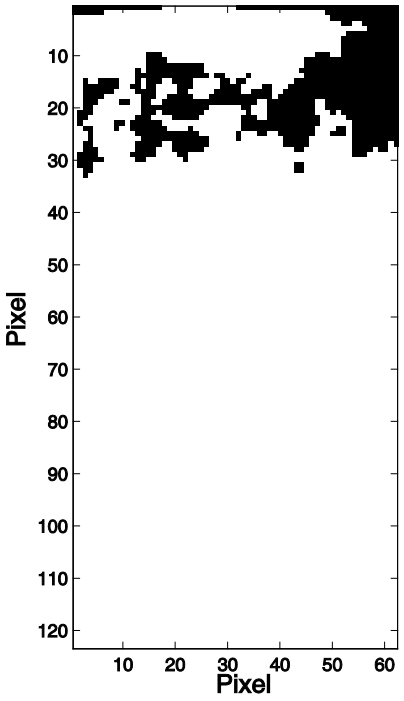
Pixel
Pixel
10
20
30
40
50
60
70
80
90
100
110
120

(a)

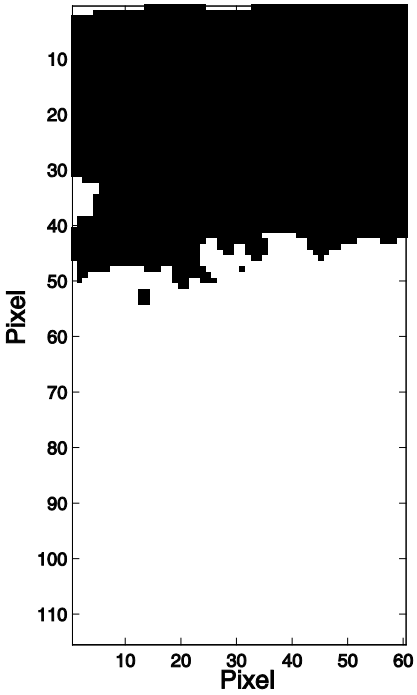
Pixel
Pixel
10
20
30
40
50
60
70
80
90
100
110

(b)

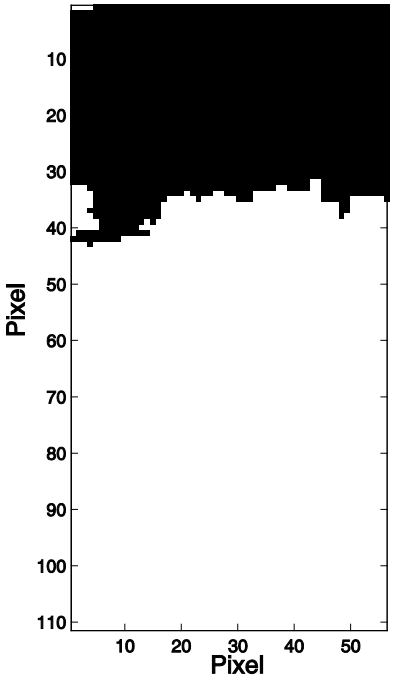
Pixel
Pixel
10
20
30
40
50
60
70
80
90
100
110

(c)

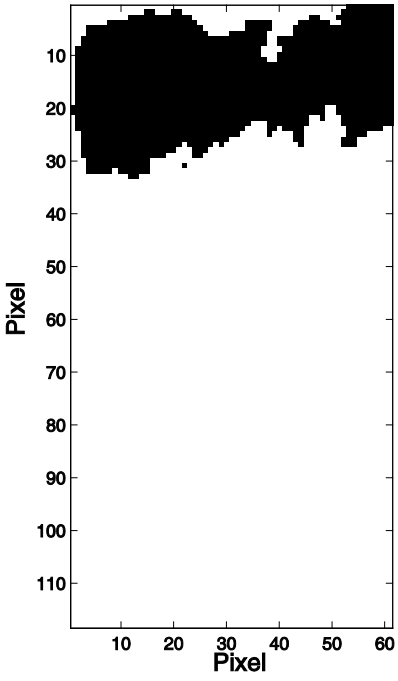
Pixel
Pixel
10
20
30
40
50
60
70
80
90
100
110

(d)

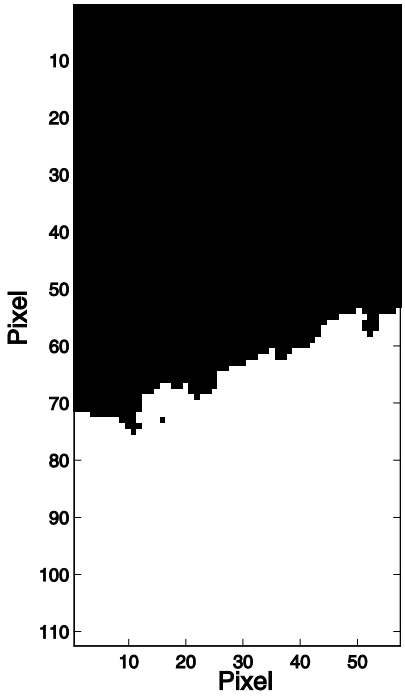
Pixel
10
20
30
40
50
60
70
80
90
100
110
10
20
30
40
50
Pixel

(e)

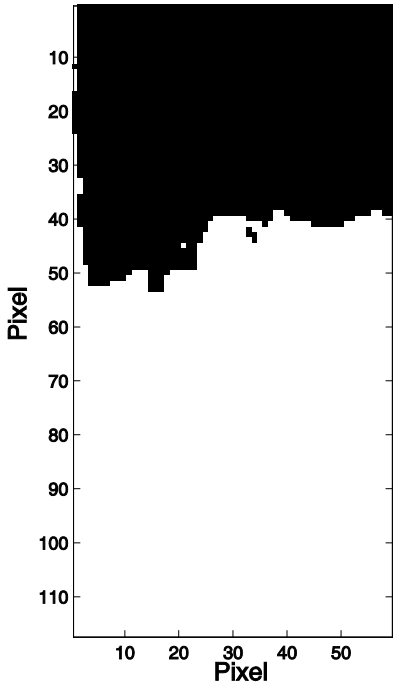
Pixel
10
20
30
40
50
60
70
80
90
100
110
10
20
30
40
50
Pixel

(f)

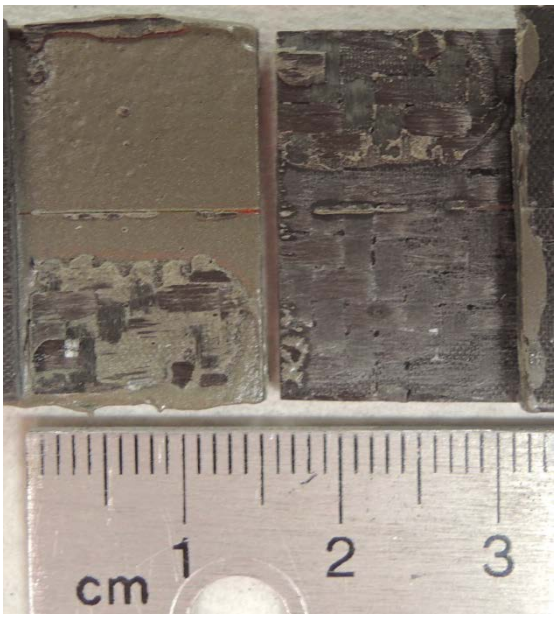

Figure 4.12 Facture surface after failure of Sample 2.

Figure 4.13 Phase image of Sample 3 (f_s = 6 Hz, N = 196, f = 0.1 Hz); (a) initial stage, (b) 200 cycles, (c) 400 cycles and pre-tension, (d) 600 cycles, (e) 800 cycles, (f) 1000 cycles, (g) 2000 cycles, (h) 3000 cycles, (i) 4000 cycles, (j) 50000 cycles. Location of joint overlap region is shown by red box in (a).

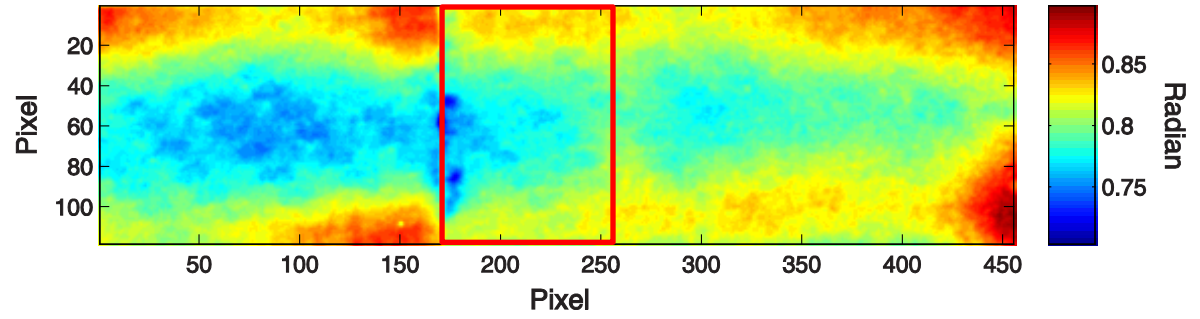
Pixel
20
40
60
80
100
50
100
150
200
250
300
350
400
450
Pixel
0.85
0.8
0.75
Radian

(a)

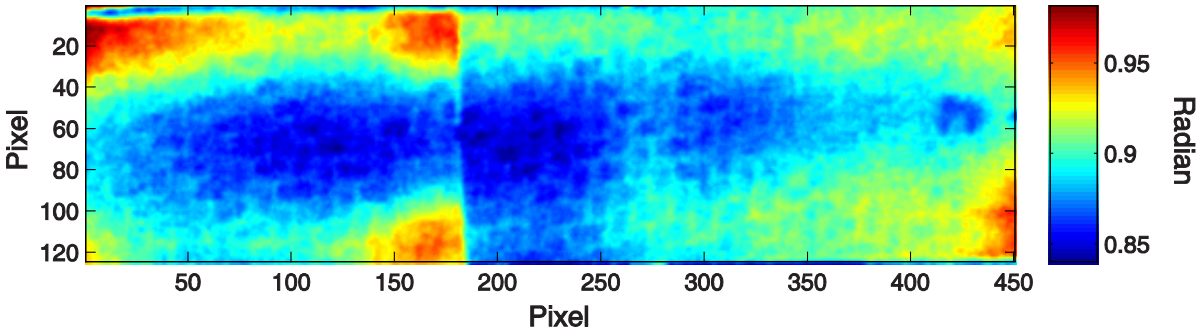
Pixel
20
40
60
80
100
120
50
100
150
200
250
300
350
400
450
Pixel
0.95
0.9
0.85
Radian

(b)

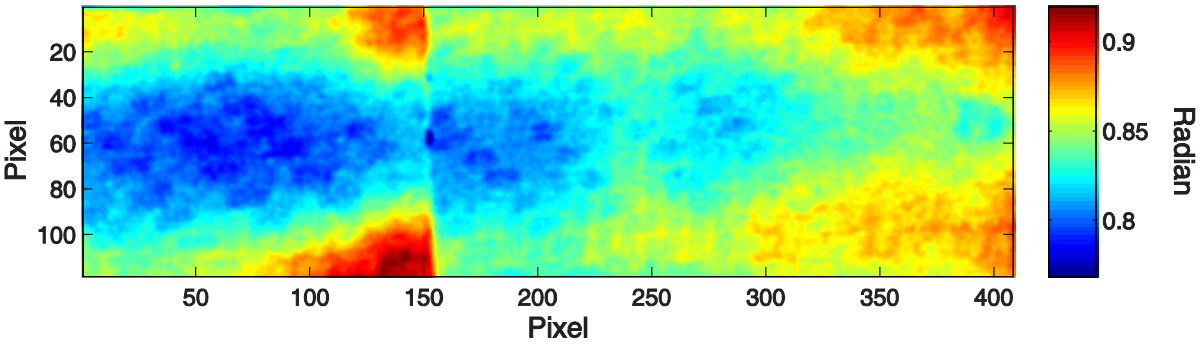
Pixel
20
40
60
80
100
50
100
150
200
250
300
350
400
Pixel
0.9
0.85
0.8
Radian

(c)

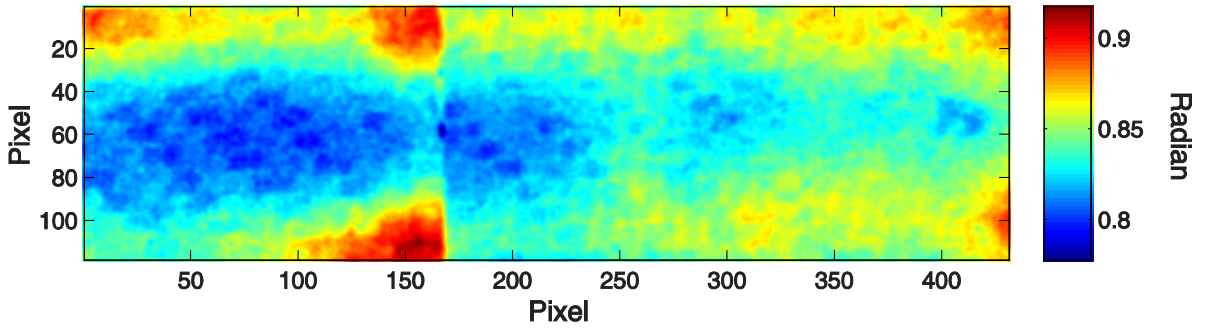
Pixel
20
40
60
80
100
50
100
150
200
250
300
350
400
Pixel
0.9
0.85
0.8
Radian

(d)

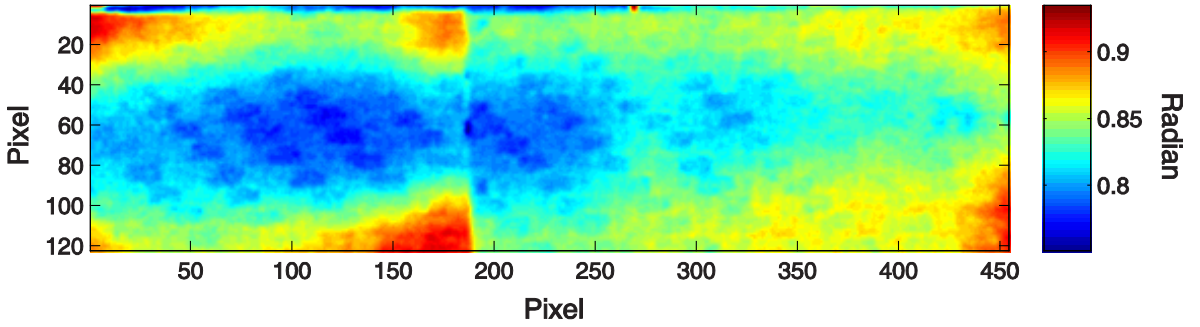
Pixel
20
40
60
80
100
120
50
100
150
200
250
300
350
400
450
Pixel
0.9
0.85
0.8
Radian

(e)

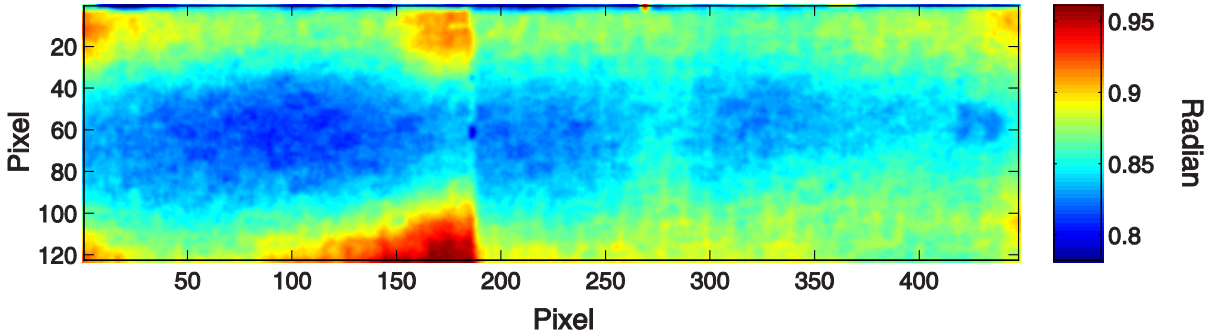
Pixel
20
40
60
80
100
120
50
100
150
200
250
300
350
400
Pixel
0.95
0.9
0.85
0.8
Radian

(f)

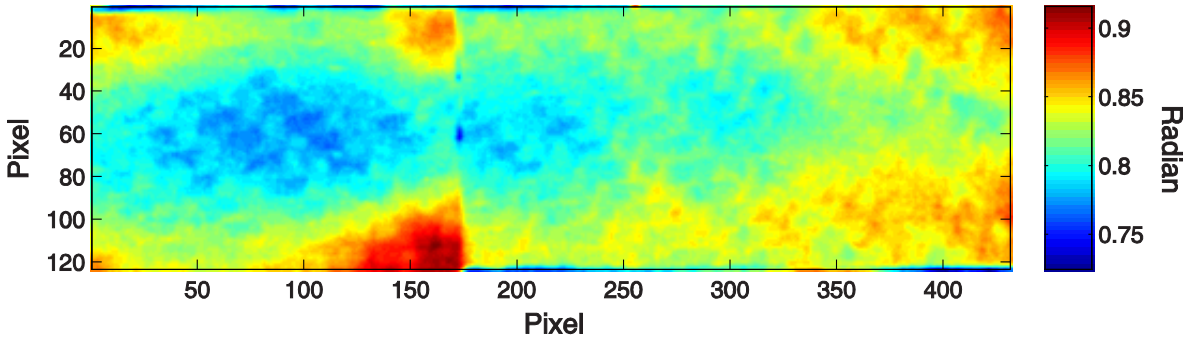
Pixel
20
40
60
80
100
120
50
100
150
200
250
300
350
400
Pixel
0.9
0.85
0.8
0.75
Radian

(g)

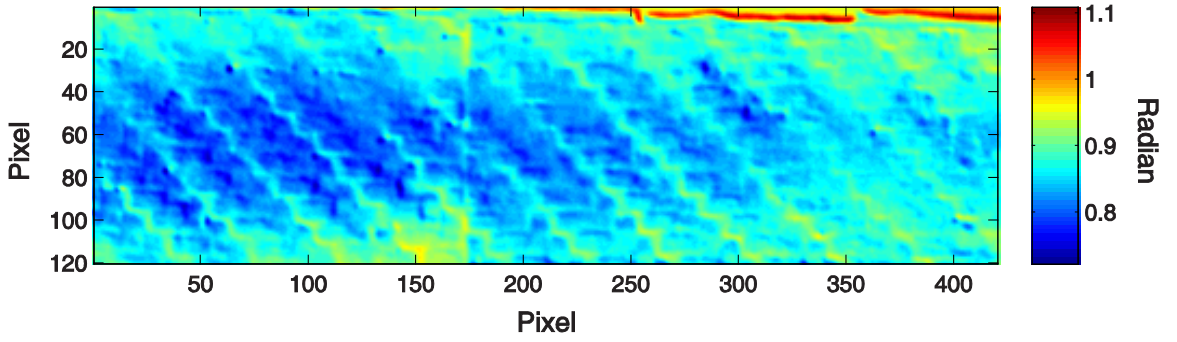
Pixel
20
40
60
80
100
120
50
100
150
200
250
300
350
400
Pixel
1.1
1
0.9
0.8
Radian

(h)

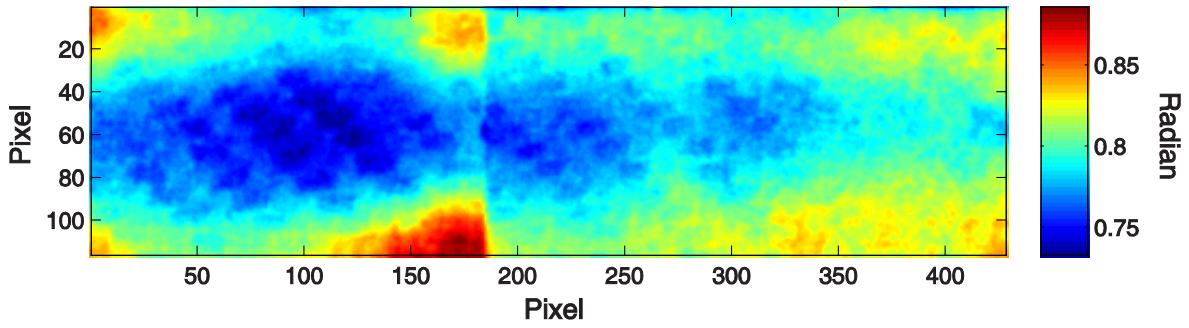
Pixel
20
40
60
80
100
50
100
150
200
250
300
350
400
Pixel
0.85
0.8
0.75
Radian

(i)

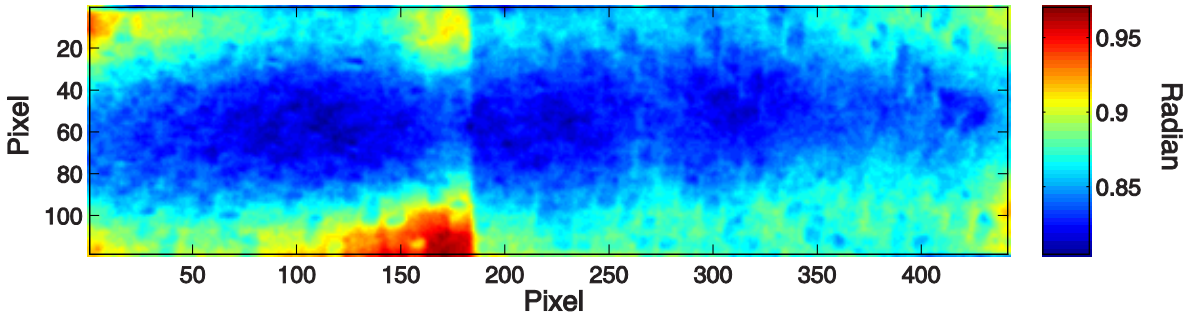
Pixel
20
40
60
80
100
50
100
150
200
250
300
350
400
Pixel
0.95
0.9
0.85
Radian

(j)

Figure 4.14 Phase contrast using multi-point user input method for Sample 3 (f_s = 6 Hz, N = 196, f = 0.1 Hz); (a) initial stage, (b) 200 cycles, (c) 400 cycles and pre-tension, (d) 600 cycles, (e) 800 cycles, (f) 1000 cycles, (g) 2000 cycles, (h) 3000 cycles, (i) 4000 cycles, (j) 50000 cycles.

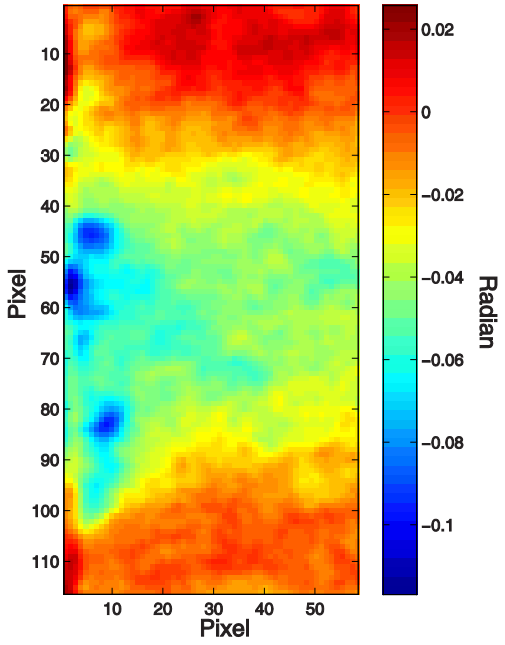
Pixel
Pixel
Radian
10
20
30
40
50
60
70
80
90
100
110
0.02
0
−0.02
−0.04
−0.06
−0.08
−0.1

(a)

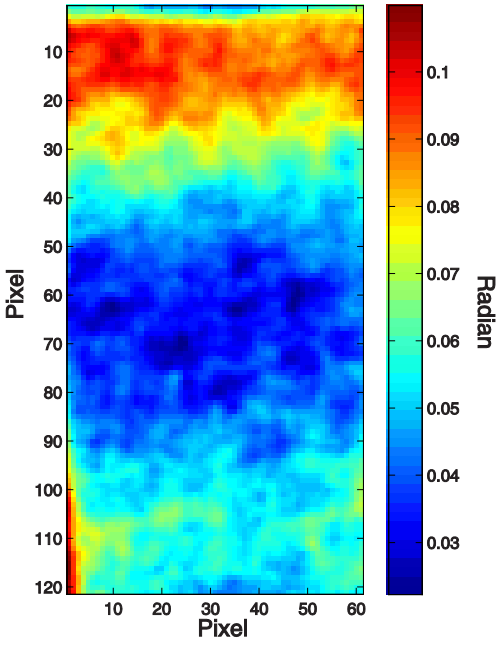
Pixel
Pixel
Radian
10
20
30
40
50
60
70
80
90
100
110
120
0.1
0.09
0.08
0.07
0.06
0.05
0.04
0.03

(b)

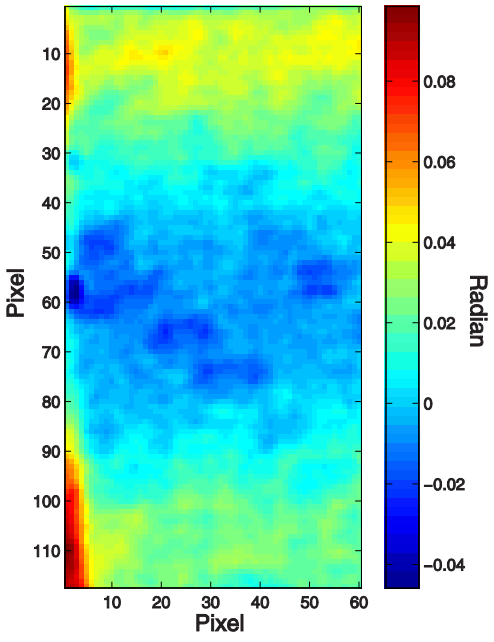
Pixel
Pixel
Radian
10
20
30
40
50
60
70
80
90
100
110
0.08
0.06
0.04
0.02
0
−0.02
−0.04

(c)

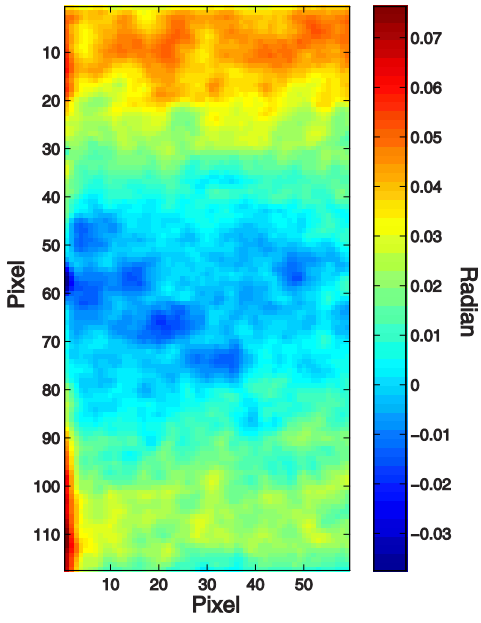
Pixel
Pixel
Radian
10
20
30
40
50
60
70
80
90
100
110
0.07
0.06
0.05
0.04
0.03
0.02
0.01
0
−0.01
−0.02
−0.03

(d)

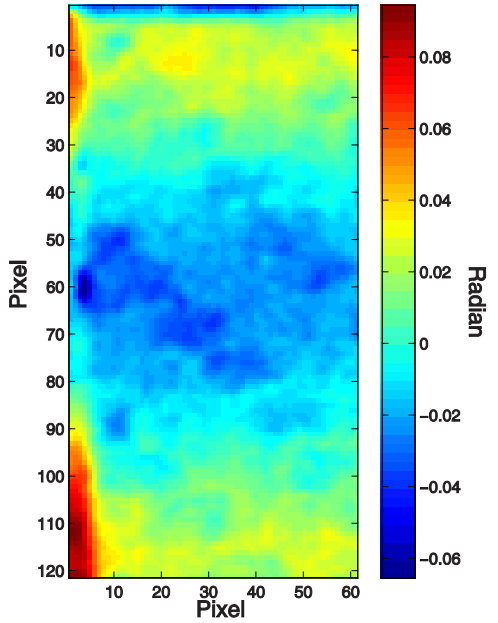
Pixel
Pixel
Radian
10
20
30
40
50
60
70
80
90
100
110
120
0.08
0.06
0.04
0.02
0
−0.02
−0.04
−0.06

(e)

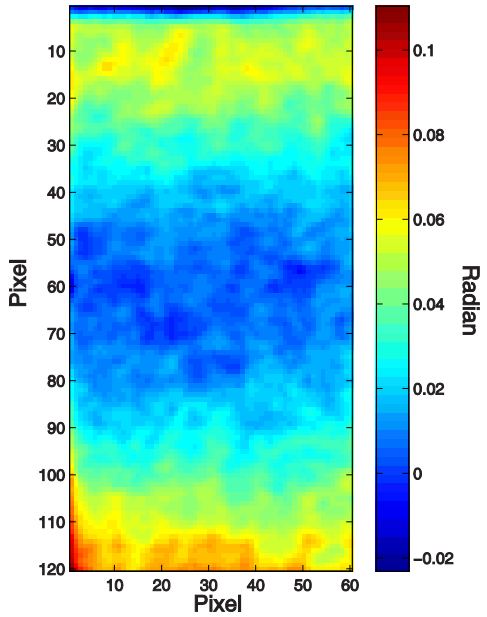
Pixel
Pixel
Radian
10
20
30
40
50
60
70
80
90
100
110
120
0.1
0.08
0.06
0.04
0.02
0
−0.02

(f)

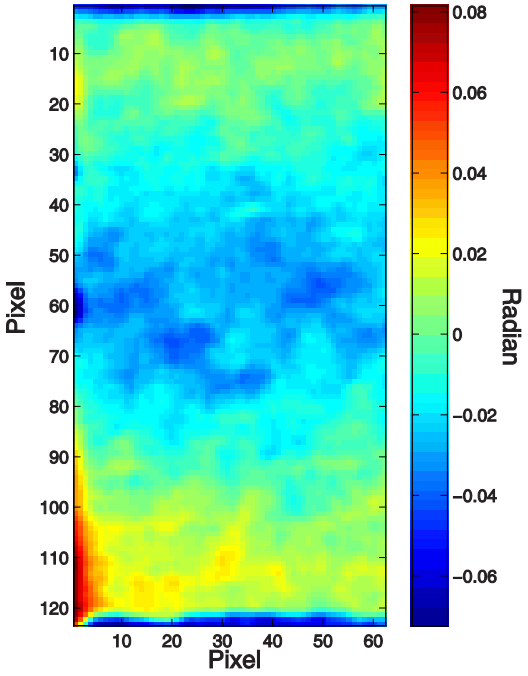
Pixel
Pixel
Radian
10
20
30
40
50
60
70
80
90
100
110
120
0.08
0.06
0.04
0.02
0
−0.02
−0.04
−0.06

(g)

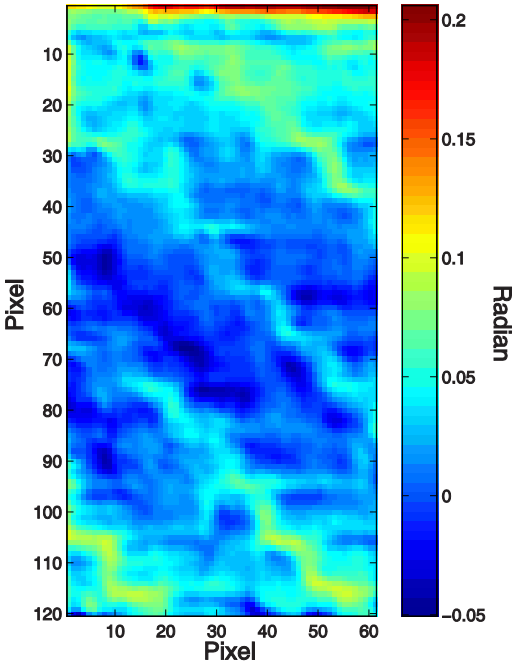
Pixel
Pixel
Radian
10
20
30
40
50
60
70
80
90
100
110
120
0.2
0.15
0.1
0.05
0
−0.05

(h)

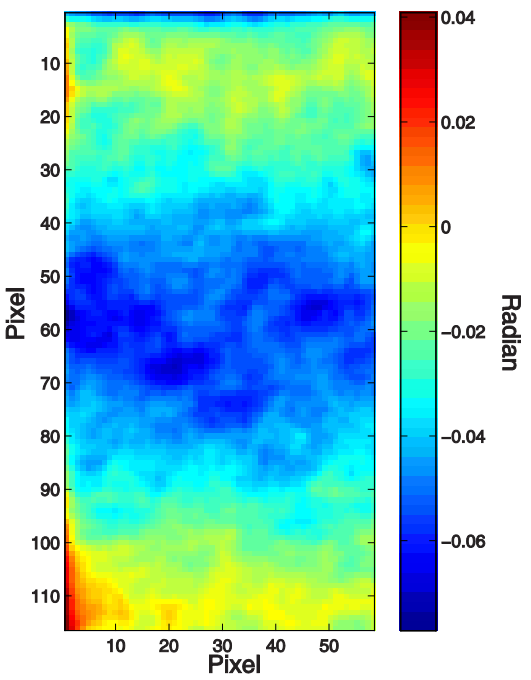
Pixel
Pixel
Radian
10
20
30
40
50
60
70
80
90
100
110
0.04
0.02
0
−0.02
−0.04
−0.06

(i)

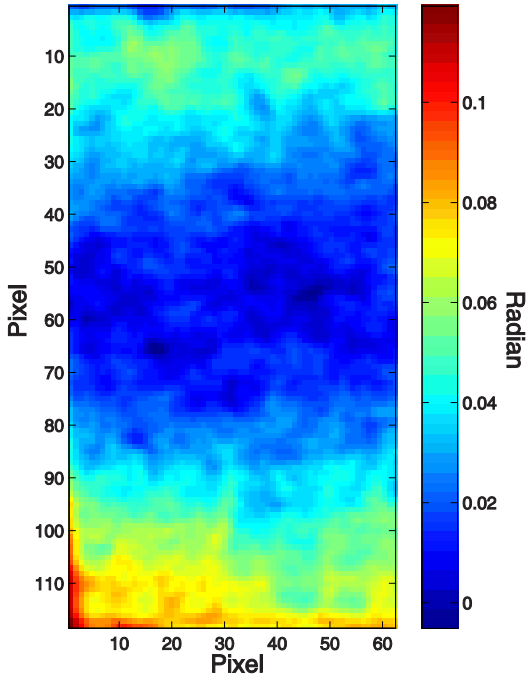
Pixel
Pixel
Radian
10
20
30
40
50
60
70
80
90
100
110
0.1
0.08
0.06
0.04
0.02
0

(j)

Figure 4.15 Binary image expression of phase contrast value in Sample 3 after applying threshold value 0.66 of maximum phase value (f_s = 6 Hz, N = 196, f = 0.1 Hz); (a) initial stage, (b) 200 cycles, (c) 400 cycles and pre-tension, (d) 600 cycles, (e) 800 cycles, (f) 1000 cycles, (g) 2000 cycles, (h) 3000 cycles, (i) 4000 cycles, (j) 50000 cycles.

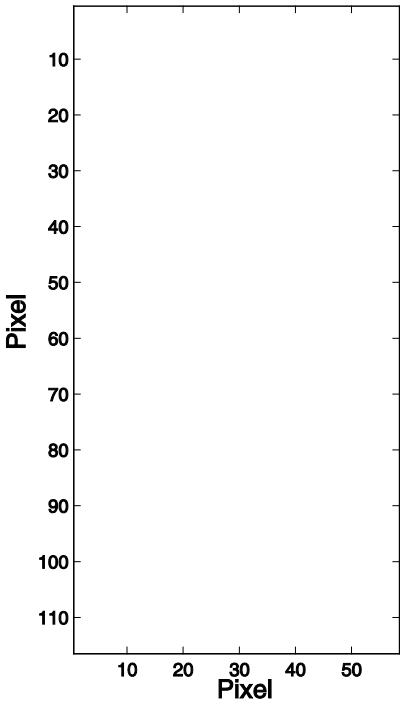
Pixel
10
20
30
40
50
60
70
80
90
100
110
Pixel
10
20
30
40
50

(a)

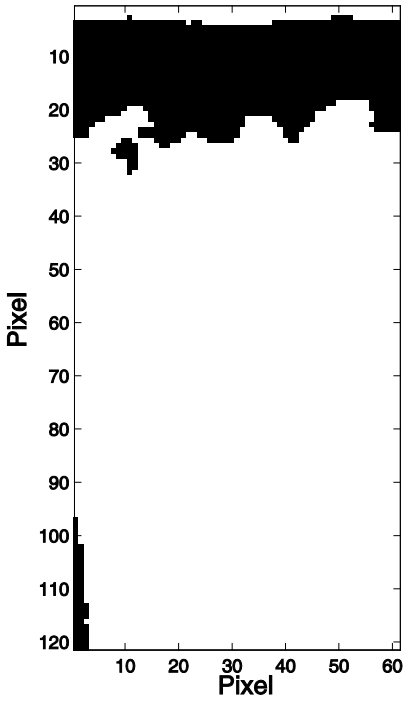
Pixel
10
20
30
40
50
60
70
80
90
100
110
120
Pixel
10
20
30
40
50
60

(b)

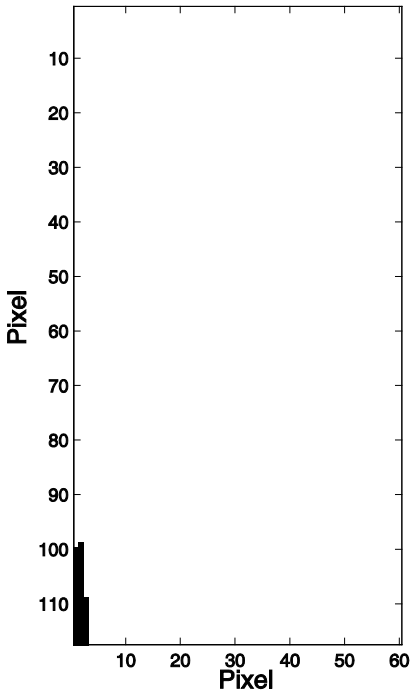
Pixel
10
20
30
40
50
60
70
80
90
100
110
Pixel
10
20
30
40
50
60

(c)

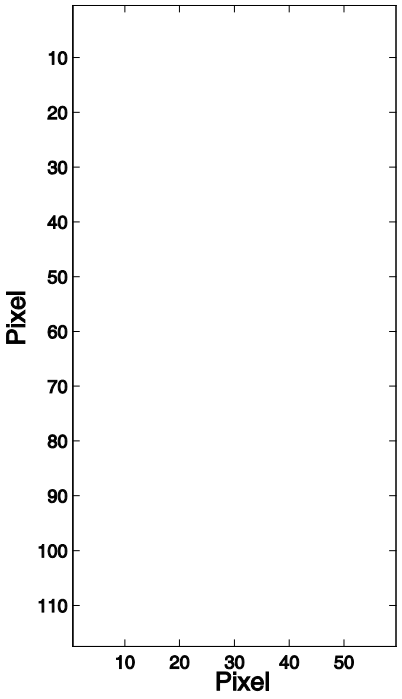
Pixel
10
20
30
40
50
60
70
80
90
100
110
Pixel
10
20
30
40
50

(d)

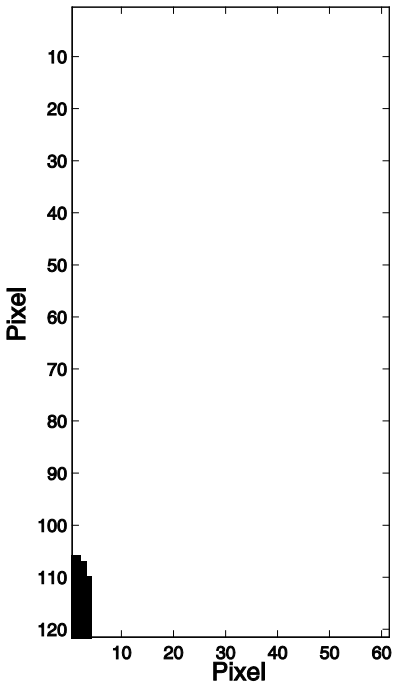
Pixel
Pixel
10
20
30
40
50
60
70
80
90
100
110
120

(e)

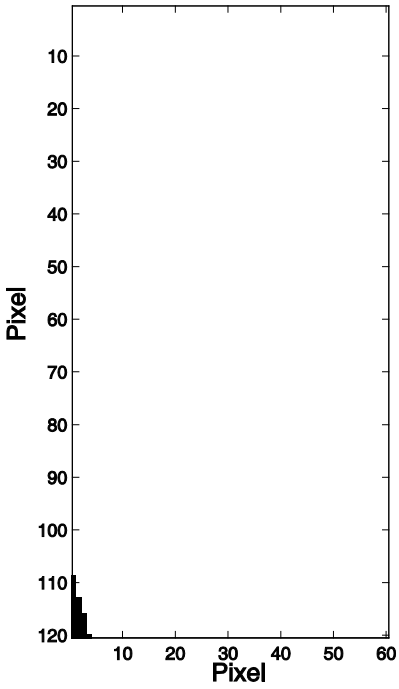
Pixel
Pixel
10
20
30
40
50
60
70
80
90
100
110
120

(f)

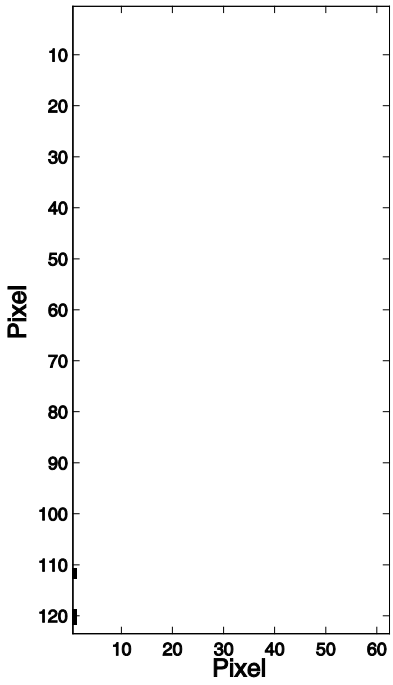
Pixel
Pixel
10
20
30
40
50
60
70
80
90
100
110
120

(g)

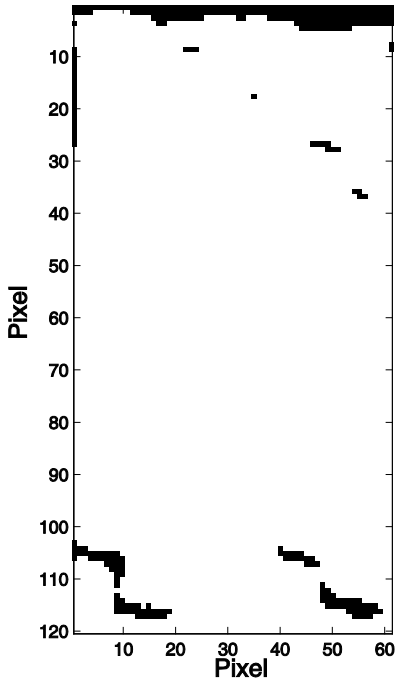
Pixel
Pixel
10
20
30
40
50
60
70
80
90
100
110
120

(h)

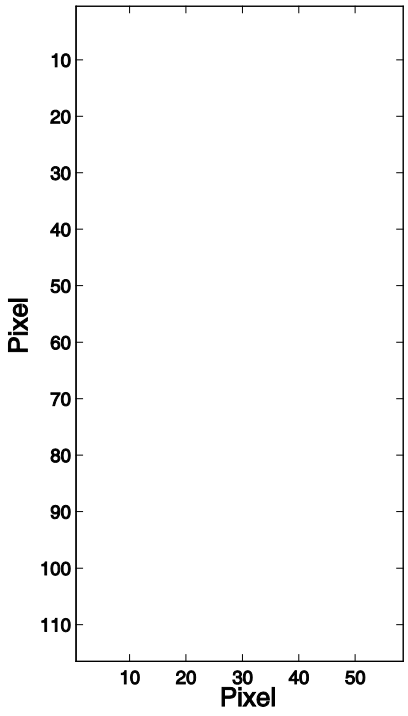
Pixel
10
20
30
40
50
60
70
80
90
100
110
10
20
30
40
50
Pixel

(i)

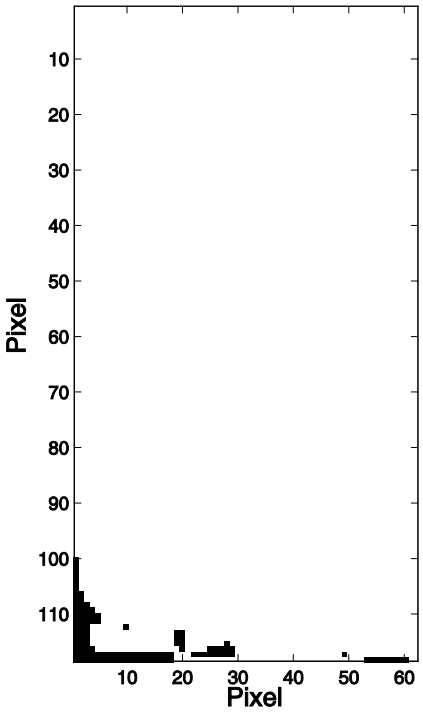
Pixel
10
20
30
40
50
60
70
80
90
100
110
10
20
30
40
50
60
Pixel

(j)

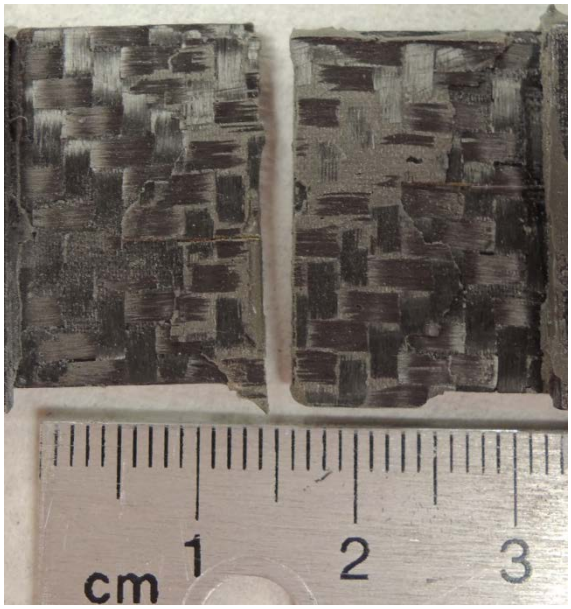

Figure 4.16 Facture surface after failure of Sample 3.

CHAPTER 5 CONCLUSIONS

This study was conducted to address damage progression in an adhesively bonded carbon fiber epoxy laminate single lap joint, under fatigue cycles using the pulsed phase thermography technique. This research was motivated by wide variations in damage detection results that depend on the operator, and inconsistency in damage boundary definitions within phase images. From a previous study, the threshold filtering method was selected to define the damage area from the phase images. During the experiments, the relative sample angle and location slightly varied from inspection to inspection within the same specimen. However, the effect of this error is negligible compared to other effects.

The calibration experiment using artificial inserts, at a known size and depth, successfully confirmed that PPT can detect the damage area. Also, a noticeable amount of manufacturing flaws were detected during this inspection. Establishing threshold values from the ratio between the maximum phase value of defects and average phase value of the boundary of inserted defects, provided a mathematical algorithm for consistent threshold value. These threshold values varied depending on the thickness of inserted defect, however, this variation was negligibly small enough to utilize its average value. Despite the visibility of the fiber weave patterns, the binary plot accurately mapped the area of the thinnest and thickest artificial defect inserts by applying the threshold value.

Fatigue loading was next introduced on the bonded joint specimens to replicate a realistic flight condition. The lifetime of individual samples were correlated to manufacturing

qualities which were detected by the PPT immediately followed by the fabrication process. The phase image after certain set of fatigue load cycles was analyzed to determine damage progress in the overlap region. The threshold filtering method, using user input for multi-point selection of the estimated minimum location, improved the consistency in phase contrast images of the lap joint area. Applying the threshold value, found from the maximum phase contrast value of the final loading cycle and the threshold factor from the calibration sample result, damage progression was seen to grow at the initial defect location from manufacturing flaws. These damages were mostly adhesive failure, debonding phenomenon between adherend and adhesive, and light-fiber-tear failure due to weak surface bonding. The fracture surface after complete failure of the bonded joint region highly agreed with the threshold binary graphs for those cases. The sample with strong surface bonding, which indicates a relatively high quality of sample manufacturing, showed barely any indication of damage in the threshold plots. The fracture surface of this sample presented strong characteristics of fiber tear failure, and based on the load envelope the sample failure was caused by brittle behavior.

Further study needs to be done to be able to use the pulsed phase thermography technique to predict fiber-tear and brittle fracture failure behavior of bonded lap joints under fatigue load cycles to be able to utilize this method in actual field applications. Also, improvements in the fabrication process are necessary to provide more consistent bonding strength between the adherend surface and adhesive. The adhesive applied and the surface preparation that was done manually contributed to inconsistent life cycle data from sample to

sample. These initial flaws introduced in manufacturing furthermore contributed to damage progression during cyclic loading.

REFERENCES

Achenbach, J.D., “Quantitative nondestructive evaluation,” International Journal of Solids and Structures, Vol. 37, Issue 1–2, 13-27, 2000.

Adams, R.D. and Cawley, P., “A review of defect types and nondestructive testing techniques for composites and bonded joints,” NDT International, Vol. 21, Issue 4, 208–222, 1988.

Adam, R.D. and Drinkwater, B.W., “Nondestructive testing of adhesively-bonded joints,” NDT&E International, Vol. 30, Issue 2, 93-98, 1997.

“Aloha 737 Fuselage Skin, Structures Undergo Detailed Fatigue Inspections,” Aviation Week & Space Technology Vol. 131, No. 12, 129, 1989.

“ALTAIR Reference Guide,” Croissy-Beaubourg, France: Cedip, n.d. 3-5. User Manual.

Ashcroft, I.A., Hughes, D.J., and Shaw, S.J., "Adhesive bonding of fibre reinforced polymer composite materials", Assembly Automation, Vol. 20, Issue 2, 150-161, 2000.

“ASTM Standard D3165 Standard Test Method for Strength Properties of Adhesives in Shear by Tension Loading of Single-Lap-Joint Laminated Assemblies," ASTM International, Oct 1, 2007.

Brigham, E. Oran. *The Fast Fourier Transform and Its Applications*. Englewood Cliffs, NJ: Prentice Hall, 1988. 96-97. Book.

Genest, M., Martinez, M., Mrad, N., Renaud, G., Fahr, A., “Pulsed thermography for non-destructive evaluation and damage growth monitoring of bonded repairs,” Composite Structures, Vol. 88, Issue 1, 112-120, 2009.

Ibarra-Castanedo, C., “Quantitative subsurface defect evaluation by pulsed phase thermography: depth retrieval with the phase,” University of Laval, 2005. Dissertation.

Ibarra-Castanedo, C., Genest, M., Servais, P., Maldague X.P.V., and Bendada A., "Qualitative and quantitative assessment of aerospace structures by pulsed thermography," Nondestructive Testing and Evaluation, Vol. 22, Issue 2-3, 199-215, 2007.

Klein, M.T., Ibarra-Castanedo, C., Maldague X.P., and Bendada A., "A straightforward graphical user interface for basic and advanced signal processing of thermographic infrared sequences," Proceedings of SPIE Vol. 6939, 2008.

Lahiri, B.B., Bagavathiappan, S., Reshmi, P. R., Philip, J., Jayakumar, T., and Raj, B., "Quantification of defects in composites and rubber materials using active thermography," Infrared Physics & Technology, Vol. 55, Issues 2–3, 191-199, 2012.

Maldague, X., "Introduction to NDT by active infrared thermography," Materials Evaluation, Vol.6, Issue 9, 1060-1073, 2002.

Maldague, X., Galmiche, F., and Ziadi, A., "Advances in pulsed phase thermography," Infrared Physics & Technology, Vol. 43, Issue 3–5, 175-181, 2002.

Maldague, X. and Marinetti, S., "Pulse phase infrared thermography," Journal of Applied Physics, Vol. 79, Issue 5, 2695-2698, 1996.

Meneghetti, G., Quaresimin, M., and Ricotta, M., "Damage mechanism in composite bonded joints under fatigue loading," Composites Part B: Engineering, Vol. 43, Issue 2, 210-220, 2012.

Quaresimin, M. and Ricotta, M., "Fatigue behaviour and damage evolution of single lap bonded joints in composite material," Composites Science and Technology, Vol. 66, Issue 2, 176-187, 2006.

Roach, D., "Methodology for Assessing the Reliability of Nondestructive Inspections on Wind Turbine Blades," Wind Turbine Reliability Workshop, June 2009.

Waugh, R.C., Dulieu-Barton, J.M., and Quinn, S., "Pulsed phase thermography and its application to kissing defects in adhesively bonded joints," Applied Mechanics and Materials, Vol. 70, 369-374, 2011.

Webb, S., Shin, P., Peters, K., Zikry, M.A., Chadderdon, S., Stan, N., Selfridge, R., Schultz, S., “Characterization of fatigue damage in adhesively bonded lap joints through dynamic, full-spectral interrogation of fiber Bragg grating sensors-Part 1. Experiments,” Proceeding SPIE, 2013.

APPENDICES

Appendix A: CYCLIC FATIGUE LOAD AND DISPLACEMENT VARIATION

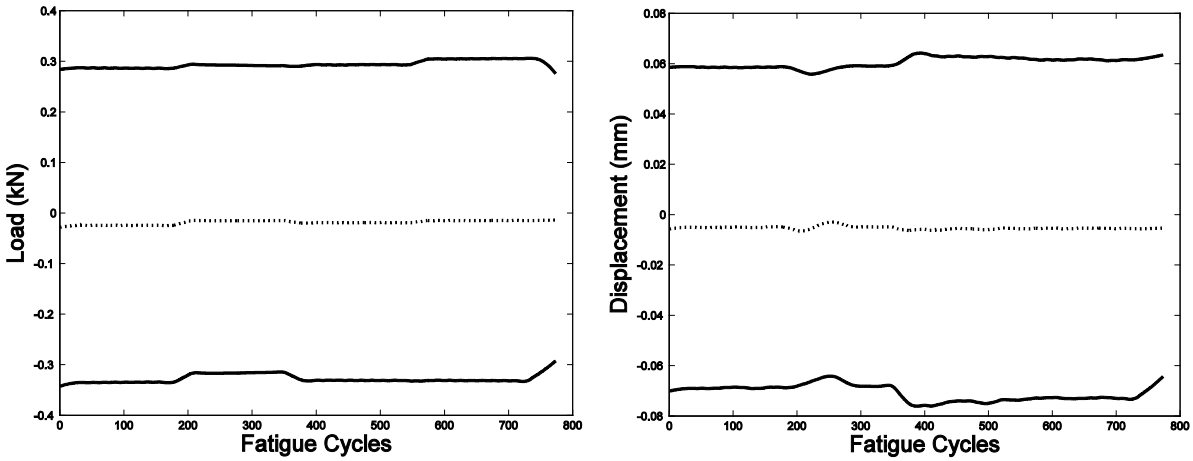

Figure A.1 Fatigue cycle envelopes (thick line) and mean values (dotted line) controller load input and corresponding displacement of the bonded joint Sample 4.

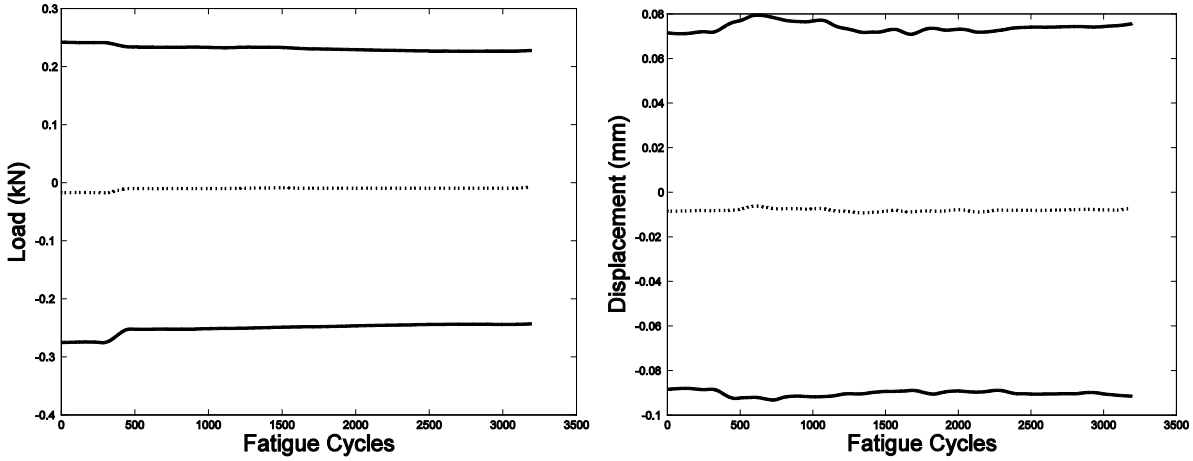

Figure A.2 Fatigue cycle envelopes (thick line) and mean values (dotted line) controller load input and corresponding displacement of the bonded joint Sample 5.

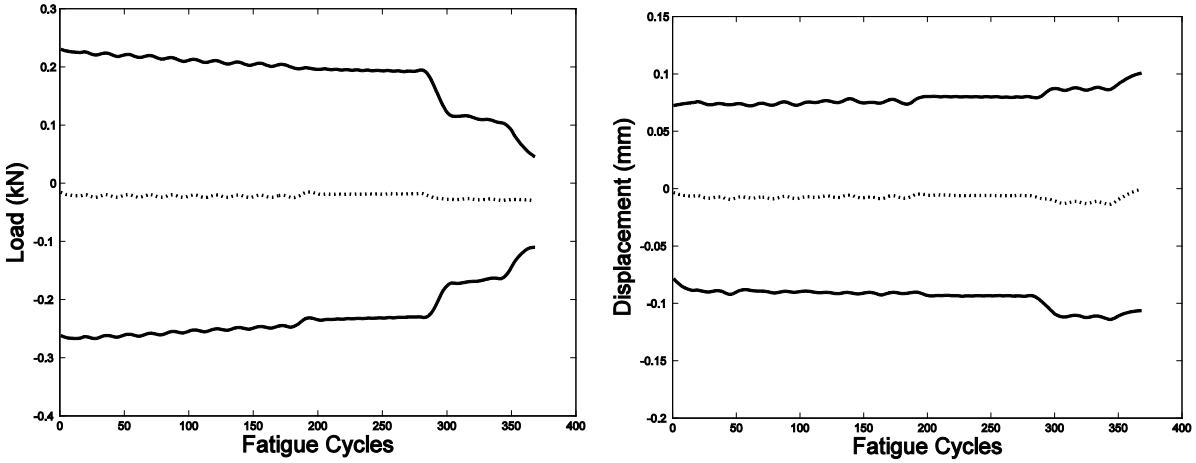

Figure A.3 Fatigue cycle envelopes (thick line) and mean values (dotted line) controller load input and corresponding displacement of the bonded joint Sample 6.

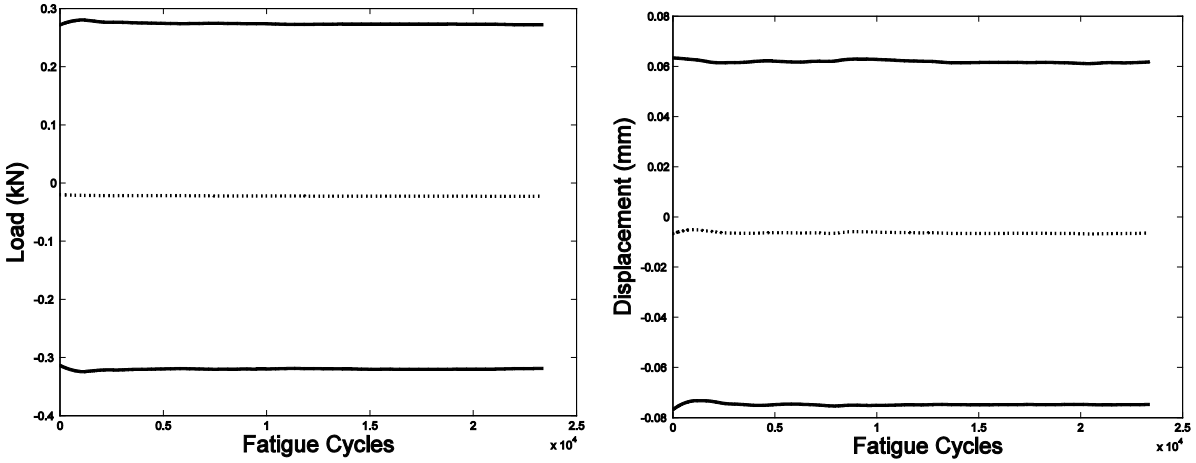

Figure A.4 Fatigue cycle envelopes (thick line) and mean values (dotted line) controller load input and corresponding displacement of the bonded joint Sample 7.

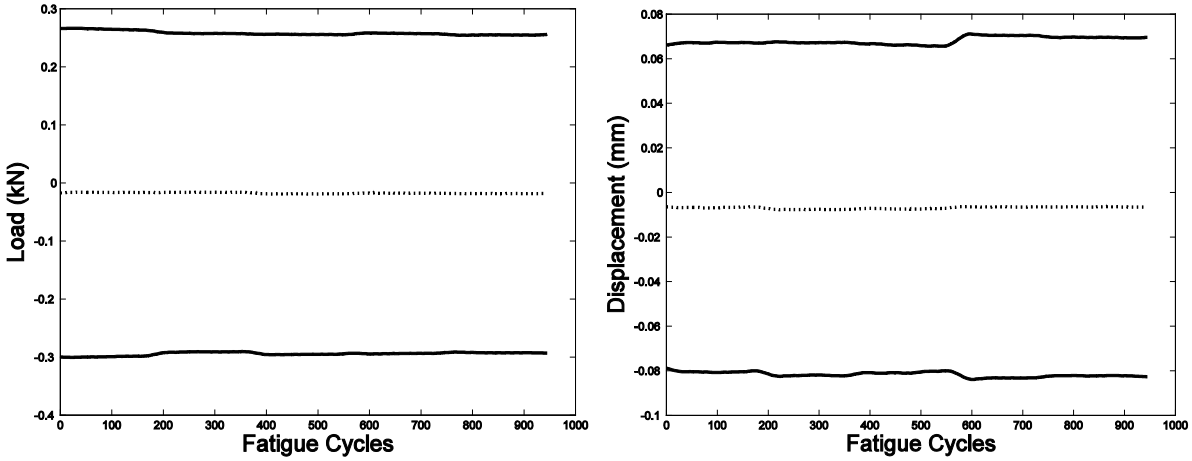

Figure A.5 Fatigue cycle envelopes (thick line) and mean values (dotted line) controller load input and corresponding displacement of the bonded joint Sample 8.

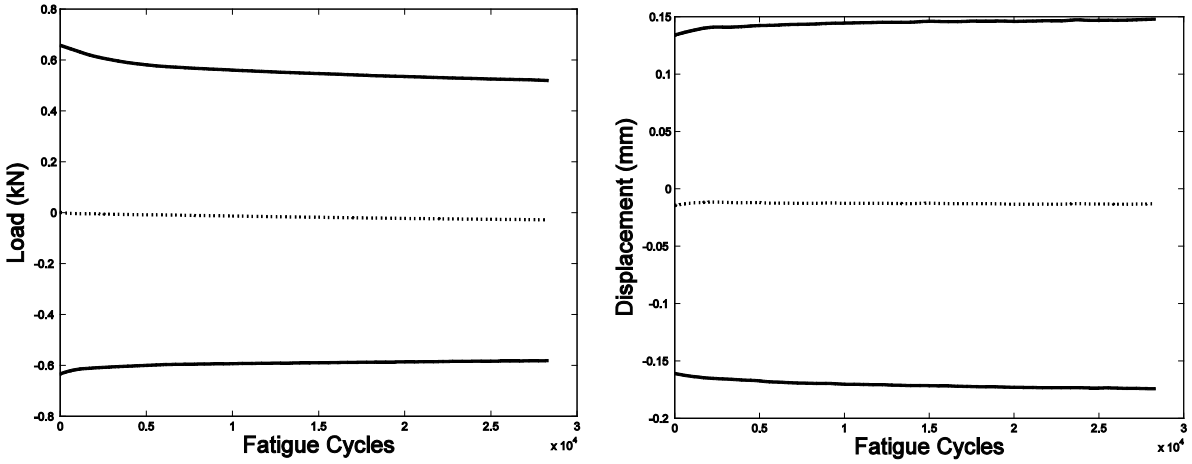

Figure A.6 Fatigue cycle envelopes (thick line) and mean values (dotted line) controller load input and corresponding displacement of the bonded joint Sample 9.

Appendix B: PULSED PHASE THERMOGRAPHY IMAGE

Figure B.1 Phase image of Sample 4 (f_s = 6 Hz, N = 196, f = 0.1 Hz); (a) initial stage, (b) 200 cycles, (c) 400 cycles, (d) 600 cycles, (e) 800 cycles. Location of joint overlap region is shown by red box in (a).

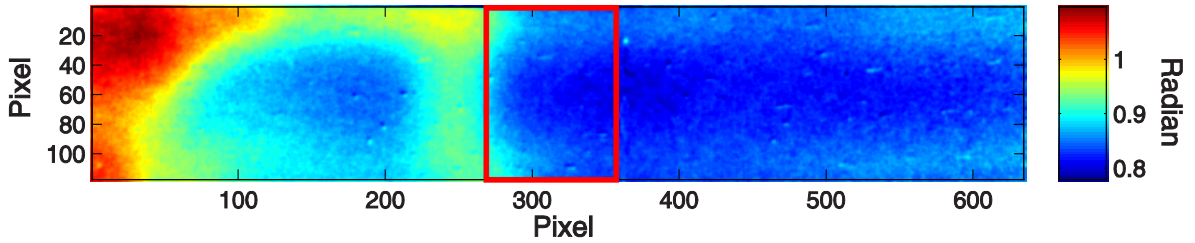
Pixel
20
40
60
80
100
100
200
300
400
500
600
Pixel
Radian
1
0.9
0.8

(a)

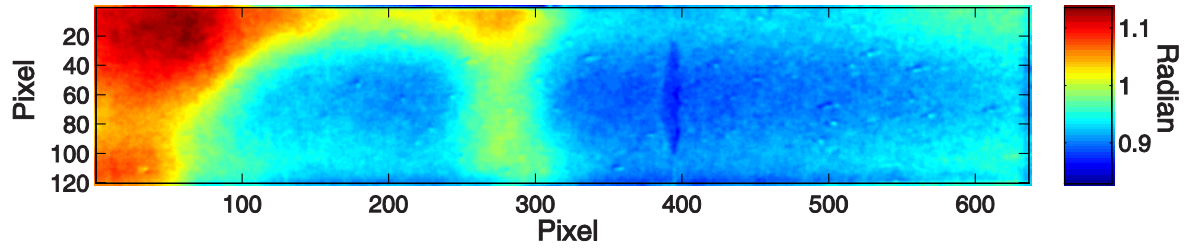
Pixel
20
40
60
80
100
120
100
200
300
400
500
600
Pixel
Radian
1.1
1
0.9

(b)

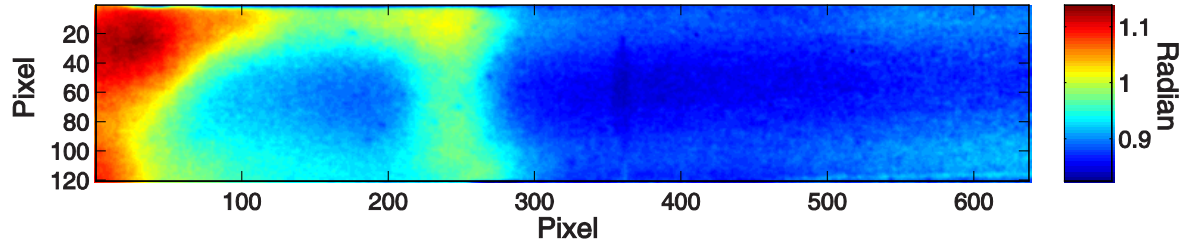
Pixel
20
40
60
80
100
120
100
200
300
400
500
600
Pixel
Radian
1.1
1
0.9

(c)

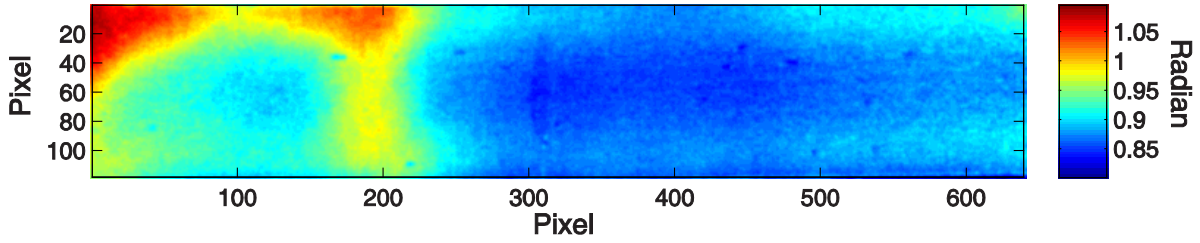
Pixel
20
40
60
80
100
100
200
300
400
500
600
Pixel
Radian
1.05
1
0.95
0.9
0.85

(d)

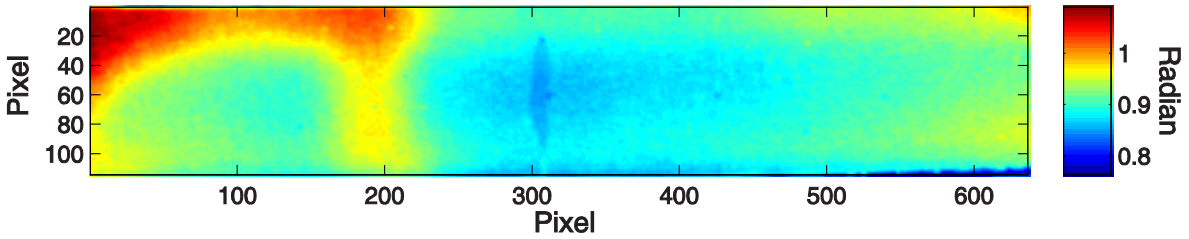
Pixel
20
40
60
80
100
100
200
300
400
500
600
Pixel
1
0.9
0.8
Radian

(e)

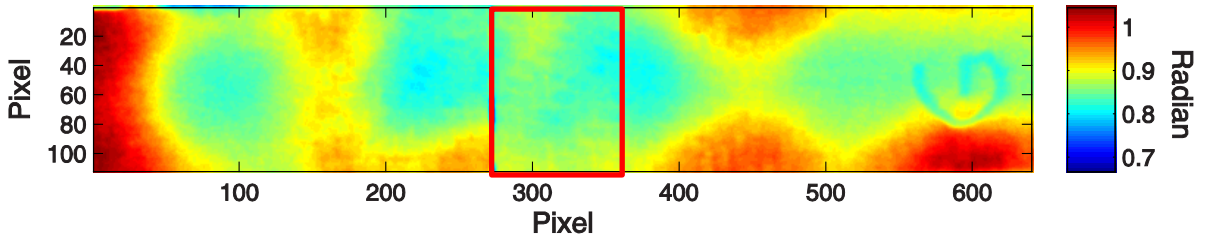

(a)

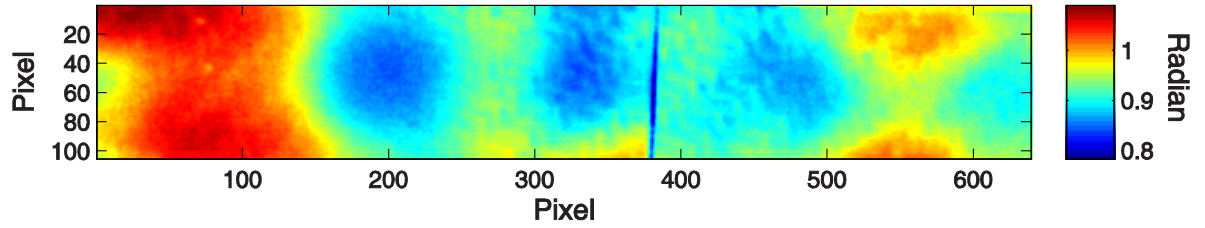

(b)

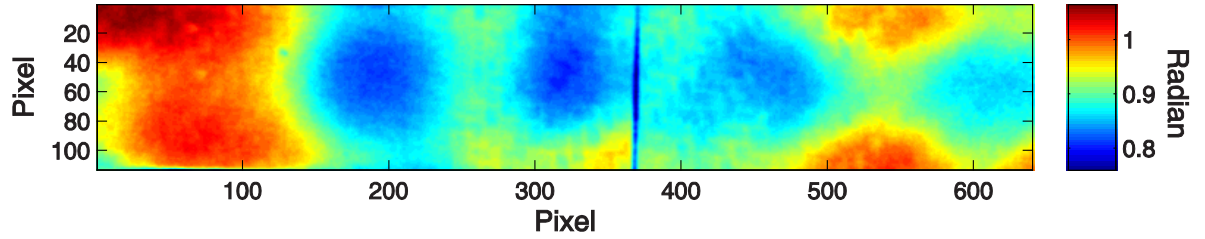

(c)

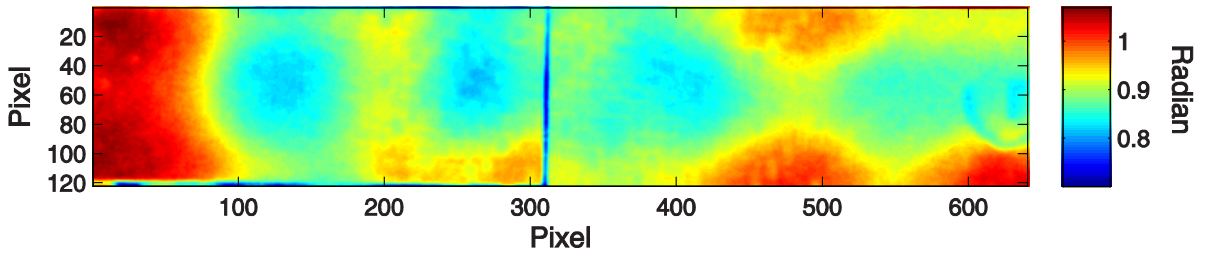

(d)

Figure B.2 Phase image of Sample 5 (f_s = 6 Hz, N = 196, f = 0.1 Hz); (a) initial stage, (b) 200 cycles, (c) 200 cycles and pre-tension, (d) 400 cycles. Location of joint overlap region is shown by red box in (a).

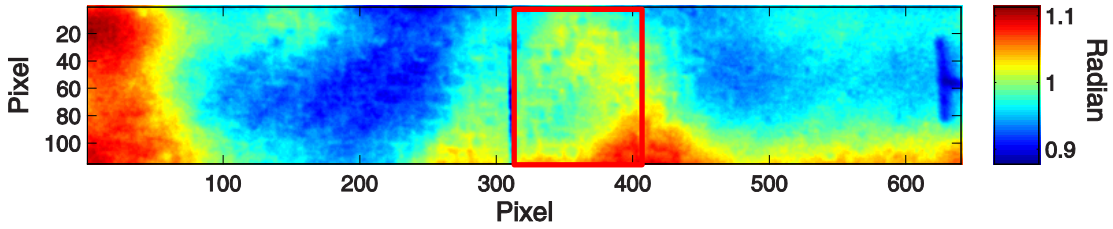

(a)

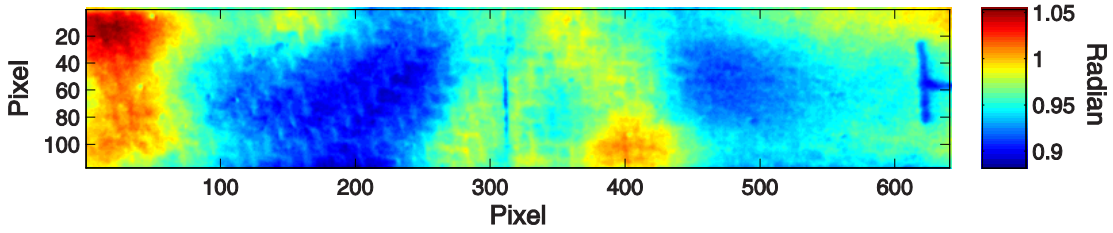

(b)

Figure B.3 Phase image of Sample 6 (f_s = 6 Hz, N = 196, f = 0.1 Hz); (a) initial stage, (b) 200 cycles. Location of joint overlap region is shown by red box in (a).

Figure B.4 Phase image of Sample 7 (f_s = 6 Hz, N = 196, f = 0.1 Hz); (a) initial stage, (b) 200 cycles, (c) 200 cycles and pre-tension, (d) 400 cycles, (e) 24744 cycles. Location of joint overlap region is shown by red box in (a).

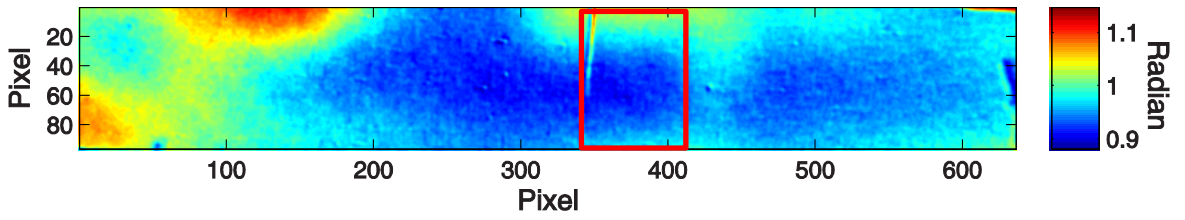
Pixel
20
40
60
80
100
200
300
400
500
600
Pixel
1.1
1
0.9
Radian

(a)

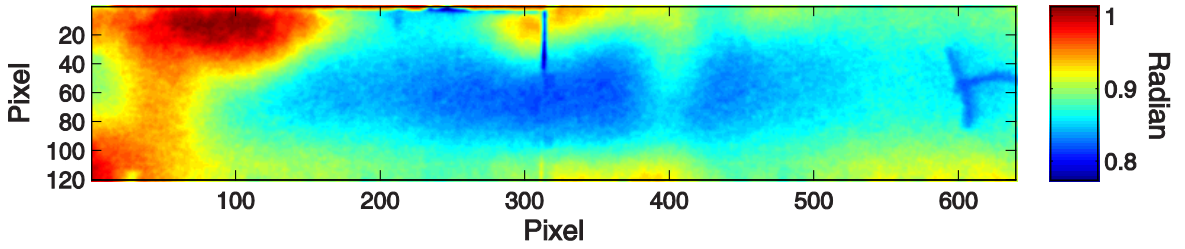
Pixel
20
40
60
80
100
120
100
200
300
400
500
600
Pixel
1
0.9
0.8
Radian

(b)

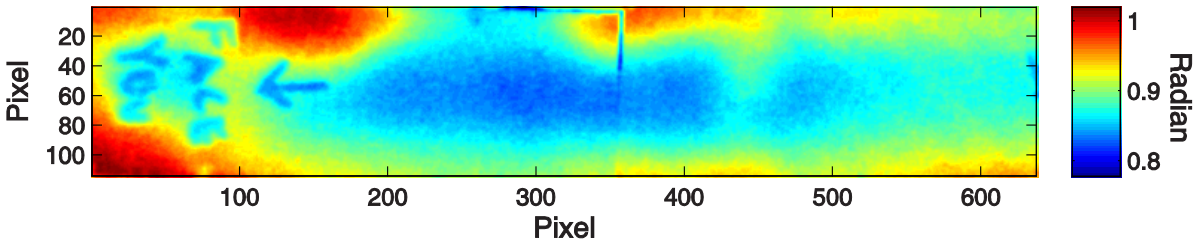
Pixel
20
40
60
80
100
100
200
300
400
500
600
Pixel
1
0.9
0.8
Radian

(c)

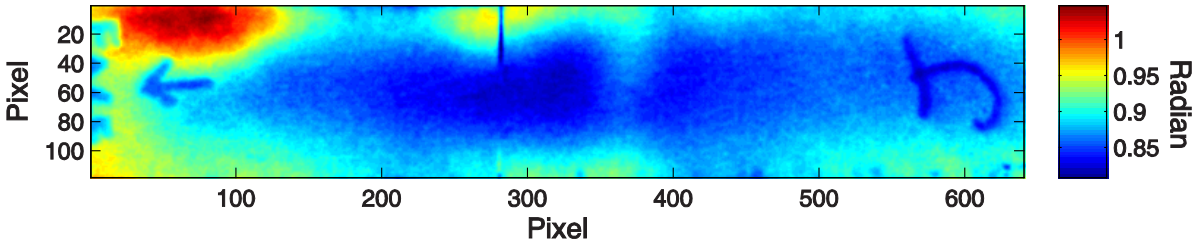
Pixel
20
40
60
80
100
100
200
300
400
500
600
Pixel
1
0.95
0.9
0.85
Radian

(d)

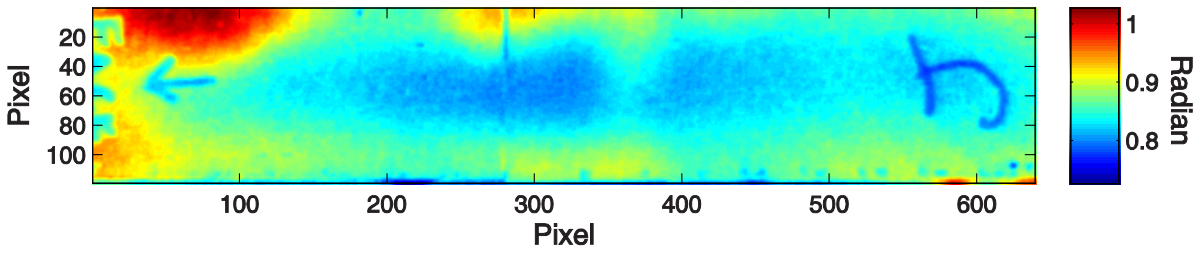
Pixel
20
40
60
80
100
100
200
300
400
500
600
Pixel
1
0.9
0.8
Radian

(e)

Figure B.5 Phase image of Sample 8 (f_s = 6 Hz, N = 196, f = 0.1 Hz); (a) initial stage, (b) 200 cycles, (c) 200 cycles and pre-tension, (d) 400 cycles, (e) 400 cycles and pre-tension, (f) 600 cycles, (g) 600 cycles and pre-tension, (h) 800 cycles, (i) 800 cycles and pre-tension, (j) 1000 cycles, (k) 1000 cycles and pre-tension. Location of joint overlap region is shown by red box in (a).

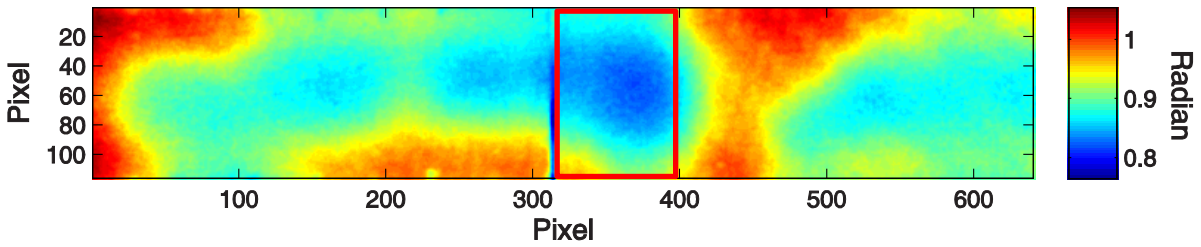
Pixel
20
40
60
80
100
100
200
300
400
500
600
Pixel
Radian
1
0.9
0.8

(a)

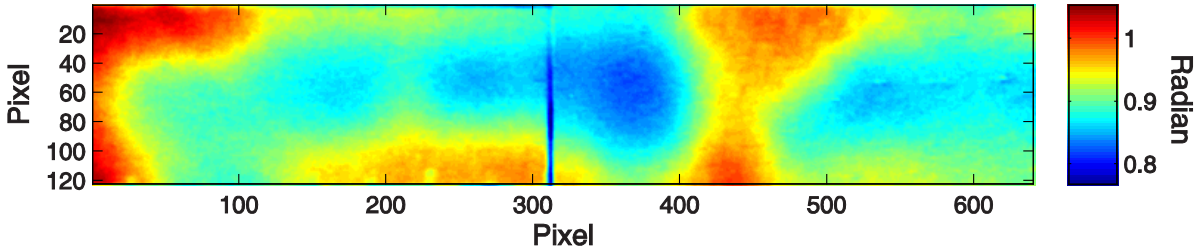
Pixel
20
40
60
80
100
120
100
200
300
400
500
600
Pixel
Radian
1
0.9
0.8

(b)

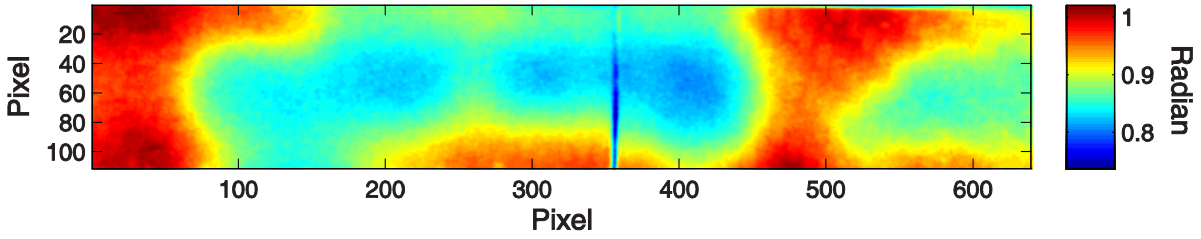
Pixel
20
40
60
80
100
100
200
300
400
500
600
Pixel
Radian
1
0.9
0.8

(c)

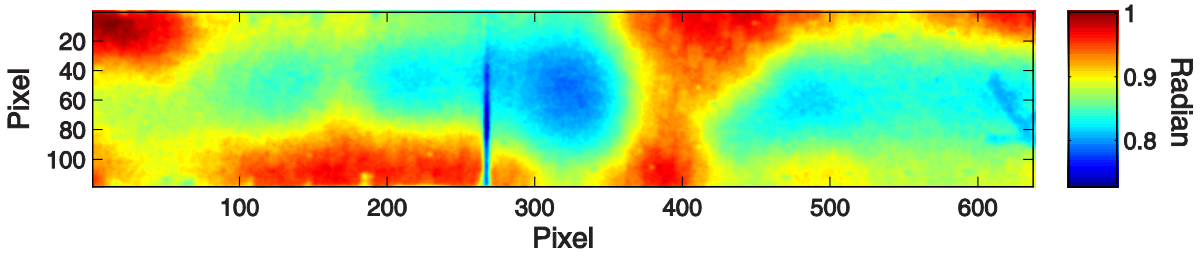
Pixel
20
40
60
80
100
100
200
300
400
500
600
Pixel
Radian
1
0.9
0.8

(d)

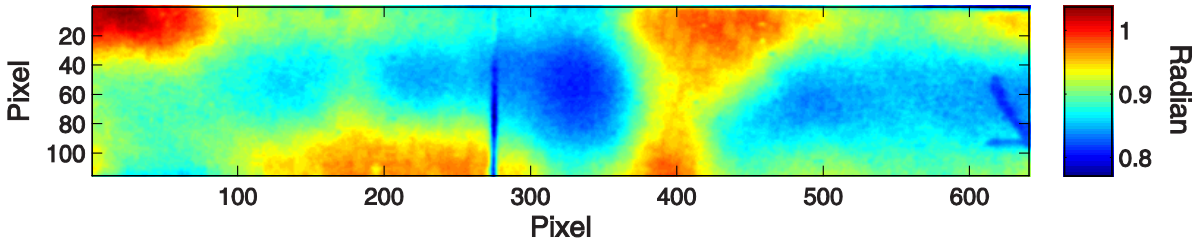
Pixel
20
40
60
80
100
100
200
300
400
500
600
Pixel
1
0.9
0.8
Radian

(e)

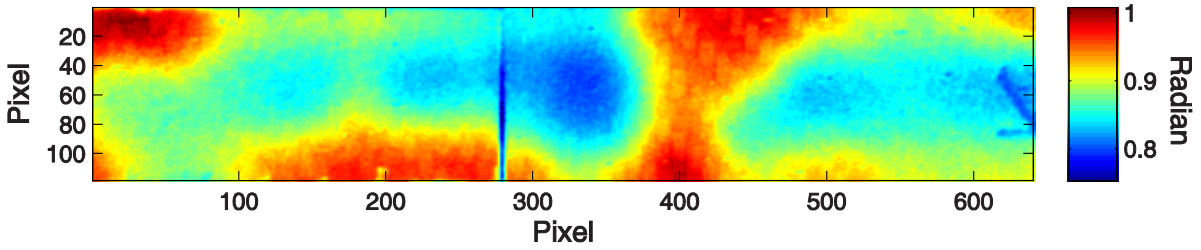
Pixel
20
40
60
80
100
100
200
300
400
500
600
Pixel
1
0.9
0.8
Radian

(f)

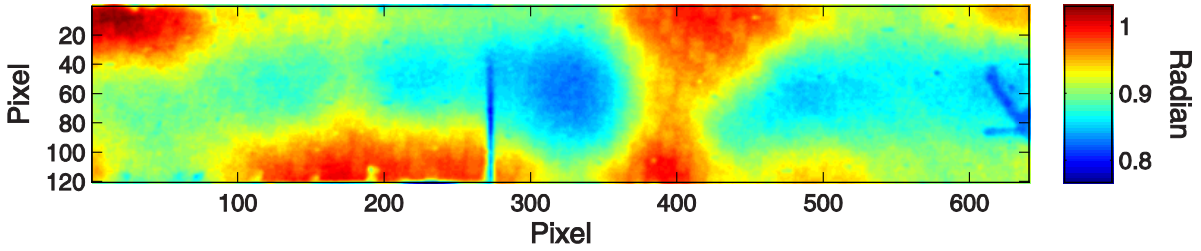
Pixel
20
40
60
80
100
120
100
200
300
400
500
600
Pixel
1
0.9
0.8
Radian

(g)

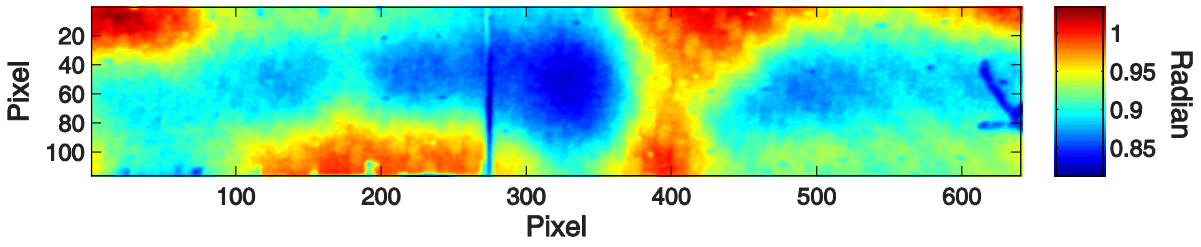
Pixel
20
40
60
80
100
100
200
300
400
500
600
Pixel
1
0.95
0.9
0.85
Radian

(h)

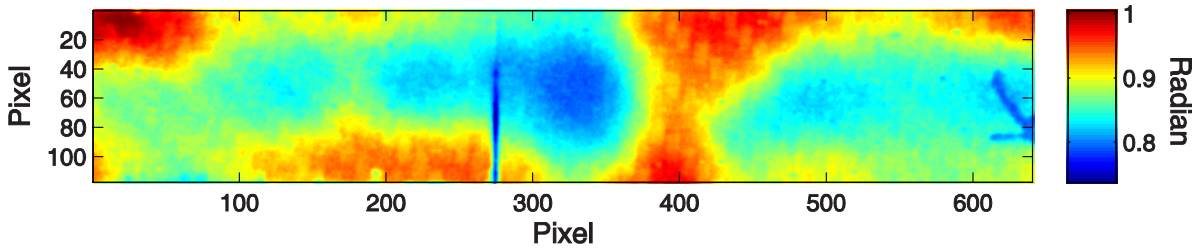
Pixel
20
40
60
80
100
100
200
300
400
500
600
Pixel
1
0.9
0.8
Radian

(i)

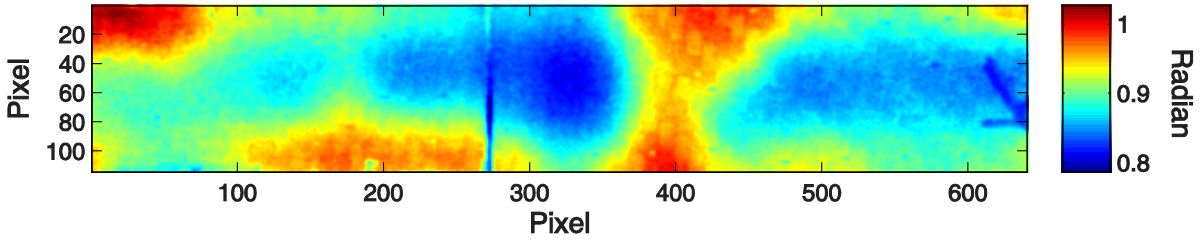
Pixel
20
40
60
80
100
100
200
300
400
500
600
Pixel
1
0.9
0.8
Radian

(j)

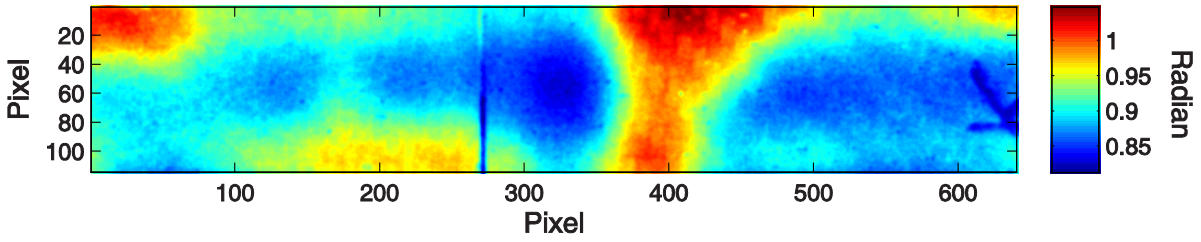
Pixel
20
40
60
80
100
100
200
300
400
500
600
Pixel
1
0.95
0.9
0.85
Radian

(k)

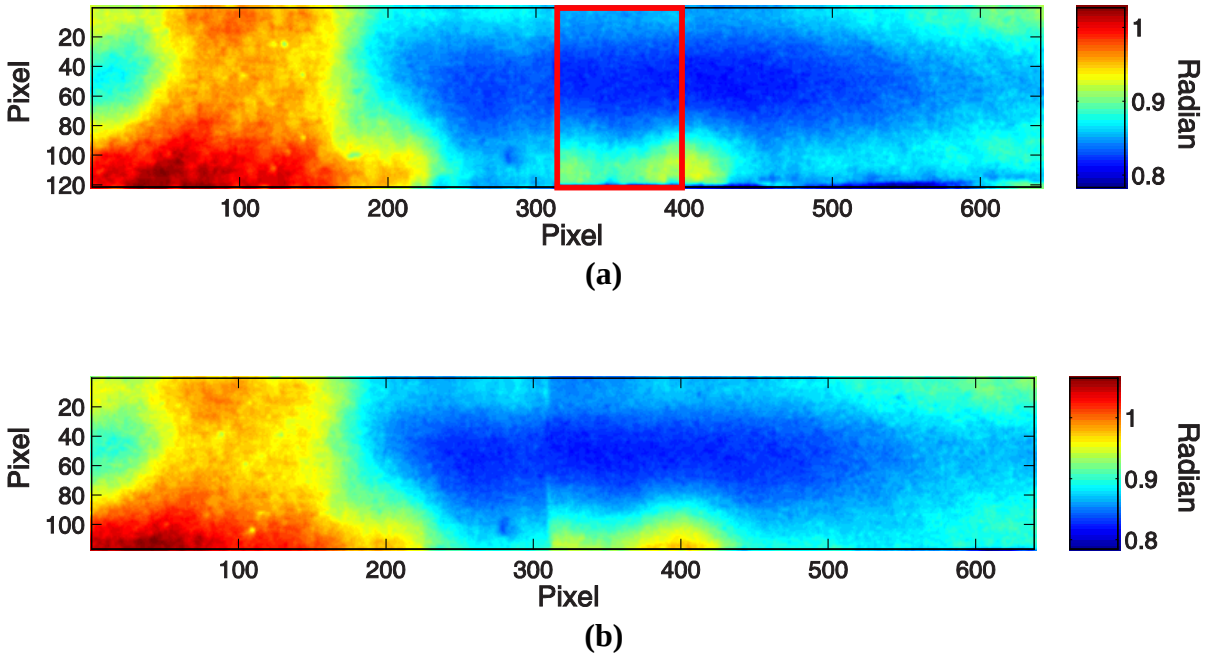

Figure B.6 Phase image of Sample 9 (f_s = 6 Hz, N = 196, f = 0.1 Hz); (a) initial stage, (b) 30000 cycles. Location of joint overlap region is shown by red box in (a).

Appendix C: MATLAB CODE LISTING

C1: SUBFRAME EXTRACTION

```
%{
*****************************************************************
*                                                               *
*             Extract subframes into .asc files                 *
*                                                               *
*                                                               *
* This program creates individual .asc file for each subframe   *
* in a matrix form by loading the .asc of entire frames.        *
* It creates a new folder called "subframe" and                 *
* saves the extracted matrix data in a new name AA#.asc,        *
* where file  number starts from 1 to n                         *
*                                                               *
*                                                               *
* Peter Shin                                                    *
* North Carolina State University                               *
* Mechanical and Aerospace Engineering Dept                     *
* 4/10/2012                                                     *
*                                                               *
*****************************************************************
%}
clear all;
clc;
profile on;

% size of the IR thermal image matrix
row = 512;
col = 640;

% select target file
[filenames,pathname] = uigetfile('*.asc','Select Thermography Image to
Extract');

afile = fullfile(pathname,filenames);
mkdir(pathname,'subframe_asc');  % Create a directory for saving
subframe

%% open file and position
tic; % start measuring process time
fileID = fopen(afile,'r');  % Open and read the file
message = ferror(fileID);   % Information about file I/O errors

%% skip the first 28 lines
skip_1 = fscanf(fileID,...
    '%*s %*s %*s \n\n %*s %*s %*s %*s %*s %*s %*s \n %*s %*s %*s %*s %d
\n %*s %*s %d \n %*s %d %d \n\n\n %*s %*s %*s \n\n %*s %*s \n %*s %*s \n
%*s %f \n %*s %*s %f %*s \n %*s %f %*s \n %*s %f %*s \n %*s %*s %f %*s
```

```
\n %*s %*s %f %*s \n %*s %*s %f %*s  \n %*s %*s %f %*s \n %*s %*s %f %*s
\n %*s %f %*s  \n %*s %*s %f %*s \n %*s %*s %f %*s \n\n\n',16);


%% Read Each Set of Frames until the end
n = 1;
 while ~feof(fileID);
    skip_2 = fscanf(fileID,'%s %s %s \n',4); % Hide Image Data:
characters
    frame(n).frm_num = fscanf(fileID,'%*s %d \n',1);  % Frame number
    frame(n).time = fscanf(fileID,'%s %s',2);         % Time stamp

    % fscanf fills the array in column order, so transpose the results
    frame(n).temp = fscanf(fileID,'%f',[col, row])';
    ascfilename = ['AA',num2str(n),'.asc']; % create file name
'AA'frame#.asc

% write subframe data to file
dlmwrite(fullfile(pathname,'subframe_asc',ascfilename),frame(n).temp,'de
limiter','\t');

    n = n +1;
 end

fclose('all');           % close all opened file
toc;                     % end measuring process time

profile viewer;
```

C2: LOADING IR-VIEW

```
%{
**************************************************************************
*                                                                        *
*                 Loadi1ng Multiple Files into MATLAB                    *
*                                                                        *
*                                                                        *
* This program reads multiple .asc files.                                *
* Then creates a 3-D matrix variable "three_D".                          *
* User input is necessary for subframe rate.                             *
* Sampling frequency is indicated as variable "sampling_freq".          *
*                                                                        *
*                                                                        *
* Peter Shin                                                             *
* North Carolina State University                                        *
* Mechanical and Aerospace Engineering Dept.                             *
* 10/20/2011                                                             *
*                                                                        *
```

```
**************************************************************************
%}

clear all; clc;
com.mathworks.mlservices.MLCommandHistoryServices.removeAll

[filenames,pathname] = uigetfile('MultiSelect','on','.asc'); % select
the files
all_files = cellstr(filenames); % list all .asc files in the MATLAB
current folder
fileNameOnly = regexp(filenames,'(\w*).asc','tokens');       % Get file
names without extensions
fileNamelist = getit(fileNameOnly);                          % Use getit
function file to get cell array in cell array

%% User input for determination of subframe rate
sub_frame = input('Enter the number of subframe rate(only in integer):
')

if isempty(sub_frame)           % Default value for the subframe rate
    sub_frame = 1
end

sampling_freq = 6 % sampling frequency in Hz

% Display the frequency of images
frequency = sampling_freq/sub_frame;               % Frequency
t = 1/frequency;                          % Time between each frames
(Delta_t)
frequency = num2str(frequency);
disp(['The image frequency is: ',frequency,' Hz']);

%%  Load the files
j=1;
for i=1:sub_frame:length(all_files); % from the first file of .asc to
last file of .asc
    C = all_files{i};
    eval(['load ' C ' -ascii']); % load the -ascii files to MATLAB

    imagelist(j)=fileNamelist(i);
    j=j+1;
end

%%  Create the list with comma separation
imagelist = vec2str(imagelist,[],1);  %  Import cell array with comma
separation
imagelist = strrep(imagelist,'''','');imagelist =
strrep(imagelist,'{','');imagelist = strrep(imagelist,'}','');

three_D = eval(['cat(3,' imagelist ')']); % 3D matrix of the selected
```

```
images

%% Run IR-View
ir_view(three_D(:,:,:),100*t,1);
```

C3: INSERTED DEFECT SIZE CALIBRATION

```
%{
**************************************************************************
*                                                                        *
*          Calibration sample damage size measurement                    *
*                                                                        *
*                                                                        *
* User selects two points of a measured geometry                         *
* and then calculates the phase contrast values in the joint region.     *
* Within this area the maximum phase contrast value is used to           *
* find the threshold value along with the calibrated factor,             *
* which then enables to express the area in binary image.                *
*                                                                        *
* Peter Shin                                                             *
* North Carolina State University                                        *
* Mechanical and Aerospace Engineering Dept                              *
* 2/19/2013                                                              *
*                                                                        *
**************************************************************************
%}

% fixed scale data
clear all;
clc; clf; close all; hold off

% check value of line 218 (variable name "factor1")

%% call in and load the .mat file
[filenames,pathname] = uigetfile('MultiSelect','on','.mat'); % select
the files

all_files = cellstr(filenames) % list all .mat files in the MATLAB
current folder

%%  Load the files, read matrix, and find min & max
for i=1:1:length(all_files); % from the first file of .asc to last file
of .asc
    filename = all_files{i};
    load(filename); % load the .mat files to MATLAB

    a = whos('-file',filename);  % separate the arrays in .mat file
```

```
    a_0 = a.name;  % new variable for array name
    matrix_name(i) = cellstr(a_0);
    A = eval([matrix_name{1,i}]);  % read each matrix values
    A_max(i) = max(max(A(:)));  % maximum of single array
    A_min(i) = min(min(A(:)));  % minimum of single array

    A_ult_max = max(max(A_max(:)));  % maximum of all array
    A_ult_min = min(min(A_min(:)));  % minimum of all array
end

scale = [A_ult_min A_ult_max]  % determine fixed scale

%% image plotting
for i=1:1:length(all_files)
    matrix = eval([matrix_name{1,i}]);
    figure(i);
    M = imagesc(matrix(:,:),scale);

    axis image; set(gcf,'color','w'); colorbar; title(matrix_name{1,i});
    xlabel('Pixel');ylabel('Pixel');

end

%% select x-y coordinates to determine pixel to length measure the
distance
hold on
[X(:,1),X(:,2)] = ginput(2);  % pick points using the mouse clicks
plot(X(:,1),X(:,2),'-rs','LineWidth',2,...
'MarkerEdgeColor','k',...
'MarkerFaceColor','g',...
'MarkerSize',5)

wdth = sqrt((X(1,1)-X(2,1))^2+(X(1,2)-X(2,2))^2); % calculate the
width(or any length) in number of pixels
prompt = {'Enter measured length:'}% input here the measured length of
the two points
dlg_title = 'Input measured value';
num_lines = 1;
length = inputdlg(prompt,dlg_title,num_lines);
actual_length =str2double(length(1,1))
pix_per_mm = wdth/actual_length
str1 = fprintf('actual length %f is displayed as %f
pixels',actual_length,wdth)

%% Select the region of interest and crop

I = imcrop(M);  % crop the image by selecting menu from right click
K=I;
I = I(:,:)-min(min(I(:)));  % calculate phase contrast
I_max = max(max(I(:)));  % maximum of single array
```

```
I_min = min(min(I(:)));  % minimum of single array
scale2 = [I_min I_max]  % determine new scale based on croped image

figure(100)
imagesc(I,scale2);
axis image; set(gcf,'color','w'); colorbar;
xlabel('Pixel');ylabel('Pixel');

%% Select the region of defected area by clicking (rectangle)
hold on
h = imrect;  % select a rectangle
pos = [5 5 20 20]  % create a square box
setPosition(h,pos)
position = wait(h)

%% Plot the actual size on the image
x_origin = position(1)+0.5*position(3);  % Define x-axis origin of the
local coordinate system
y_origin = position(2)+0.5*position(4);  % Define y-axis origin of the
local coordinate system
defect_size_mm = 25.4;  % 1 inch square shaped defect in millimeters
defect_size_pixel = defect_size_mm*pix_per_mm;  % Defect size in pixels
x_plus = x_origin+0.5*defect_size_pixel;  % actual xy position of actual
artificial defect
x_minus = x_origin-0.5*defect_size_pixel;
y_plus = y_origin+0.5*defect_size_pixel;
y_minus = y_origin-0.5*defect_size_pixel;

% Matrix of the xy-coordinate of the 4 points
D(1,1) = x_minus;    D(1,2) = y_minus;
D(2,1) = x_plus;     D(2,2) = y_minus;
D(3,1) = x_plus;     D(3,2) = y_plus;
D(4,1) = x_minus;    D(4,2) = y_plus;
D(5,1) = D(1,1);     D(5,2) = D(1,2);

% plot actual defect on image
plot(D(:,1),D(:,2),'-r','LineWidth',2);


%% Selecting the critarions
critarions = imrect;  % select another ROI
position2 = wait(critarions);  % double click after selection
zero_base = I(:,:)-min(I(:));  % critarion based on zero base
zero_max = max(zero_base(:));  % maximum value of the zero base plot
croppedImage = imcrop(zero_base,position2);  % crop the selected
max_croppedImage = max(croppedImage(:))

Size = size(zero_base(:,:));    % Pixels of the height
half_height = Size(1,1)/2;        % Middle of the hieght
 % Plot cross-section of the midplane
figure(2);plot(zero_base(round(half_height),:));grid on;
```

```
set(gcf,'color','w'); title(matrix_name{1,i});
xlabel('Pixel');ylabel('\Delta\phi (rad)');

% plot the region of interest around a high peak value
scale3 = [0 zero_max];
figure(1000);
imagesc(croppedImage,scale3);
axis image; set(gcf,'color','w'); colorbar;
xlabel('Pixel');ylabel('Pixel');

round_x_minus = round(x_minus);round_y_minus = round(y_minus);
round_x_plus = round(x_plus);round_y_plus = round(y_plus);

% Note that the y position is row and x position is column
line_1 = zero_base(round_y_minus,round_x_minus:round_x_plus);
line_2 = zero_base(round_y_minus:round_y_plus,round_x_plus);
line_3 = zero_base(round_y_plus,round_x_minus:round_x_plus);
line_4 = zero_base(round_y_minus:round_y_plus,round_x_minus);
avg_red_line = (mean(line_1)+mean(line_2)+mean(line_3)+mean(line_4))/4%
calculate average of the red line

factor = avg_red_line/max_croppedImage


size_zero_base = size(zero_base);
cutoff_value = factor*max_croppedImage

for j = 1:size_zero_base(1,1);
    for k = 1:size_zero_base(1,2);
        if zero_base(j,k) >= cutoff_value;
           C(j,k) = zero_base(j,k);
        else
           C(j,k) = 0;
        end
    end
end

figure(200)
imagesc(C,scale3);load('MyColormaps','mycmap');  % Make sure to keep
'MyColormaps' file within the same folder
set(get(0,'CurrentFigure'),'Colormap',mycmap);
axis image; set(gcf,'color','w'); colorbar;
xlabel('Pixel');ylabel('Pixel');
hold off


%% black or white
% Select 2 different regions
% call back the figure of the plate
figure(100)
```

```
delete(h)
delete(critarions)
sel_roi1 = imrect;
pos_roi1 = wait(sel_roi1);
if round(pos_roi1(1)) <= 0
    pos_roi1(1) = 1
else
end

% first region
row_roi1 = round(pos_roi1(2)):round(pos_roi1(2)+pos_roi1(4))+1;
col_roi1 = round(pos_roi1(1)):round(pos_roi1(1)+pos_roi1(3));
roi1 = zero_base(row_roi1,col_roi1);
[max_roi1 idx1] = max(roi1(:));
[find_row1, find_col1] = ind2sub(size(zero_base),idx1);
row1 = find_row1 + round(pos_roi1(2))-1;
col1 = find_col1 + round(pos_roi1(1))-1;

% second region
sel_roi2 = imrect;
pos_roi2 = wait(sel_roi2);
row_roi2 = round(pos_roi2(2)):round(pos_roi2(2)+pos_roi2(4));
col_roi2 = round(pos_roi2(1)):round(pos_roi2(1)+pos_roi2(3));
roi2 = zero_base(row_roi2,col_roi2);
[max_roi2 idx2] = max(roi2(:));
[find_row2, find_col2] = ind2sub(size(zero_base),idx2);
row2 = find_row2 + round(pos_roi2(2))-1;
col2 = find_col2 + round(pos_roi2(1))-1;

size_zero_base = size(zero_base);
% factor1 = 0.720988249;
factor1 = 0.661486;

C = zeros(size_zero_base);
C_01 = zeros(size_zero_base);

 for j = 1:size_zero_base(1);
    for k = 1:size_zero_base(2);
        % compare the distance from each point and find minimum
        dist(1) = sqrt((row1-j)^2 + (col1-k)^2);
        dist(2) = sqrt((row2-j)^2 + (col2-k)^2);

        % find which distance is the minimum
        [Value,Ind]=min(dist(:));
        [N]=ind2sub(size(dist),Ind);

        if N == 1
            cutoff_value = max_roi1*factor1;
        elseif N == 2
            cutoff_value = max_roi2*factor1;
        end
```

```
        if zero_base(j,k) >= cutoff_value;
           C_01(j,k) = 1;
           C(j,k) = zero_base(j,k);
        else
           C_01(j,k) = 0;
           C(j,k) = 0;
        end
    end
end

figure(300)
imagesc(C,scale3);load('MyColormaps','mycmap');  % Make sure to keep
'MyColormaps' file within the same folder
set(get(0,'CurrentFigure'),'Colormap',mycmap);
axis image; set(gcf,'color','w'); colorbar;
xlabel('Pixel');ylabel('Pixel');

figure(400)
imagesc(C_01);colormap(flipud(gray));
axis image; set(gcf,'color','w'); colorbar;
xlabel('Pixel');ylabel('Pixel');

hold off

%% plot actual defect for the two selected defect
h1 = imrect;  % select a rectangle
pos1 = [5 5 20 20]  % create a square box
setPosition(h1,pos1)
position3 = wait(h1)
hold on
h2 = imrect;  % select a rectangle
pos2 = [55 55 20 20]  % create a square box
setPosition(h2,pos2)
position4 = wait(h2)
hold on

delete(h1)
delete(h2)

%% Plot the actual size on the image
x_origin1 = position3(1)+0.5*position3(3);  % Define x-axis origin of
the local coordinate system
y_origin1 = position3(2)+0.5*position3(4);  % Define y-axis origin of
the local coordinate system
x_plus1 = x_origin1+0.5*defect_size_pixel;  % actual xy position of
actual artificial defect
x_minus1 = x_origin1-0.5*defect_size_pixel;
y_plus1 = y_origin1+0.5*defect_size_pixel;
y_minus1 = y_origin1-0.5*defect_size_pixel;
```

```
% Matrix of the xy-coordinate of the 4 points
D1(1,1) = x_minus1;    D1(1,2) = y_minus1;
D1(2,1) = x_plus1;     D1(2,2) = y_minus1;
D1(3,1) = x_plus1;     D1(3,2) = y_plus1;
D1(4,1) = x_minus1;    D1(4,2) = y_plus1;
D1(5,1) = D1(1,1);     D1(5,2) = D1(1,2);

% plot actual defect on image
plot(D1(:,1),D1(:,2),'-r','LineWidth',2);

%% Plot the actual size on the image
x_origin2 = position4(1)+0.5*position4(3);  % Define x-axis origin of
the local coordinate system
y_origin2 = position4(2)+0.5*position4(4);  % Define y-axis origin of
the local coordinate system
x_plus2 = x_origin2+0.5*defect_size_pixel;  % actual xy position of
actual artificial defect
x_minus2 = x_origin2-0.5*defect_size_pixel;
y_plus2 = y_origin2+0.5*defect_size_pixel;
y_minus2 = y_origin2-0.5*defect_size_pixel;

% Matrix of the xy-coordinate of the 4 points
D2(1,1) = x_minus2;    D2(1,2) = y_minus2;
D2(2,1) = x_plus2;     D2(2,2) = y_minus2;
D2(3,1) = x_plus2;     D2(3,2) = y_plus2;
D2(4,1) = x_minus2;    D2(4,2) = y_plus2;
D2(5,1) = D2(1,1);     D2(5,2) = D2(1,2);

% plot actual defect on image
plot(D2(:,1),D2(:,2),'-r','LineWidth',2);
```

C4 : FATIGUE LOAD AND DISPLACEMENT CALCULATION

```
%{
**********************************************************************
*                                                                    *
*                  Fatigue load and displacement calculation         *
*                                                                    *
*                                                                    *
* This program calculates and plots the normalized load              *
* and displacement of the entire life cycle of the specimen.         *
*                                                                    *
* Peter Shin                                                         *
* North Carolina State University                                    *
* Mechanical and Aerospace Engineering Dept                          *
* 11/27/2012                                                         *
*                                                                    *
```

```
**********************************************************************
%}

clear all; hold off
clc;clf; close all;

% fatigue displacement and load plot
% saving switch
saveoption.disp = 1; % save displacement plot switch 1: on, 2: off
saveoption.load = 1; % save load plot switch 1: on, 2: off

filename = 'C_combined'; % .mat file name of the combined load and
displacement information in 2 column matrix
load(filename) ; % load the .mat file
A = eval([filename]);
size_A = size(A,1);
cnt = 1;
inc = 1;

%% calculate normalized displacement (first column in the data)
for i = 1:inc:round(size_A/6);
    if i < round(size_A/6)
        st = 6*(i-1)+1;
        ed = 6*(i-1)+6;
        N(cnt) = i;
        zero_factor(cnt) = mean(A(st:ed,1)); % mean value of
corresponding period
        max_disp(cnt) = max(A(st:ed,1))-zero_factor(cnt); % max value of
corresponding period
        min_disp(cnt) = min(A(st:ed,1))-zero_factor(cnt);  % min value
of corresponding period
        avg_disp(cnt) = (max_disp(cnt)+min_disp(cnt))/2; % mean value of
min and max
        cnt = cnt+1;
    else
    end
end

max_disp=smooth(N,max_disp,0.1,'rloess');
min_disp=smooth(N,min_disp,0.1,'rloess');
avg_disp=smooth(N,avg_disp,0.1,'rloess');

% plot the maximum, minimum, and average of the two (min and max)
figure(1)
hold on;box on;set(gcf,'color','w');

plot(N,max_disp,'-k','LineWidth',2)
plot(N,min_disp,'-k','LineWidth',2)
plot(N,avg_disp,':k','LineWidth',2);xlabel('Fatigue
Cycles','fontsize',20);ylabel('Displacement (mm)','fontsize',20);
hold off
```

```
B = strcat(filename,'_disp')
if saveoption.disp == 1;
    saveas(gcf,[B],'eps')
    saveas(gcf,[B],'fig')
else
end

%% calculate normalized load (second column in the data)
cnt = 1;
for j = 1:inc:round(size_A/6);
    if j < round(size_A/6);
        st = 6*(j-1)+1;
        ed = 6*(j-1)+6;
        N(cnt) = j;
        zero_factor(cnt) = mean(A(st:ed,2)); % mean value of
corresponding period
        max_load(cnt) = (max(A(st:ed,2))-zero_factor(cnt))*4.4482/1000;
% max value of corresponding period
        min_load(cnt) = (min(A(st:ed,2))-zero_factor(cnt))*4.4482/1000;
% min value of corresponding period
        avg_load(cnt) = ((max_load(cnt)+min_load(cnt))/2); % mean value
of min and max
        cnt = cnt+1;
    else
    end
end

max_load=smooth(N,max_load,0.1,'rloess');
min_load=smooth(N,min_load,0.1,'rloess');
avg_load=smooth(N,avg_load,0.1,'rloess');

% plot the maximum, minimum, and average of the two (min and max)
figure(2)
hold on;box on;set(gcf,'color','w');
plot(N,max_load,'-k','LineWidth',2)
plot(N,min_load,'-k','LineWidth',2)
plot(N,avg_load,':k','LineWidth',2);xlabel('Fatigue
Cycles','fontsize',20);ylabel('Load (kN)','fontsize',20);
hold off

C = strcat(filename,'_load')
if saveoption.load == 1;
    saveas(gcf,[C],'eps')
    saveas(gcf,[C],'fig')
else
end
```

C5: FATIGUE DAMAGE DETECTION

```
%{
**************************************************************************
*                                                                        *
*                  Fatigue sample damage size measurement                *
*                                                                        *
*                                                                        *
* This program selects three low phase area by a user select,            *
* and then calculates the phase contrast values in the joint region.     *
* Within this area the maximum phase contrast value is used to           *
* find the threshold value along with the calibrated factor,             *
* which then enables to express the area in binary image.                *
*                                                                        *
* Peter Shin                                                             *
* North Carolina State University                                        *
* Mechanical and Aerospace Engineering Dept.                             *
* 2/19/2013                                                              *
*                                                                        *
**************************************************************************
%}

clear all; hold off;
clc; clf; close all;
com.mathworks.mlservices.MLCommandHistoryServices.removeAll

%% Joining area direction relative to laminate gap 1: Right 2: Left
roi.direction = 1;

%% Save options ** both cannot be 1 at the same time!!
storage.raw = 2;  % 1 for saving entire ROI
storage.bondedroi = 2;  % 1 for saving bonded area
storage.bondedBW = 2;  % 1 for saving binary filtered bounded area
% storage.bondedflt = 2;  % 1 for saving color filtered bounded area

%% call in and load the .mat file
[filenames,pathname] = uigetfile('MultiSelect','on','.mat'); % select
the files
all_files = cellstr(filenames); % list all file names selected .mat
files into string

%%  Load the files, read matrix, and find min & max of all images (ult
max & min)
for i=1:1:length(all_files); % from the first file of .asc to last file
of .asc
    filename = all_files{i};
    load(filename); % load the .mat files to MATLAB

    a = whos('-file',filename);  % separate the arrays in .mat file
    a_0 = a.name;  % new variable for array name
    matrix_name(i) = cellstr(a_0);
```

```
    A = eval([matrix_name{1,i}]);  % read each matrix values
    A_max(i) = max(max(A(:)));  % maximum of single array
    A_min(i) = min(min(A(:)));  % minimum of single array

end

%% plot the last image
figure(1000);
M = imagesc(A(:,:));
axis image; set(gcf,'color','w'); colorbar; title(matrix_name{1,i});
xlabel('Pixel');ylabel('Pixel');

hold on

%% find maximum value of the the last image with in joining area
% select three points then calculate average around the points for
minimum phase value
% area 1
[last_min_x1,last_min_y1] = ginput(1);

        plot(last_min_x1,last_min_y1,'r^',...
            'MarkerSize',5); % plot the selected point

IMinVC1 = imcrop(A,[round(last_min_x1) round(last_min_y1) 5 5]);   % min
value calculation
last_avg_min_candidate(1) = mean(mean(IMinVC1));

% area 2
[last_min_x2,last_min_y2] = ginput(1);

        plot(last_min_x2,last_min_y2,'r^',...
            'MarkerSize',5); % plot the selected point

IMinVC2 = imcrop(A,[round(last_min_x2) round(last_min_y2) 5 5]);   %
initial min value calculation
last_avg_min_candidate(2) = mean(mean(IMinVC2));

% area 3
[last_min_x3,last_min_y3] = ginput(1);

        plot(last_min_x3,last_min_y3,'r^',...
            'MarkerSize',5); % plot the selected point

IMinVC3 = imcrop(A,[round(last_min_x3) round(last_min_y3) 5 5]);   %
initial min value calculation
last_avg_min_candidate(3) = mean(mean(IMinVC3));

last_avg_min = min(last_avg_min_candidate(:));
last_phase_cont = A-last_avg_min;  % phase contrast
```

```
% user selects the 25.4mm width
[X(:,1),X(:,2)] = ginput(2);
wdth = sqrt((X(1,1)-X(2,1))^2+(X(1,2)-X(2,2))^2); % calculate point-to-
point length
actual_length = 25.4; %length of measurement in this case it's always
the width (25.4mm)
pix_per_mm = wdth/actual_length;
mm_per_pix = 1/pix_per_mm;
actual_length_pixels = actual_length*pix_per_mm;

    if round(X(1,2)) <= 0;
        X(1,2) = 1;
    elseif round(X(2,2)) >= size(last_phase_cont(:,:),1);
        X(2,2) = size(last_phase_cont(:,:),1);
    end
        plot(X(:,1),X(:,2),'r^',...
            'MarkerFaceColor','b',...
            'MarkerSize',5);
hold off;

        if roi.direction == 1;  % when joining region is to the
rightside of the laminate gap
            M2_last = imcrop(last_phase_cont,[X(1,1) X(1,2)
actual_length_pixels/2 actual_length_pixels]);
        elseif roi.direction == 2;  % when joining region is to the
leftside of the laminate gap
            M2_last = imcrop(last_phase_cont,[X(1,1)-
actual_length_pixels/2 X(1,2) actual_length_pixels/2
actual_length_pixels]);
        end

factor = 0.661486;  % From calibration we know that 66.15% of max phase
value determines the damaged boundary
calibration = max(max(M2_last))*factor;

for i=1:1:length(all_files);
    matrix = eval([matrix_name{1,i}]);

    %% plot the entire sample
    figure(i);
    M = imagesc(matrix(:,:));
    axis image; set(gcf,'color','w'); colorbar; title(matrix_name{1,i});
    xlabel('Pixel','fontsize',12);ylabel('Pixel','fontsize',12);

        if storage.raw == 1;
            saveas(figure(i),[matrix_name{1,i} 'raw'],'epsc');
            saveas(figure(i),[matrix_name{1,i} 'raw'],'fig');
        else
        end
```

```
    hold on;
    if i < length(all_files);
        % select three average low area for phase contrast calculation
        % area 1
        [min_x1,min_y1] = ginput(1);

                plot(min_x1,min_y1,'r^',...
                    'MarkerSize',5); % plot the selected point
        IMinVC1 = imcrop(A,[round(min_x1) round(min_y1) 5 5]);   %
initial min value calculation
        avg_min_candidate(1) = mean(mean(IMinVC1));

        % area 2
        [min_x2,min_y2] = ginput(1);

                plot(min_x2,min_y2,'r^',...
                    'MarkerSize',5); % plot the selected point
        IMinVC2 = imcrop(A,[round(min_x2) round(min_y2) 5 5]);   %
initial min value calculation
        avg_min_candidate(2) = mean(mean(IMinVC2));

        % area 3
        [min_x3,min_y3] = ginput(1);

                plot(min_x3,min_y3,'r^',...
                    'MarkerSize',5); % plot the selected point
        IMinVC3 = imcrop(A,[round(min_x3) round(min_y3) 5 5]);   %
initial min value calculation
        avg_min_candidate(3) = mean(mean(IMinVC3));

        avg_min = min(avg_min_candidate(:));
        phase_cont = matrix-avg_min;  % phase contrast

        %% pick two points using the mouse clicks
        figure(i);
        [X(:,1),X(:,2)] = ginput(2);

            if round(X(1,2)) <= 0;
                X(1,2) = 1;
            elseif round(X(2,2)) >= size(phase_cont(:,:),1);
                X(2,2) = size(phase_cont(:,:),1);
            end

        wdth = sqrt((X(1,1)-X(2,1))^2+(X(1,2)-X(2,2))^2); % calculate
point-to-point length
        actual_length = 25.4; %length of measurement in this case it's
always the width (25.4mm)
        pix_per_mm = wdth/actual_length;
        mm_per_pix = 1/pix_per_mm;
        actual_length_pixels = actual_length*pix_per_mm;
```

```
        plot(X(:,1),X(:,2),'-rs','LineWidth',2,...
            'MarkerEdgeColor','k',...
            'MarkerFaceColor','g',...
            'MarkerSize',5);
        hold off;

        %%crop the bonded area based on measurement
        % map the actual size of bonded area
        if roi.direction == 1;  % when joining region is to the
rightside of the laminate gap
            M2 = imcrop(phase_cont,[X(1,1) X(1,2) actual_length_pixels/2
actual_length_pixels]);
        elseif roi.direction == 2;  % when joining region is to the
leftside of the laminate gap
            M2 = imcrop(phase_cont,[X(1,1)-actual_length_pixels/2 X(1,2)
actual_length_pixels/2 actual_length_pixels]);
        end

    elseif i == length(all_files);
          M2 = M2_last;
    end

        %% plot the phase contrast ROI (bonded region)
        figure(11*i);
        imagesc(M2);
        axis image; set(gcf,'color','w'); colorbar;
title(matrix_name{1,i});
        xlabel('Pixel','fontsize',14); ylabel('Pixel','fontsize',14);
set(gca,'XTick',0:10:size(M2,2));
        set(gca,'YTick',0:10:size(M2,1));

          % save as .eps files and .fig files when storage.bondedroi = 1
            if storage.bondedroi == 1;
                saveas(figure(11*i),[matrix_name{1,i}
'bondedroi'],'epsc');
                saveas(figure(11*i),[matrix_name{1,i}
'bondedroi'],'fig');
            else
            end

    %% threshold filter
    C_BW = im2bw(M2,calibration);

    %% plot the binary image
    figure(111*i);
    imagesc(C_BW);colormap(flipud(gray));
    axis image; set(gcf,'color','w'); set(gca,'XTick',0:10:size(M2,2));

xlabel('Pixel','fontsize',14);ylabel('Pixel','fontsize',14);set(gca,'YTi
ck',0:10:size(M2,1));
```

```
        % save as .eps files and .fig files when storage.bondedBW = 1
        if storage.bondedBW == 1
            saveas(figure(111*i),[matrix_name{1,i} 'bondedBW'],'eps');
            saveas(figure(111*i),[matrix_name{1,i} 'bondedBW'],'fig');
        else
        end
end
```